Abundance analysis of normal and mercury-manganese type late-B stars from optical spectra

Caroline Sarah Allen

Thesis submitted for the degree of Doctor of Philosophy,
in the Faculty of Science of the University of London

Department of Physics & Astronomy
UNIVERSITY · COLLEGE · LONDON

12th October 1997

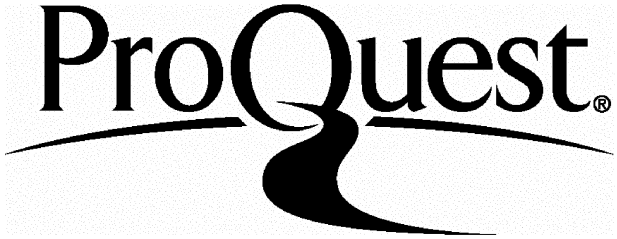

Dedication

To Charles Edward Kempson Roe

1941-1992

Abundance analysis of normal and mercury-manganese type late-B stars from optical spectra

Abstract

The aim of this project was to perform an abundance analysis of a selection of mercury-manganese and normal A and B-type stars. Observations of thirteen stars were taken using the Hamilton Échelle Spectrograph and coudé auxilliary telescope (CAT) situated at Lick Observatory. The high signal-to-noise optical spectra were reduced with the aid of the software packages FIGARO and VISTA. A technique for measuring the parasitic light parallel to the dispersion of the spectrum was devised; none was found (mean P = $-1.0\pm0.8\%$), which implies that measured equivalent widths should be free of this important systematic error.

Measurements were made of the wavelengths and equivalent widths of unblended spectral lines. The spectra were modelled using ATLAS-6 model atmospheres and the synthesis package UCLSYN. Effective temperatures and surface gravities for the programme stars were adopted from Smith and Dworetsky (1993). Abundances were generally determined by comparing synthetic equivalent widths to measured equivalent widths. Where line blends made this impossible, the observed spectra were compared to the synthetic spectra. The instrumental profile was determined from arc calibration lines and was found to be asymmetric; the profile was measured and was convolved with the synthetic spectra to allow a comparison with observations to be made.

Microturbulence parameters for these stars were determined according to the method of Magain (1984); stars with effective temperatures below 11 000K showed a positive value, but stars above this temperature yielded microturbulences consistent with zero.

The abundances generally compare well with the literature and are in many cases an improvement on existing work. Phosphorus showed a positive correlation with effective temperature in HgMn stars and manganese also exhibits a strong correlation, in agreement with previous observations. The strong manganese line at λ4206.367 was found to exhibit a systematic discrepancy with respect to other manganese lines at high abundances; this is probably due to hyperfine structure and it is recommended that this line not be used for abundance analysis in the future unless its structure can be modelled explicitly.

Contents

List of Tables

List of Figures

Chapter 1

Introduction

1.1 Overview

This thesis provides an analysis of the abundance of elements observed in mercury manganese stars. Mercury-manganese (HgMn) stars are a class of B-type main sequence stars whose spectra exhibit strong lines of mercury and/or manganese. It is possible to determine the chemical compositions of these stars from direct observations and subsequent analysis of their spectra.

1.1.1 Aim and Objectives

The HgMn phenomenon is not currently fully explained, although progress has been made for some elements in the area of diffusion theory. This thesis will constitute an important contribution to the science of HgMn stars through its meticulous selection of spectral lines and careful data handling.

One of the aims of this project was to obtain abundances for a number of HgMn stars and compare them to the results predicted by theory; another was to ensure the data were as accurate and wide ranging in their element coverage as possible. This ensures that this work is not simply an addition to but an improvement on existing data on this class of stars.

It was also hoped that this thesis could introduce an improved means of determining the nature and quantity of contamination of the spectrum due to scattered

and parasitic light, and of removing it if it were present. This would then give improved equivalent width measurements and therefore improved abundances.

Finally, it was worth using the research time to investigate anomalies reported by other authors, such as the differences in abundances between different ionisation stages seen in the results of Adelman (1991) and possibly to identify new ones. Confirmation or rejection of reported abundance trends for some elements would also be possible.

In order to monitor systematic error in the abundance calculations the sample should include both HgMn and a control sample of solar abundance or 'normal' stars.

The thesis should be a considerable improvement on the work of Heacox (1979), whose analysis of HgMn stars contained obvious systematic errors, and Lemke's (1990) work which, because of the narrow spectral range of the data used, only used the Ca I resonance line for its abundance determination. The work will also provide magnesium abundances which appear to be free of known systematic error and improved abundances for the normal star ζ Dra, as well as vanadium, yttrium and zirconium abundances.

It will also be more extensive in its study of the abundances of different elements than work in the field by other authors than Adelman (1989, 1991, 1994). Most published work deals with an in-depth study of a few elements (i.e., Heacox (1979), Lemke (1990), Sadakane et al (1983)) and in order to obtain a full picture of the abundances of individual chemically peculiar stars it would be necessary to combine these results. This would not be an ideal situation as the methods, spectra and software used by each researcher would be different. Instead, this thesis will follow the approach of Adelman, which is to study in depth the abundances of as many elements as possible, to allow a picture to be built up of the stellar abundance of each star using a single source of data.

Finally, the approach of this thesis can be considered superior to the recent work of Adelman (1989, 1991, 1994), but in a different way than to other work. The abundances obtained here will be calculated using only those lines which meet the necessary criteria of being unblended, with known atomic data and on the linear

Table 1.1: The ten stages of the project

Objective	Stage	Chapter
Selection of programme stars	1	2
Observing	2	2
Plan analysis	3	2
Reduce data	4	2
Measure wavelengths	5	3
Measure equivalent widths	6	3
Select atomic data	7	4
Spectrum synthesis	8	5
Error determination	9	5
Comparison	10	6

portion of the curve-of-growth. In contrast, the work of Adelman contains a large selection of lines of varying strengths and oscillator strength quality.

1.1.2 Structure of the thesis

The method adopted in this thesis for abundance determination involved a number of distinct stages. The initial stage was to obtain high resolution échelle spectra of thirteen stars. Next a technique was devised for the reduction of these spectra which minimises systematic error. The spectrum of one of these stars, the HgMn star υ—Her, was examined in great detail and the wavelengths of the spectral lines measured and the lines identified. A full list of the wavelengths and the line identifications for υ Her was compiled in order to aid the selection of lines from which the equivalent widths of the other twelve stars can be measured. The final stages involved the synthesis of stellar spectra and calculations of chemical abundances for each star and estimation of the internal and external errors in the calculation. Finally the efficacy of the method is tested by comparison of the normal star spectra with published work.

The ten stages of the project are shown in Table 1.1.

1.2 Background information

1.2.1 A and B-type main-sequence stars

A- and B-type main sequence stars are found in the temperature range 7 500 – 30 000K (A7V – B0V). Not all A- and B-type main- sequence stars can automatically be assumed to show solar-type chemical abundances in their spectra, and stars which do not show solar abundances, the 'chemically peculiar' (or CP) stars, appear frequently throughout the narrow temperature range between 9 000 and 16 000K (Wolff 1983).

Normal early A and late B-type stars occur in the $T_{\rm eff}$ range where photospheric mass motions are expected to be small. They do not appear to have the surface anomalies characteristic of CP stars, are found to have similar compositions to the Sun when analysed under LTE conditions and have no observed periodic or non-periodic variability (Wolff 1983). But normal stars in the CP star temperature range may be a rarity rather than a common occurrence; Cowley (1969) states that one-fifth of A-stars have conspicuous spectral anomalies while Gray (1992) writes that CP stars may comprise anything upwards of one-third of all A and B stars, and Ramella *et al* (1989), Lemke (1989,1990) suggest that sharp-lined normal A- and B-type stars may be the exception rather than the rule. Indeed, the case of Vega (α Lyr, a program star), which authors from Hunger (1955) to Smith and Dworetsky (1993) found to be metal deficient, helps to illustrate the scarcity of normal stars around A0 (Wolff 1983), when it is recalled that Vega is considered to be a 'standard' A0V star.

There are several classes of main sequence CP stars; the Ap, Am, HgMn, λBoo, and He-wk stars. Some CP stars are found to exhibit measurable magnetic fields (Preston 1971). Cowley's 1980 classification scheme places both the Ap and silicon-overabundant helium-weak stars into the magnetic CP star class. The AmFm stars are non-magnetic and are given their name because of the abnormally strong metal lines in their spectra (Conti 1970). The other non-magnetic CP A- and B-type stars are: another type of 'helium-weak' [He-wk] star which shows enhanced phosphorus and gallium, a class of He-wk star which shows titanium and strontium enhancements and the non-magnetic mercury-manganese [HgMn] stars which show overabundances

of mercury, manganese, gallium and phosphorus. Details of all three of the He-wk classes can be found in Borra, Landstreet and Thompson (1983). The stars from each CP class sometimes vary a great deal in detail but still share the common properties of the class. Some apparently normal stellar spectra show chemical peculiarities only at high resolution; these are the 'superficially normal' stars (Cowley 1980, Cowley *et al* 1982).

1.2.2 The CP stars of the main-sequence

The Ap stars are known to have magnetic fields (Preston 1971, Dworetsky 1993) and Zeeman effect measurements confirm this (Conti 1970). They are found in the upper region of the A-star temperature range but Ap stars have bluer colours for their spectroscopic temperatures than normal stars; i.e., A0p corresponds in colour and luminosity to B8 normal stars. Deutsch (1947) found that the helium lines in the spectra of these stars are abnormally weak. The chemical abundances of Ap stars also show a tendency to increase with $T_{\rm eff}$ but do not correlate with $v \sin i$ or magnetic field strength (Adelman 1973). Ap stars also show unusual properties regarding chromium and silicon abundances. The ratio of silicon to magnesium in hotter stars is more than a factor of 25 greater than that seen in cooler Ap stars. The cooler stars show abundances of chromium and silicon which, though they vary from star to star, are consistent with normal stars. However, hotter Ap stars show overabundances of chromium. Generally the chemical abundances of Ap stars show scatter from star to star. Wolff (1983) draws attention to a temperature dependent classification scheme first drawn up by Jaschek (1958) for magnetic A-stars. The bluest and hottest stars are called λ4200 Si stars, and the sequence passes through the Si, Sr-Cr-Eu and Eu-Cr-Sr to Sr, the coolest and least-blue stars. Jaschek and Jaschek (1967) found that the correlation between $T_{\rm eff}$ and peculiarity is statistically significant.

The Am stars were first defined by Roman et al (1948) and were classified as those stars 'for which spectral type derived from the K line of Ca II is five subclasses earlier than the type corresponding to metal line strength' (Wolff 1983). Am stars also have weaker hydrogen Balmer lines than would be expected for a main sequence star of the apparent spectral type of the Am star and they are not thought to be

magnetic (Preston 1971). There are three distinct types of Am stars; those which exhibit both weak calcium and scandium lines and strong metal lines, stars with weak calcium and scandium lines alone, and stars which show only the strong metal lines.

The chemically peculiar λ Boo stars are characterised by weak metal lines and $v \sin i$ values anywhere between 5 and 200kms^{-1}. Sargent (1965) estimates λ Boo stars comprise 1-2 percent of A-type dwarfs. The review paper of Gerbaldi and Faraggiana (1993) expands this definition further and defines λ Boo stars as those having a deficiency of a factor of 3 in the iron-group elements Sr, Fe, Ti and Sc. These stars are also normal in oxygen abundance and deficient in Mg and Ca when compared to the star's iron abundance. It is not thought that λ Boo stars evolve through radiative diffusion processes; instead it has been proposed that these stars are in the late phases of pre-main sequence evolution; this hypothesis is strengthened by the detection of a narrow Ca II K line and the Na II D doublet, both of which signify the presence of circumstellar matter surrounding these stars.

The 'Helium-rich' [He-rich] stars can be divided into two subclasses (Hunger 1975), one of which is highly evolved and of low mass, and one of which is on the main sequence. The temperature range of the latter class does not have a well-defined boundary but appears not to extend into the O-star range. Five of the ten He-rich main-sequence stars observed by Borra and Landstreet (1979) have rotational velocities greater than 150kms^{-1}.

The 'Helium-weak' [He-wk] stars (Borra, Landstreet and Thompson 1983, Wolff 1983) occupy the spectral range B3-B7 and exhibit a discrepancy between photometric colours and spectral type, as well as a helium deficiency anywhere between 2 and 15 times that observed in normal stars. The magnetic Si-overabundant stars show spectra similar to the magnetic λ 4200 stars of the Ap class, the non-magnetic P-Ga stars show spectra much like hot versions of mercury-manganese B-type stars with an overabundance of ^{3}He with respect to ^{4}He (Hartoog and Cowley 1979) and another class shows enhanced titanium and strontium which implies that there may be a temperature dependent continuum of these stellar types.

Mercury-manganese stars are CP non-magnetic late B-stars. Their characteristics are further discussed in Section 1.2.3.

1.2.3 Mercury-manganese stars

Mercury-manganese stars were first discovered and classified as manganese stars by Morgan (1931), although Morgan was not able to identify the λ3984 line which was later identified as Hg II by Bidelman (1962*a*,*b*). The current classification criteria are the strength of the manganese and mercury lines in visible spectra observed at a classification dispersion (50Åmm^{-1}, Jaschek and Jaschek 1987) as well as the strength of the helium line at λ4026, which is weaker in these stars than normal stars of a similar spectroscopic effective temperature.

Wolff and Wolff (1974) state that because Balmer and helium line strength are used as luminosity classification criteria, the weak helium lined HgMn stars appear to correspond to a later but more luminous spectral type with the same Balmer-line strength as the corresponding main sequence HgMn star. Strömgren (1966) photometry places these stars firmly on the main sequence (Hauck and Mermilliod 1980).

HgMn stars are thought to be older than 10^7 years from studies of open clusters by Abt (1979), who detected no HgMn stars in clusters below this age. Surface gravity can be an indicator of stellar age; in this study the random error in $\log g$ makes any conclusions about the age of these stars impossible to make (see 7.1.2 for further details).

Reviews of previous work on HgMn stars can be found in Dworetsky (1986, 1993), Guthrie (1984), Wolff (1983) and the thesis of Smith (1992). Observational results and analyses can be found in Heacox (1979), Wolff and Preston (1978), Guthrie (1984), Smith and Dworetsky (1993), Smith (1993, 1995, 1996) and the papers of Adelman (1989, 1994).

General properties

HgMn stars occur in the $T_{\rm eff}$ range 10 000 to 16 000K (Wolff and Wolff 1974). The Wolff and Preston (1978) high dispersion field-star study (at a reciprocal dispersion of 2-4Å mm^{-1}) revealed 36 HgMn stars out of a total of 256 late B-type stars, which is approximately 14 per cent of the sample. They found that at 11 000K the frequency of HgMn stars in their sample was 8 per cent, which rose to 25 per cent of

the sample at 15 000K. Abt (1979) studied the incidence of HgMn stars in galactic clusters and found no HgMn stars below an age of 10^7 years, which implies that the development of the HgMn phenomenon may be age-related.

HgMn stars rotate at speeds below 100kms^{-1}, although normal stars are also found to rotate at these speeds. Aikman (1971) argues that this observed low $v \sin i$ in HgMn stars is genuinely indicative of slow rotation and not orbital inclination because studies of binary stars show that orbital inclinations are randomly distributed; however it is not completely clear whether *normal* stars with low observed $v \sin i$ are simply those few seen nearly pole-on, or whether any of them are genuinely slow rotators (Gulliver *et al* 1994). For further discussion of this problem, see Chapter 2.

HgMn stars have not been found to be magnetic (Preston 1971, Borra and Landstreet 1979). Mathys and Lanz (1990) suggested that HgMn stars could have a disordered solar-type magnetic field which may not be easy to detect.

Abundance characteristics

At classification dispersion manganese and mercury are not always exhibited simultaneously in the spectra of all HgMn stars; *e.g.* 53 Tau only shows the strong Mn II line at λ4206; conversely in χ Lupi only the Hg II line at λ3984 appears in the spectrum. Wolff and Wolff (1974) noted these differences and defined three distinct types; Mn, Hg and HgMn. The appelation *HgMn* will be used throughout this thesis for stars exhibiting one or both of these features.

Aller's (1970) study of the HgMn star κ Cnc was the first to raise the possibility that manganese may be correlated with T_{eff}. Since that time Heacox (1979), Guthrie (1984), Adelman (1989), Smith and Dworetsky (1993) have all been able to confirm and extend this finding, although not all the HgMn stars studied by these authors have shown a dependence between abundance and temperature; the consistency of the stellar abundances between the work of different authors on individual stars suggests this is not an experimental error but a property of the individual stars and cosmic scatter.

Takada-Hidai *et al* (1986) performed a UV analysis of a sample of HgMn stars and found gallium also to be correlated with T_{eff}. This has been confirmed by Smith

(1996), who also proposed a successful two-layer model to account for differences in the abundances between Ga II and III ions (Smith 1995).

Sadakane *et al* (1983) found aluminium is generally underabundant in HgMn stars, as did Smith (1993) who found some HgMn stars were underabundant by 2 dex.

Nickel (Adelman 1991 and 1994) has been found to be consistently underabundant in the spectra of HgMn stars but not correlated in any way with effective temperature. Magnesium is also underabundant in HgMn stars (Adelman 1991, 1994, Guthrie 1984, Smith 1993). The elements carbon, nitrogen and oxygen are normal, underabundant and close to normal respectively in typical HgMn stars (Roby and Lambert 1990, Smith and Dworetsky 1990).

Smith and Dworetsky (1993) found silicon was of solar abundance and that magnesium was underabundant in HgMn stars. Optical analysis by Guthrie (1984) illustrated that chromium, titanium and iron scatter widely about the solar abundance; indeed normal stars, analysed by Adelman (1991), do not show such a considerable scatter. Yttrium, scandium, strontium and barium are typically enhanced (Guthrie 1984) and mercury, phenomenally overabundant in most HgMn stars, shows evidence of non-terrestrial isotopic composition (White *et al* 1976), as does platinum (Wahlgren *et al* 1995).

The first analysis of ϕ Her (Zimmerman, Aller and Ross 1970) revealed an overabundance of zirconium in this star, but despite being present in the spectrum of this cool HgMn star, and that of χ Lup (Wahlgren *et al* 1994*a*), zirconium is not particularly anomalous in the spectra of most HgMn stars. Guthrie (1985) found neodymium in the spectrum of HR7775, whilst gold lines and thallium lines, due to the heavy isotope Tl-205, which exhibit hyperfine structure have been seen in the UV spectra obtained using the Hubble telescope (Leckrone *et al* 1994). Wahlgren *et al* (1994*b*) state that As II lines at λ1375.07 and Bi II lines at λ1372.6 and 1902.3Å have been seen in the spectrum of χ Lup which illustrate overabundances in these elements of $\sim$2 orders of magnitude; however bismuth is blended and an uncertainty in the wavelength calibration could cast some doubt on the results for this element. More research is needed. A spectrum of Sirius analysed by the same authors shows no absorption lines at these wavelength positions, which lends weight to their results.

1.2.4 Theories about the origin of HgMn stars

Much speculation has been made about the mechanisms of formation for HgMn stars. Some early theories have now been largely discredited. Fowler *et al* (1965) suggested that rare earth elements are manufactured from iron-peak elements by the *s-process*, a process of slow neutron addition which is thought to occur in stars which have evolved off the main sequence, entered the giant phase and returned to the vicinity of the main-sequence. The nucleosynthesised products are then mixed to the surface. The stars are expected to appear photometrically at the edge of the main sequence despite not being main-sequence stars, because one effect of line blanketing is to increase the blue flux in the spectra and alter the star's photometric indices, apparently placing the star on the main sequence. Fowler *et al* (1965) also presented a theory on Ap-star formation which suggested that a white dwarf secondary star is magnetically linked to the Ap star and transfers mass onto the companion. However, Sargent and Searle (1967) confirmed that the anomalies were confined to the surface of the star and so the star would have to be young and on the hydrogen burning main sequence, not the giant required by Fowler's theory.

The nucleosynthetic explanation for the formation of mercury manganese stars has been recently resurrected, but only partly, by Wahlgren *et al* (1995) who suggest that *s*-process elements could contribute to abundance anomalies found in binary systems and make them more extreme than they otherwise would be. Wahlgren states that the abundance ratio between gold and platinum [Au/Pt] will vary depending on the nuclear process (*r* or *s* process) producing these elements. The authors admit that the sensitivity of this test precludes accurate diagnostics until abundances can be known to better than 0.1 dex, and it would seem this hypothesis is unprovable.

Cameron (1971) wrote that a supernova outburst could not be responsible for HgMn star formation in clusters, which showers the atmosphere of the precursor star with heavy elements. He suggested that the force of the outburst would sweep away the stellar envelope. The evolved HgMn star is also expected to gain radial velocities in excess of 10 kms^{-1}, and studies of these stars in clusters demonstrate that they do not have relative velocities in excess of the cluster escape velocity of approximately $2\,\mathrm{kms}^{-1}$ (Abt 1979). This means the star is not in the process of passing through

the cluster and the presence of these stars in clusters must be explained some other way.

Vauclair (1976) expressed a view that mixing in the atmosphere due to meridional circulation may be responsible for the presence of normal stars with high $v \sin i$ values. Meridional circulation is the motion of deep currents within a star, mixing layers and leading to a uniform composition throughout the star, including the surface layers. This process begins to become important at v_e values above $100\,\mathrm{kms}^{-1}$ (Gray 1992). Not all main-sequence A and B-type stars with low $v \sin i$ values are HgMn stars. This may be because the HgMn pattern takes time to develop and the slow-rotating normal stars are therefore younger stars which have not had time to form their surface abundances, or because apparently normal stars are pole-on to the observer and have higher v_e values. An example of the latter can be found in the spectrum of Vega. Gulliver *et al* (1994) examined three lines, including the λ4528 Fe I line, in the spectrum of Vega to see if the curious trapezoidal profiles seen in weak lines in the spectrum of Vega could be explained using a model of a pole-on rapidly rotating star instead of a slowly-rotating model. The authors used a grid of inclinations and rotational velocities to obtain a fit to the data using an inclination of $\sim$5 degrees and a $v \sin i$ of $21.8\mathrm{kms}^{-1}$ (which corrresponds to an equatorial velocity of $250\mathrm{kms}^{-1}$). Fits to the spectral lines using a fixed iron abundance were much better using the pole-on model, including reproduction of the trapezoidal profile.

Press, Witta and Smarr (1975) speculated that low $v \sin i$ normal stars in the HgMn T_{eff} range may form instead of becoming HgMn stars because of outside factors such as mass transfer between binary companions. Mass transfer can prevent development of HgMn peculiarities because turbulence can destroy ordered patterns int he stellar atmosphere or prevent them emerging.

Burbidge and Burbidge (1955), and Fowler, Burbidge and Burbidge (1955) proposed surface nuclear reactions as a mechanism for forming CP stars. Alpha particles, deuterons and neutrons strike the stellar atmosphere and react to produce heavy elements. A magnetic field is required to accelerate the particles.

Havnes and Conti (1970) proposed that a star moving through the interstellar medium could capture elements in its magnetosphere which then accumulate onto its surface. HgMn stars are non-magnetic, so this is not a viable model for these

stars.

1.2.5 Michaud's parameter-free model

Michaud's basic parameter-free diffusion model, first proposed in 1970, describes how both the magnitude and direction of the stellar radiation field shapes the atmosphere of a precursor star to give rise to abundance anomalies. The main features of the diffusion model are shown in Table 1.2. It is assumed that elements are initially contained in an atmospheric reservoir of solar composition, which is continually replenished and unaffected by large scale mass motions. Interactions between photons from the radiation field and particles within this atmospheric 'reservoir' result in a transfer of momentum from photon to particle. Given enough collisions with photons emerging from the lower boundary of the photospheric reservoir, atoms with lines in the same energy region as the radiation will absorb momentum and slowly drift upwards. The converse is true for elements without lines in the energy region of the radiation. These elements will sink if the atmosphere can no longer support them, and appear as underabundant elements once mass motions cease.

The diffusion velocity v_D is given by Michaud (1986) as

$$v_D = -D_{12}\left[\frac{\partial \ln c}{\partial r} + (g - g_R)\frac{m_p}{KT} - k_T\frac{\partial \ln T}{\partial r}\right] \tag{1.1}$$

where D_{12} is a 'molecular diffusion coefficient', $c = \frac{N}{N_H}$ is the concentration of the element undergoing diffusion, g and g_R are the accelerations due to gravity and radiation respectively, m_p is the mass of the proton and other symbols take conventional meanings.

This equation has three terms. The first term is the classical or 'chemical' diffusion term. Chemical diffusion takes place in order to 'neutralise' a concentration gradient in the atmosphere. In stellar models this term is set to zero at t=0, the beginning of the main sequence (ZAMS). The second term is the resultant force on each atom due to differences in the accelerations due to gravity (g) and to radiation pressure (g_R), and the third term covers thermal diffusion due to the presence of temperature gradients in the stellar atmosphere.

The process of gradual drifting is labelled 'radiative diffusion' because although

Table 1.2: Main features of the parameter-free model

•Star is free of large-scale mass motions
•No free parameters should be required for a fit
•The star's gravitational field acts 'inwards' on all atoms in the atmosphere
•Radiation pressure acts 'outwards' on all atoms in the atmosphere
•Atoms 'diffuse' outwards or inwards in the direction of the resultant force

the motion of the atoms is a random walk process, the net motion of the atoms and ions is in the radial direction of the radiation field or gravity, whichever dominates. The rising particle travels to lower optical depths beyond the optical line forming region where the electron density drops. This means that the atoms which rise have a higher probability of ionisation which shifts the ionisation balance towards higher stages.

Higher ionisation stages of 'opaque' ions may be transparent to the photospheric radiation and therefore not experience any net outward force. If a layer of such ions builds up in the outer atmosphere then an overabundant layer forms below this region which, if it happens to be in the line forming region, manifests itself as an overabundance. The two layers are in dynamic equilibrium. If no equilibrium forms in the photosphere then the material may leave the star altogether.

A He II convection zone is present in young A and B stars (less than 10^6 years) and is thought to continuously mix the stellar atmosphere and prevent the appearance of over and under-abundances (Michaud et al 1979). Diffusion will still take place in stable regions outside the convection zone, but the diffusing elements cannot pass through the convection zone without becoming fully mixed. The He II in the convection zone gradually sinks under the influence of gravity and is thought to dominate element motion in the stellar atmosphere. After 10^6 years the helium is depleted by a factor of 3 (Vauclair, Vauclair and Pamjatnikh 1974) leading to the disappearance of the convection zone and this is when the atmosphere is thought to become stable enough for diffusion to progress through the atmosphere. The presence of this zone may also help explain why HgMn stars do not appear in clusters younger than 10^7 years (Abt 1979).

Meridional circulation, which begins to dominate in rapid rotators ($v \sin i$ above

100 kms^{-1}; Gray 1992) can also interfere with the slow diffusion of elements. The Tassoul and Tassoul (1982) model of meridional circulation was used by Michaud (1982) to show that the He II zone does not disappear in stars which rotate more rapidly than $90\,\mathrm{kms}^{-1}$. Both these considerations may explain why HgMn stars are not observed at $v \sin i$ values above $100\,\mathrm{kms}^{-1}$ (Wolff and Preston 1978).

Cooler stars with an effective temperature of less than 10 500K are thought to possess a hydrogen convection zone which may not allow enough stability in the outer atmosphere. Indeed the characteristic HgMn pattern is not seen in stars at or below this temperature (Wolff and Wolff 1974, Wolff and Wolff 1976, Wolff and Preston 1978), although the anomalies common to the AmFm and Ap stars are. Furthermore, the absence of a detectable (Preston 1971, Conti 1970) magnetic field in HgMn stars implies that the net direction of the resultant force acting on individual atoms is radial. No spots or rings have been observed on the surfaces of HgMn stars, and a uniformly radial force is likely to give rise to surface abundance anomalies which are uniformly distributed.

Light induced drift

It was proposed by Leblanc and Michaud (1993) that a phenomenon known as light induced drift should be included in radiative calculations. Light induced drift occurs in the profiles of one or more Doppler-broadened lines of a particular element when the radiation field in the line is anisotropic. Such a situation could occur when the flux of excited atoms moving away from the star is greater than the flux moving towards the star, which means that radiative acceleration should already be dominating small scale motions in the stellar atmosphere. A drift velocity is set up in the stellar atmosphere which is in the direction of the least-excited atoms. This additional drift velocity has a greater magnitude for neutral species than for ionised species and so a large light induced drift will occur in regions where the atoms are excited but rarely ionised.

1.3 The methodology of abundance determinations.

In order to obtain accurate abundances the atmospheric parameters of the star must be well-known, the line strengths or equivalent widths must be reliable, the lines must be identified correctly and the atomic data must be known precisely. Armed with these data, there are four techniques which can be used to obtain chemical abundances; differential analysis, curve of growth analysis, spectrum synthesis and the estimation of a star's 'metallicity' from photometric observations.

A differential analysis compares the spectrum of the programme star to a well-known standard star (Gray 1992). It is important to choose a reference star as spectroscopically similar to the sample star as possible to prevent spectral differences due to temperature becoming important. The main advantage of this method is that it is possible to obviate atomic data uncertainties when deriving abundances, but it requires that the abundances of the comparison star be accurately known, absolutely derived, or assumed to be particular values, usually consistent with solar quantities.

The modern curve-of-growth analysis technique involves the calculation of abundances by comparing the theoretical and empirical curves of growth. To perform this calculation it is first necessary to know the reduced equivalent width, which is defined as the ratio of the equivalent width of a line (W_λ) and the line's wavelength λ, (*i.e.* W_λ/λ). The curve of growth is then the logarithmic relationship between the reduced equivalent width of an absorption line and the effective number of absorbers in the line forming region relative to the amount of continuum absorption at wavelength lambda, which depends on many factors which vary from line to line, but which is directly proportional to the abundance of the element relative to hydrogen.

The first curve-of-growth analyses were performed by Voigt (1912) and van der Held (1931); these models used a simple model atmosphere with a single temperature layer. The first published abundance analysis was performed for the Sun by H.N. Russell (1929) where Russell's calculation for the solar composition was based on measurements made from a single saturated hydrogen line. The 'exact' curve-of-growth method used in this project calculates the curve of growth for a single line of an element, providing a unique abundance for each spectral line.

Spectrum synthesis is the process of computation of a complete spectrum interval

including one or more lines using a model atmosphere. This is a 'trial and error' technique, often with many free parameters which require fitting, where the effects of instrumental profiles, line broadening, line blends and the abundances are adjusted until the observed spectrum and the model match. The technique relies strongly on the perception and judgement of the observer but has the advantage of providing simultaneous fitting to several lines of an element by synthesising many lines from one element over a single spectral interval. A particular advantage of this technique is that it can also deal very well with line blends.

Model atmospheres have seen much improvement since the first rudimentary model atmosphere was published (Milne 1922). Modern model atmospheres take into account the effects of convective transport (Hearnshaw 1990), and line-blanketing (Mihalas 1965) and offer a real insight into the mechanisms at work in stellar envelopes. Model atmospheres are founded on the assumption of local thermodynamic equilibrium, which states that the Boltzmann, Saha and Maxwell distributions describing the properties of the atmosphere are consistent with those found in a gas at the local value of the temperature. However, the assumption of LTE may not hold in reality, as the radiative processes might dominate over collisional processes in the atmosphere. In these situations, a model may be constructed which is allowed to depart from the conditions of LTE; this model is said to be in 'non-local' thermodynamic equilibrium or nLTE. Anderson (1989) and Rutten *et al*(1984) discuss the effects of nLTE and line blanketing in modern model atmospheres.

'Metallicity' can be measured by examining spectral intervals using narrow band filters. Strömgren $uvby\beta$, Geneva photometry and spectrophotometry lend themselves well to metallicity measurements (Smalley 1992). The index is calibrated by comparison of the metallicity index yielded by photometry to a full-scale abundance analysis. Straizys (1985) and Smalley and Dworetsky (1993) review several photometric systems used for measuring metallicity. Smalley notes that few metallicity calibrations exist for main-sequence A-stars and offers a calibration derived from a comparison between the flux-blocking measured for a variety of Am stars and that measured from a number of synthetic spectra at the stars' temperatures, gravities, and a range of metallicities. Smalley then plotted the stars' derived metallicities against the photometric parameter δm_0 and found a linear calibration for [M/H].

The errors on abundances can be estimated from the spread in abundances for several lines, or from errors estimated from the variables used to calculate the abundances. For the curve-of-growth and spectral synthesis methods errors can come from the stellar model and the oscillator strengths, as well as the measured equivalent widths. If these variables are assumed to be independent, they can be propagated to give an estimate for the external error. The internal error, calculated from the abundances of several lines, is given by the standard error on the mean abundance.

The external errors on the abundances obtained from photometry can be propagated from the uncertainty in the stellar effective temperature, and the flux-blocking-parameter Λ, given by

$$\Lambda = \log_{10}\left[\int_{\lambda_1}^{\lambda_2}(1 - R_\lambda)d\lambda\right] \tag{1.2}$$

where R_λ is the residual flux at λ and the equation is integrated over the range of the spectrum examined. Errors can also be present in the continuum level calibration and from noise in the spectrum. This method was not used in this thesis as the individual abundances of elements were required and not a basic metallicity parameter.

1.3.1 Summary

The abundances obtained for this project will be calculated using spectrum synthesis and exact curve-of-growth techniques. In order to perform accurate abundance analysis and satisfy the requirements set out at the beginning of this section the spectra for this project need to be of high resolution (to enable identification of single lines in elements which may not have many optical lines and to separate blends where possible) and of a high signal-to-noise ratio (s/n above 100:1 to prevent obscuration of weak or single lines). It was decided to study the region between 3900 and 4900Å as many interesting lines of calcium, singly ionised chromium, scandium and gallium can be seen in this wavelength range as well as those of more commonly seen elements. All of these data requirements could be satisfied by the Coudé Auxilliary Telescope and Hamilton Échelle Spectrograph at Lick Observatory and observations were scheduled there for May and September 1993.

Chapter 2

Observations and reduction

2.1 Choice of stars

A sample of thirteen stars, comprising 6 HgMn and 7 'normal' stars was selected for analysis with the aid of the thesis of Dworetsky (1971), work by Heacox (1979), Smith and Dworetsky (1993) and Adelman (1989), Guthrie (1984), and White *et al* (1976).

The stars chosen from the Bright Star Catalogue (Hoffleit and Jaschek 1982) were field stars, because cluster stars are too faint (Abt 1979) to allow many to be acquired using a small telescope (the CAT) and during the limited time period of an observing run.

The next criterion for the choice of stars was whether or not they were visible from the northern hemisphere. The star sample was narrowed further by the time constraints operating during both the observing run and the data reduction period. The HgMn star sample was therefore reduced to six stars and the normal star sample to seven. Care was taken to ensure the range of HgMn star effective temperatures was bracketed by a wider temperature range of the normal stars, giving an even coverage and easy comparision between the two samples. This also reduces systematic error. It would have been useful to find equivalent temperature and gravity between normal and HgMn stars, but the sample was too small for this.

There may be some doubt as to whether the rotational velocities of the sample

are unbiased. It is impossible to tell, either in single systems or well-separated binary systems, whether a star is pole-on or equator-on or at some other inclination. The stars in this project, both normal and HgMn, were chosen to have a $v \sin i$ smaller than $35\,\mathrm{kms}^{-1}$, because this faciliates line identification, analysis by measurement of equivalent widths and continuum calibration, all of which are used in this thesis. However, this value gives only a lower limit to the true equatorial velocity v_e of the star. This information is important, because the v_e of the star may have a bearing on whether HgMn stars develop. This was investigated by Smith (1992) who was unable to find any correlation between $v \sin i$ and overabundance; however a relationship may exist between v_e and abundance. It is possible that such a relationship exists because HgMn stars are found to exist at low $v \sin i$ speeds, which, considering a random sample is taken, implies that v_e is also low for these stars; otherwise there would be a random mixture of speeds as seen in normal stars. Rapid rotation would be likely to disrupt the atmospheres of HgMn stars, which appear to require a stable atmosphere to develop (Wolff and Preston 1978).

Normal stars are also seen with $v \sin i$ values below $100\mathrm{kms}^{-1}$ and these stars may be at low inclinations. This is different to HgMn stars and could explain the wide range of speeds seen for normal stars with a large, apparently random sample (Wolff and Preston 1978). The equatorial velocity of the normal stars may not necessarily be low, and some of the stars might be viewed pole-on. Vega is a case in point, as this star has been shown to be a pole-on rapid rotator (Gulliver *et al* 1994). This is not the case for all HgMn stars as the orbital inclinations of binaries systems containing HgMn stars showed random distribution of $v \sin i$ (Aikman 1976).

The six sample HgMn stars are ϕ Her, υ Her, 87 Psc, HR7361, HR7664 and HR6997, which have all been studied by Smith and Dworetsky (1993) and span the temperature range 11 000 - 15 000K; in addition ϕ Her and HR7664 can be compared directly to the work of Adelman (1988).

The normal stars were chosen as a control sample to mitigate the effects of unknown sources of systematic error and nLTE effects. Both samples of stars span the effective temperature range 9 500 to 15 000K, although the HgMn phenomenon only begins to appear above 10 500K (Wolff 1983). All of the CP stars in this study belong to the HgMn class described in Chapter 1, but they are very different in de-

Table 2.1: Programme stars

HD	HR	Star	Spectral Type	$v \sin i$[1]	V	B–V
				$km\,s^{-1}$	Magnitude	Colour index
97633	4359	θ Leo	A2V	23	3.34	-0.01
147394	6092	τ Her	B5IV	32	3.89	-0.15
155763	6396	ζ Dra	B6III	34	3.17	-0.12
172167	7001	α Lyr	A0Va	23	0.03	0.00
179761	7287	21 Aql	B8II-III	19	5.15	-0.07
174567	7098	-	A0Vs	11	6.64	+0.02
209459	8404	21 Peg	B9.5V	4	5.80	-0.07
7374	364	87 Psc	B8III	21	5.98	-0.08
144206	5982	υ Her	B9III	11	4.76	-0.11
145389	6023	ϕ Her	B9p Mn	10	4.26	-0.07
172044	6997	-	B8II-III pHg	34	5.42	-0.10
182308	7361	-	B9pHgMn	9	6.52	-0.04
190229	7664	-	B9pHgMn	8	5.67	-0.10

1: vsini derived by Smith and Dworetsky(1993)

Spectral type and photometry adopted from Hoffleit and Jaschek (1982).

tail. Previous work on these stars by the authors listed above reveal that ϕ Her is a cool HgMn star ($T_{\rm eff}$=11 670K, Smith and Dworetsky 1993; $T_{\rm eff}$=11 325K, Adelman 1989) with only mildly enhanced manganese; υ Her is a narrow-lined HgMn star ($v \sin\ i$=11kms^{-1} Smith and Dworetsky 1993) and HR7664 shows a curious deficiency in magnesium (the abundance is 6.25 dex, Adelman 1989), whereas HR7361 shows a deficiency in sulphur. HR6997 is a hot star ($T_{\rm eff}$=14 520K, Smith and Dworetsky 1993) at the upper temperature boundary of the HgMn class with a projected rotation velocity of 34 kms^{-1} (Smith 1992) which shows a large manganese overabundance (3 dex, Smith and Dworetsky 1993) above solar, and 87 Psc exhibits a very low iron abundance ($\sim$1 dex below solar, according to Smith and Dworetsky 1993).

Summaries of the basic data on these stars can be seen in Table 2.1. Epoch 2000.0 coordinates for the programme stars are shown in Table 2.2, while Tables 2.3 and 2.4 show the complete Lick observation set.

Data on these programme stars were obtained in 1993 at the Lick Observatory

Table 2.2: Programme stars and their coordinates

HD	HR	Star	α 2000.0	δ 2000.0
			h m s	^{o} ' "
97633	4359	θ Leo	11 14 14.3	+15 25 46
147394	6092	τ Her	16 19 44.3	+46 14 48
155763	6396	ζ Dra	17 08 47.1	+65 42 53
172167	7001	α Lyr	18 36 56.2	+38 47 01
179761	7287	21 Aql	19 13 42.6	+02 17 38
174567	7098	–	18 49 43.9	+31 37 45
209459	8404	21 Peg	22 03 18.9	+11 23 11
7374	364	87 Psc	01 14 07.6	+16 08 01
144206	5982	υ Her	16 02 46.1	+46 02 12
145389	6023	ϕ Her	16 08 46.1	+44 56 06
172044	6997	–	18 36 37.1	+33 28 08
182308	7361	–	19 19 46	+64 23 27
190229	7664	–	20 03 29.9	+16 01 53

in California with the Hamilton Échelle Spectrograph. These échelle data were then extracted, flat-fielded, wavelength-calibrated and transformed into the laboratory rest-frame. The presence of scattered light in the spectra was found to be negligible. The data were finally summed according to a photon-count based weighting scheme and normalised using the DIPSO software package.

2.2 Observations of the programme stars

The Coudé Auxilliary Telescope (CAT) at Lick Observatory, Mount Hamilton, California, was used to obtain échelle spectra in May and September 1993. The CAT feed is situated on the south side of the main 3-m telescope dome. The two telescopes share the Hamilton Échelle Spectrograph and observations with the CAT and Hamilton were scheduled during dark runs.

The Hamilton Échelle Spectrograph (Vogt 1987) gives a mean reciprocal dispersion of 2.54 Åmm^{-1} in the centre of the wavelength range. The resolving power ($\lambda/\Delta\lambda$) was quoted theoretically as 48 000 over the entire format (Misch 1991), and the dispersion for any particular order, along with further details on the detector and spectrograph, can be found listed in Misch (1991). The actual wavelength-dependent resolution measured (see Figure 2.6 and 2.7) was in the range 30 000 to 35 000. Detectors can be fitted to the spectrograph which cover the wavelength range 3900–$\sim$8900 Å, but for this study a thinned blue-sensitive 800×800 chip was used with a wavelength range set between 3900–4900 Å. This region covers many metal lines (including calcium, manganese, zirconium and vanadium) and so is sufficient for this study. This did not cover the entire free spectral range of the grating. Use of a chip covering the full wavelength range would have meant loss of blue sensitivity. The detector is a Texas Instruments 800×800 back-illuminated charge-coupled device (CCD) with a 'red' (4900Å) quantum efficiency of 65% and a 'blue' (3900Å) quantum efficiency of 45%. The chip dimensions are 12mm×12mm and each pixel is 15μm in diameter.

The CCD and grating were adjusted to allow two settings to be used to record the entire FSR, hereafter referred to as RHS and LHS. (LHS and RHS refer to the appearance of the image on the VDU screen; LHS=blue, RHS=red sides of blaze).

A slit width of 600μm (5.9 arcseconds) was used in all of the observations. The slit length was adjusted for flat-field and stellar observations.

The spectrograph was focused from measurements of the mean FWHM of six randomly selected arc lines measured at different positions on the CCD format. The focus was altered until the minimum mean FHWM was determined; this point was adopted as the optimum focus position.

Calibration Observations

Observations of a Thorium-Argon lamp spectrum were used to calibrate the stellar spectra, and several observations were taken to ensure that there was a high positional accuracy when the spectra were combined and also to check whether the spectrograph settings shifted during the night. The lines of this lamp are numerous, easy to identify, and well distributed over the entire wavelength region used. They are also very sharp because there is no splitting due to hyperfine structure or the presence of isotopes. A typical Thorium-Argon data frame demonstrating the even distribution of calibration lines is shown in Figure 2.1.

Arc calibration observations were taken at the beginning and end of observations using a new setting and during each afternoon before the start of observations to ensure the spectrum had not moved during the day.

During the September observing run, weak, broad emission lines of hydrogen were seen in the arc lamp. The source of this contamination is not known. The intensity of these emission lines was much weaker than the Th-Ar lines and did not affect the wavelength calibration. Figure 2.2 shows an extracted arc exhibiting an example of these lines at Hβ (λ4861).

A line-free quartz lamp is used at Lick to produce flat-field spectra. Two sets of exposures were taken; one set with a long-slit (30 arcsecond) and one with a short-slit (12.5 arcsecond), the latter being the same length as that used for the stellar exposures. It is the convention to use a long slit when flat fielding spectra because this affords an increase in S/N and therefore a cleaner stellar continuum. Short-slit flat-fields, with narrow spatial profiles and an absence of lines, were used as a template for spectrum extraction. An example of the spatial profiles of both

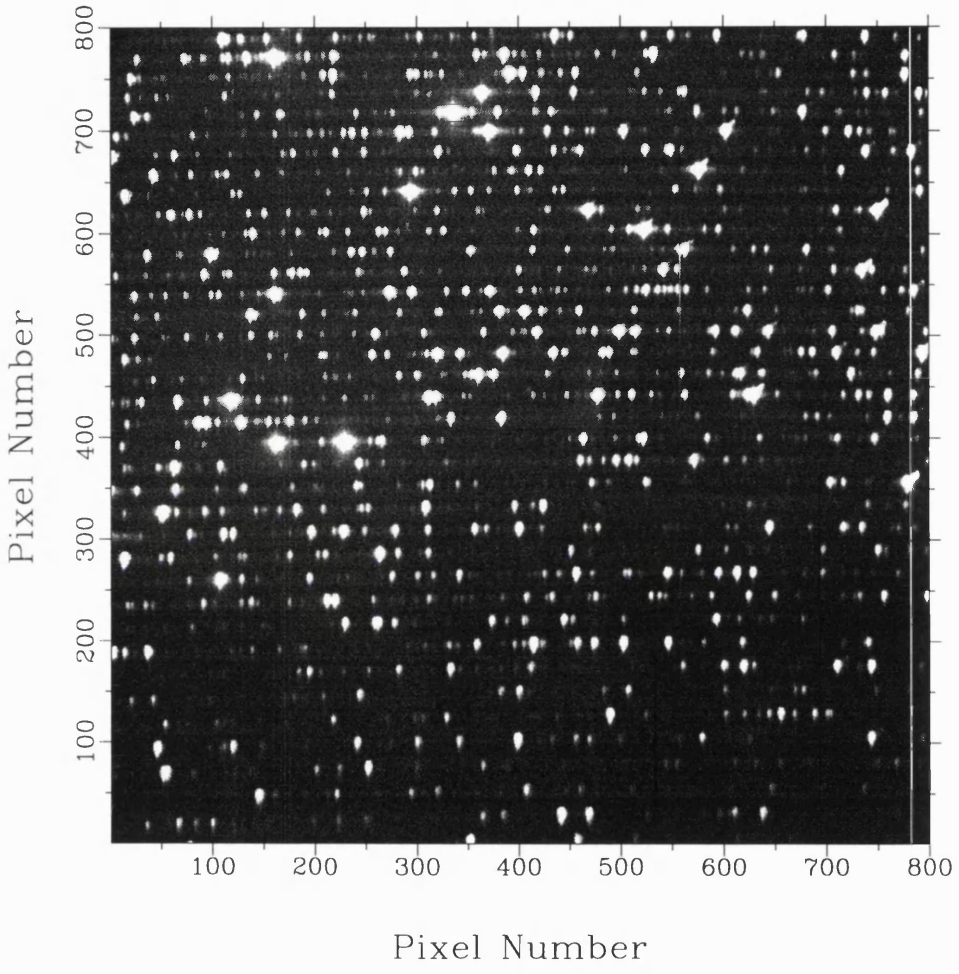

Figure 2.1: A Thorium-Argon spectrum for the right hand side of the format. There is a hot column at pixel 781. Note the even distribution of Th-Ar lines, facilitating an effective fit to the wavelength scale.

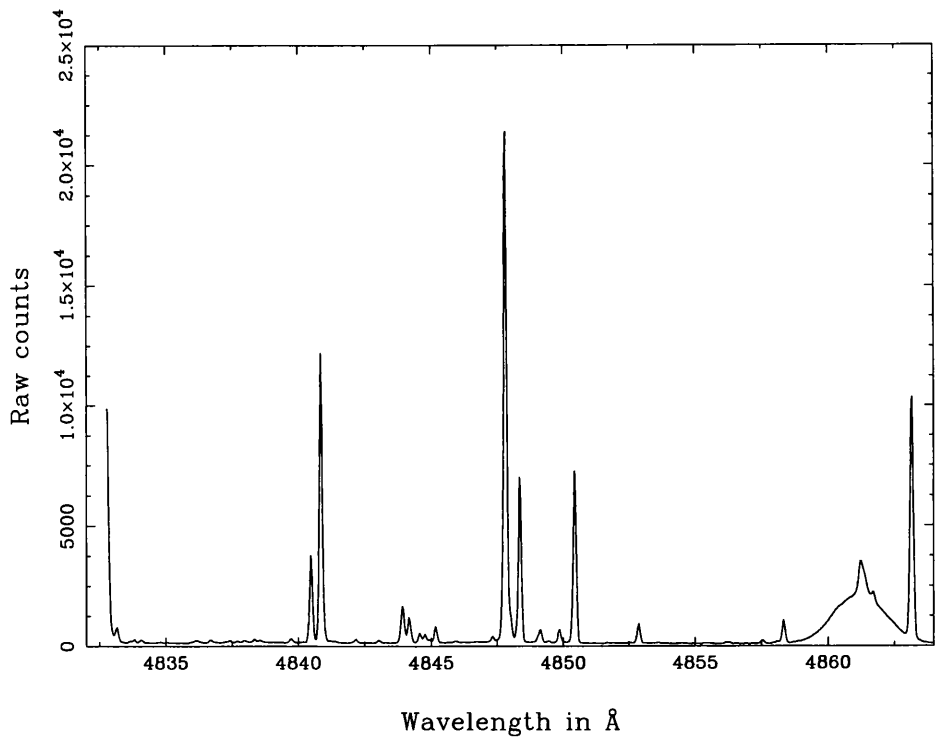

Figure 2.2: A weak, broad Hβ line in the comparison spectrum. This line appeared in arcs taken in the September observing run but was not present in May

types of flat-field is shown in Figure 2.3.

Solar spectra are also required as these can be used as a means of finding systematic errors present in the equivalent widths and line profiles of the data. Solar irradiance spectra were taken of the diffuse reflected sunlight from the telescope housing roof during the day and a comparison was made between these data and a high-resolution, high S/N solar-flux atlas (Kurucz *et al* 1984).

The bias current is automatically subtracted by the data-acquisition software. Instead of bias frames, dark frames are measured at Lick with the shutter closed which ensures stray photons do not interfere with the voltage pattern recorded on the chip. A selection of timed exposures were taken in order to measure the time dependence of the current, but zero-second exposures were forbidden by the software.

The mean count rate of a dark frame was measured using the ISTAT routine from the Starlink FIGARO package (Shortridge *et al* 1997). It was found to be linear and

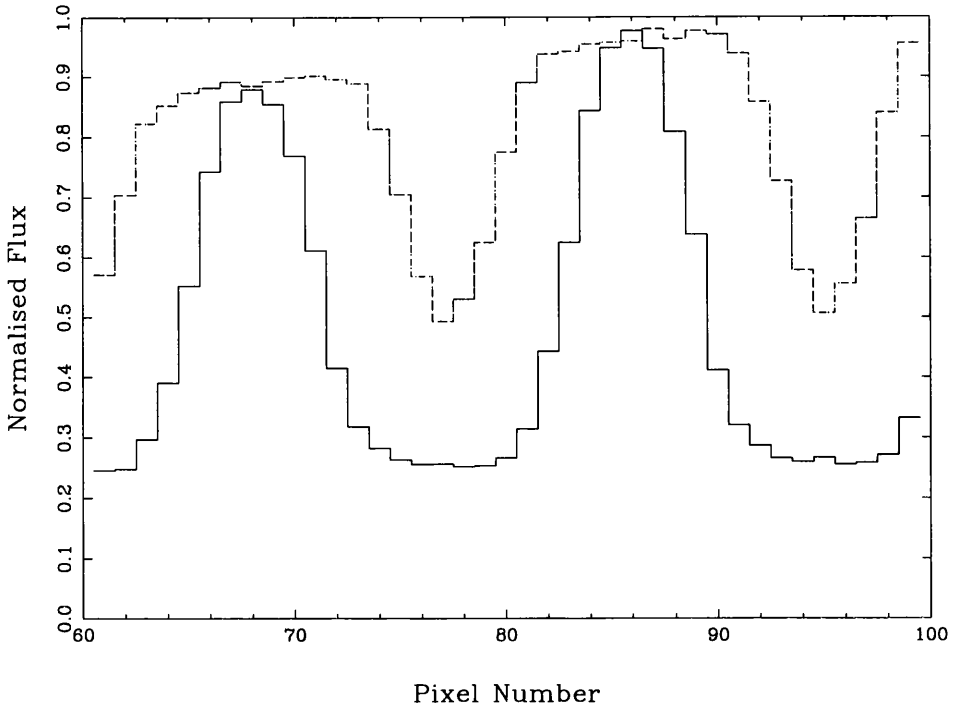

Figure 2.3: The different spatial profiles from long and short-slit data. The broken line is the long-slit spatial profile.

negligible compared to the data. A least squares fit gives

$$B = \frac{T}{2250} \tag{2.1}$$

where B is the increase in counts above the fixed mean background and T the exposure time for the frame in seconds. A plot of $B + 1.5$, where 1.5 is the mean residual count due to readout noise (which was not subtracted by the data taking software) is shown in Figure 2.4. The dark current is shown to increase at a rate of 2 counts pixel^{-1}hour^{-1}.

In addition to the dark current, the author was notified about the presence of fixed pattern interference (Pogge *et al* 1988). This is assumed to be time independent and is superposed upon the background. The fixed pattern interference can be thought of as a ripple in the counts of fixed amplitude and is a basic property of the chip when it undergoes a slow readout, as was performed at Lick. As the fixed pattern interference has an amplitude of 2 counts (Misch 1991) and so was also negligible compared to the data which often had counts of 20 000 photon events or more (1 electron corresponds to 2.5 photons, Misch 1991) no correction was made.

Table 2.3: The observing log for the programme stars taken at Lick Observatory with the Hamilton Echelle Spectrograph in May 1993

Star	Date	UT Time	Exposure time/s	Position w.r.t. blaze
θ Leo	18th May 1993	04:34	3600	left
τ Her	18th May 1993	09:52	1200	left
ϕ Her	18th May 1993	10:17	2700	left
HR6997	18th May 1993	11:15	4200	left
Day Sky	18th May 1993	21:50	3	left
Day Sky	18th May 1993	21:51	3	right
Day Sky	19th May 1993	02:38	70	right
θ Leo	19th May 1993	04:57	900	right
υ Her	22nd May 1993	06:19	3600	right
ϕ Her	22nd May 1993	07:02	1800	right
τ Her	22nd May 1993	07:43	1200	right
ζ Dra	22nd May 1993	08:08	900	right
HR6997	22nd May 1993	10:25	4200	right
21 Aql	22nd May 1993	11:39	1800	right
υ Her	23rd May 1993	04:04	3600	left
ζ Dra	23rd May 1993	05:28	900	left
21 Aql	23rd May 1993	08:19	4500	left
21 Aql	23rd May 1993	09:51	2700	right

Table 2.4: The observing log for the programme stars taken at Lick Observatory with the Hamilton Echelle Spectrograph in September 1993

Star	Date	UT Time	Exposure time/s	Position w.r.t. blaze
α Lyr	14th Sep 1993	04:58	30	left
HR7098	15th Sep 1993	04:01	7200	left
21 Peg	15th Sep 1993	08:25	5000	left
87 Psc	15th Sep 1993	10:02	4500	left
HR7361	16th Sep 1993	05:40	5000	left
HR7664	16th Sep 1993	07:45	4500	left
Day Sky	19th Sep 1993	23:09	3	left
Day Sky	19th Sep 1993	23:10	3	left
Day Sky	19th Sep 1993	23:11	3	left
HR7361	19th Sep 1993	07:00	3600	right
HR7361	19th Sep 1993	08:02	3225	right
87 Psc	19th Sep 1993	09:20	5000	right
Day Sky	19th Sep 1993	20:15	3	right
Day Sky	19th Sep 1993	20:20	3	right
Day Sky	19th Sep 1993	20:21	3	right
α Lyr	20th Sep 1993	03:55	30	right
HR7098	20th Sep 1993	04:03	3600	right
HR7098	20th Sep 1993	05:04	3600	right
HR7664	20th Sep 1993	06:10	4300	right
HR7664	20th Sep 1993	07:20	900	right
21 Peg	20th Sep 1993	07:40	5000	right

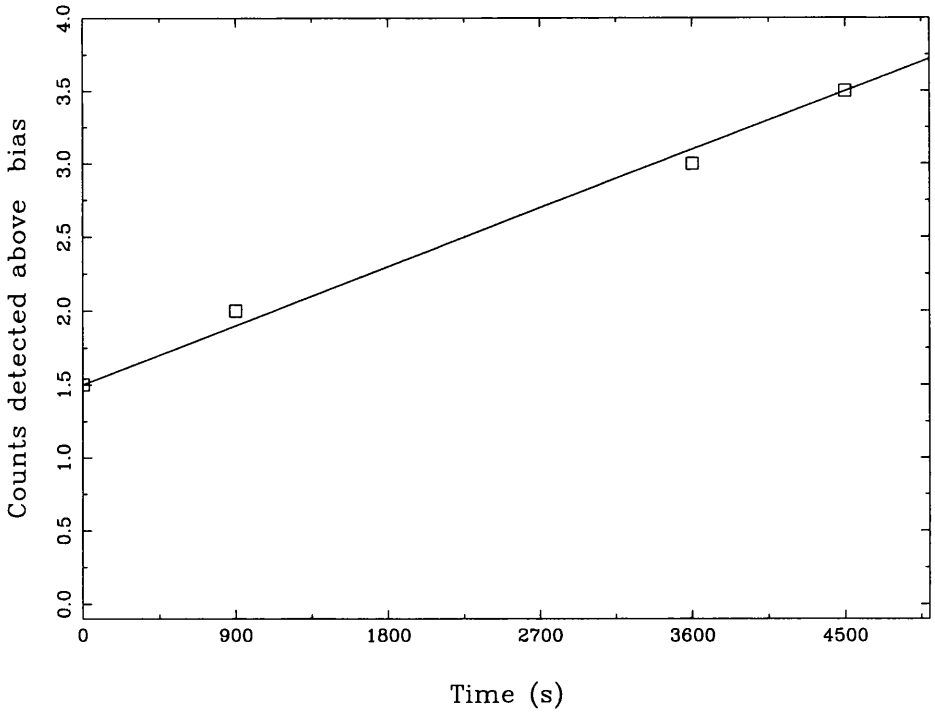

Figure 2.4: Increase in dark counts with exposure time. The best—fit straight line is superposed

2.3 Preliminary reduction procedures

The data frames contain single pixels and groups of pixels where the response is non-linear. Cosmic rays can also hit the CCD and result in a trail or an anomalously large single peak. In order to introduce redundancy, exposures longer than an hour were split into segments. The cosmic ray intensities were never much higher than $\sim$ 30 per cent above the continuum level. These features were not removed prior to reduction because the FIGARO routine available (BCLEAN) did not do a sufficiently good job—a lot of cosmic rays were missed and spectral information over several pixels sometimes destroyed. Chip defects such as bad columns and bad rows always occur at the same CCD chip position, and these were removed from all frames after initial extraction by using a binary mask. Cosmic rays were removed after final spectrum extraction by 'snipping' in DIPSO (Howarth and Murray 1991).

2.4 Extraction

All of the reduction stages which follow, except wavelength calibration, make use of the reduction package VISTA (Stover 1988). VISTA is designed specifically for Lick spectra. It can perform a complete échelle reduction and is flexible enough to allow the user to enter or leave the reduction procedures at any point.

The first stage of the reduction procedure is estimation of the position of each order centroid by eye from a 1-D plot of the first CCD column. This estimate is refined by the program and then used to fit a polynomial in the dispersion or x-direction along each order. Figure 2.5 shows an example of such a trace; note the trace does not pass through the intensity maximum of the cross-dispersed profile; this is because the 2-D point-spread-function of the Hamilton Schmidt Camera was found to exhibit a slight asymmetry, possibly due to instrumental effects and also guiding variations during the observations. A cross section of the order cross-dispersion profile and its centroid can be seen in Figure 2.5. (Although this is not documented in the literature about the spectrograph and camera; Vogt 1987, Vogt *priv comm*, suggested that a flaw in the design of the corrector and field flattener of the Schmidt camera may be responsible for the asymmetry).

VISTA follows the completed trace and records the flux in the pixels surrounding the centroid. The cross-dispersion profile is usually fifteen pixels wide from profile core to profile wings and so VISTA was set to record the flux from the seven pixels on each side of the trace. The program uses Laguerre interpolation when it encounters fractional pixels (Holzmann 1991). The pixels read by the program are simply summed and this sum stored as a 1-D spectrum containing information on x-pixel position and total recorded flux.

The level of the inter-order background is easily measured by examining the background signal between the orders. The inter-order background was assumed to be where the profile 'tail' flattens out for several pixels before rising into the next order. The orders did not overlap. VISTA was used to subtract this background, using the assumption that the background level superposed on the spectrum is not different from the mean measured between the orders.

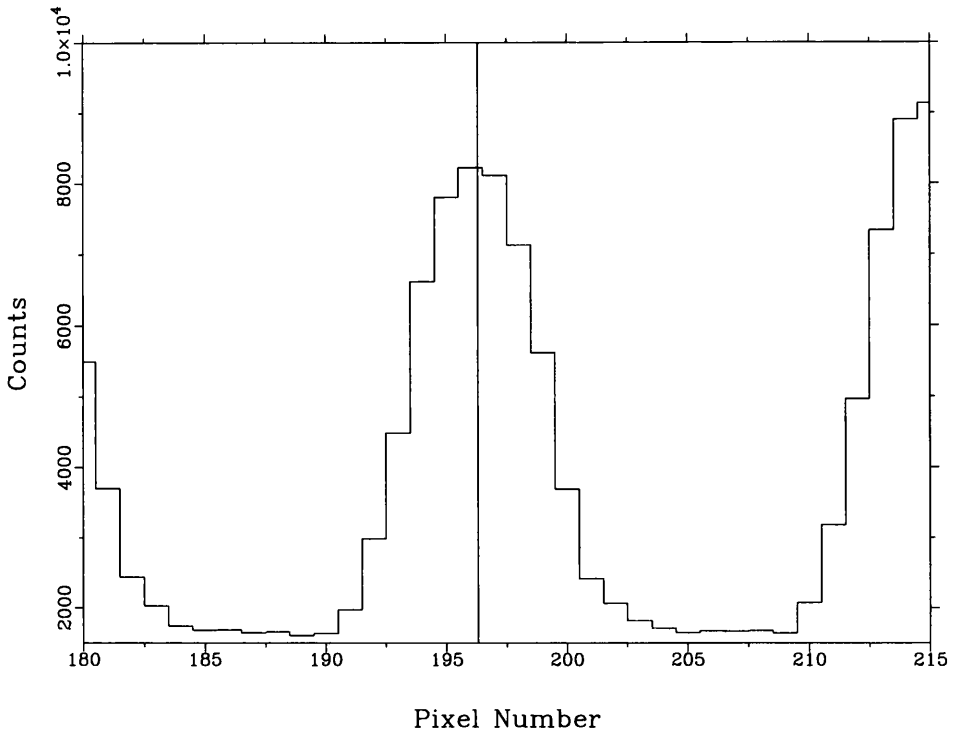

Figure 2.5: The order trace passing through the cross-dispersed short-slit narrow-dekker flat-field profile. The centroid lies close to the central pixel.

2.5 The Hamilton instrumental profile

An investigation was then made to see how the *dispersed* instrumental profile, $\phi(\lambda)$ changed along the échellogram and from order to order, and how this could be taken into account during spectrum synthesis. This profile was also found to be slightly asymmetric. Along each order a simple sum was made of normalised arc line profiles with clean, unblended cores. From measurements of each individual line, the FWHM was found to vary by no more than $\frac{1}{8}$ of a pixel along any one order, but across the entire free-spectral-range (FSR) a 'quadratic' relationship between FWHM and blaze wavelength was apparent; this is shown in Figures 2.6 and 2.7. This is not what should be expected; the relationship between $\Delta\lambda$ and λ should be a linear one if the resolving power of the detector is constant (quoted as 48 000 in Misch 1991). This is obviously not the case here. The error bars represent intra-order changes in FWHM and the minimum of the plots falls at a consistent wavelength for both formats. There was no significant change in the variation of $\phi(\lambda)$ between chip positions. No fit was made to the instrumental profile and no attempt was made to

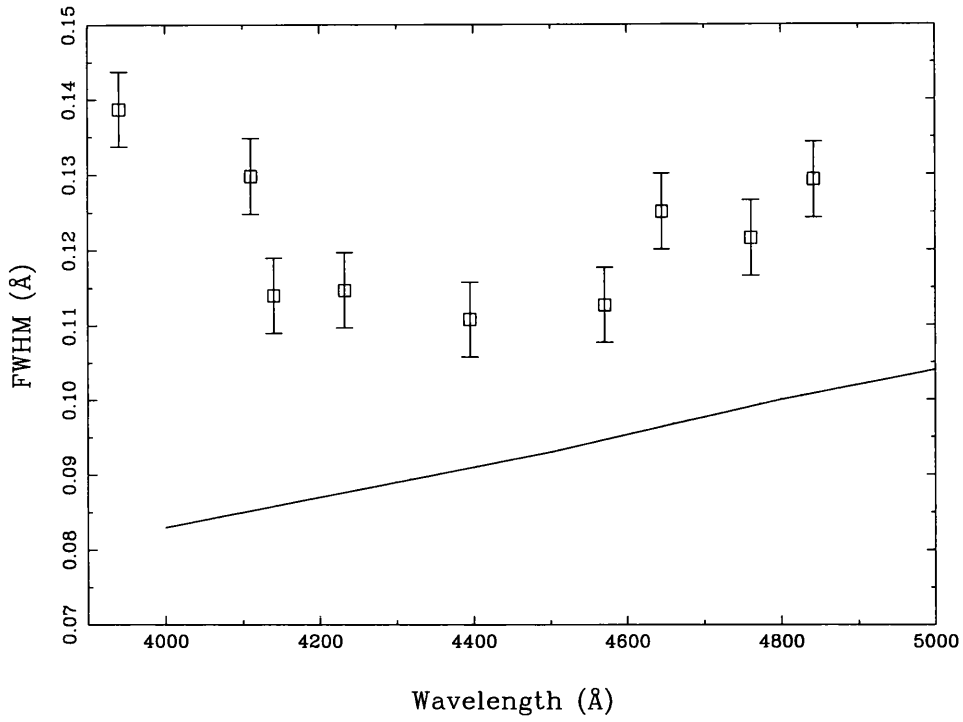

Figure 2.6: Variation in instrumental profile FWHM as a function of wavelength for the right hand format. The superposed line shows the expected variation in FWHM for a constant resolving power of R = 48 000.

model it. Instead it was measured directly from the arc lines in each order. This is because, although the FWHM variation could be fitted, it was not possible to model the profile tail and centroid so easily.

The instrumental profile may be a possible cause of background contamination. If the profile has broad, shallow wings which are hard to measure directly, these wings will convolve with the continuum, giving rise to a depressed continuum, a shallower line profile and a systematic error in the measured equivalent width (Griffin 1969). The presence of this contamination, referred to by Griffin as parasitic light, can only be verified by comparison with the spectrum of a well-known standard, e.g., the Kitt Peak Solar Flux Atlas (Kurucz *et al* 1984) which is assumed to be uncontaminated by a similar wide-winged profile.

The Solar Atlas was convolved with an oversampled dispersed instrumental profile to serve as an uncontaminated model and then rebinned to the same number of Å per pixel as the data. Data and model were normalised by dividing the two

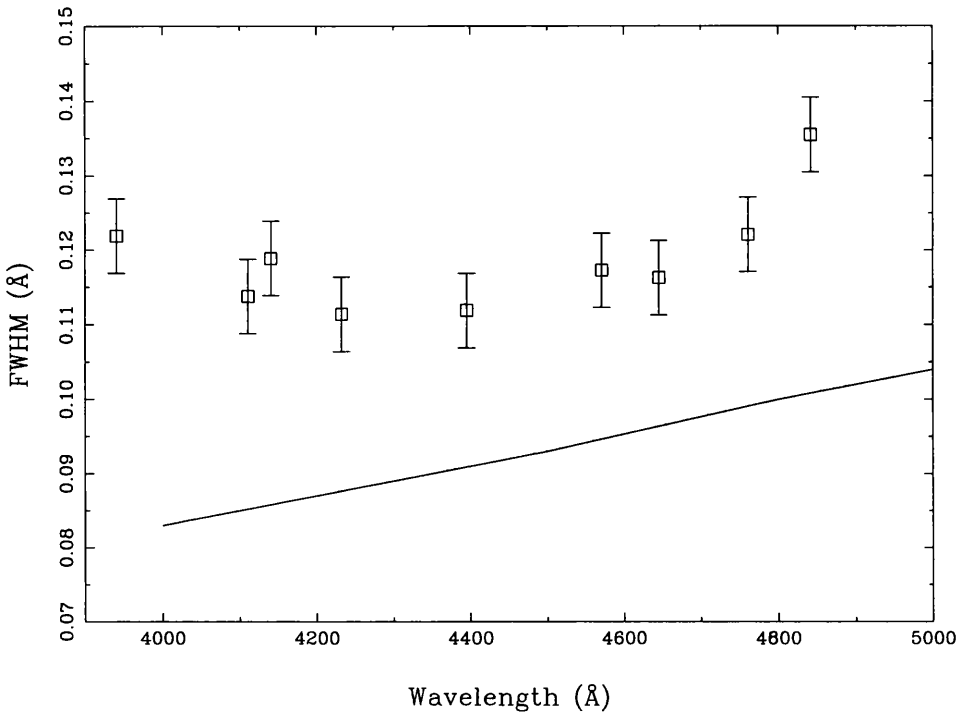

Figure 2.7: Variation in instrumental profile FWHM as a function of wavelength for the left hand format. The superposed line shows the expected variation in FWHM for a constant resolving power of R = 48 000.

spectra and then fitting a spline curve to the ratio using the spaces between strong spectral lines. Finally this ratio was divided into the observed spectrum to produce matching continua between the observed spectrum and the model.

A comparison between data and model before and after convolution is shown in Figures 2.8 and 2.9.

The equivalent widths of spectral lines from both model and data were measured for 13 orders across the whole wavelength range. The expression

$$P_{i_\lambda} = \frac{M_{i_\lambda}}{D_{i_\lambda}} - 1 \tag{2.2}$$

was used to calculate the fractional parasitic light for each line P_{i_λ} where M_{i_λ} is the equivalent width of a line from the convolved atlas, λ is order blaze wavelength from Misch (1991) and i is the *ith* line for order λ. D_{i_λ} is the equivalent width of the observed spectral line. A weighted mean, P_λ, of P_{i_λ} was calculated for each order, the weighting factor w_{i_λ} being the mean of M_{i_λ} and D_{i_λ}.

The values obtained for P_λ and ΔP_λ, along with order number N are shown in Table 2.5. A plot of P_λ vs order blaze wavelength λ is shown in Fig 2.10. There is no obvious trend in P_λ with wavelength (see Figure 2.10). The weighted mean P of P_λ was calculated using the inverse square of its error ΔP_λ as the weight w'_λ.

P was found to be consistent with zero;

$$P = -(9.91 \pm 8.39) \times 10^{-3} \tag{2.3}$$

as this is within the bounds of the experimental error a value of zero was adopted for P.

2.6 Calibrations

The data were flat-fielded in VISTA by dividing the extracted, masked flat-fields into the extracted stellar spectra. A test was performed to see if the s/n of the spectra was significantly improved by using long-slit flat fields. This was the *F-test* (Press *et al* 1986) in which one finds the ratio between the variances of two different

Table 2.5: The amount of scattered light as a percentage of the continuum in a selection of echelle orders

Order N	Parasitic Light, ($P_\lambda \pm \Delta P_\lambda$)
113	-0.0±0.9
114	+2.9±1.0
122	-0.8±0.7
123	+4.3±1.3
124	+1.5±1.6
128	-1.4±0.6
129	+0.6±0.7
134	+5.0±1.4
135	-2.4±0.6
136	+1.5±0.6
139	-5.1±0.3
140	-2.0±0.7
141	-1.7±0.6

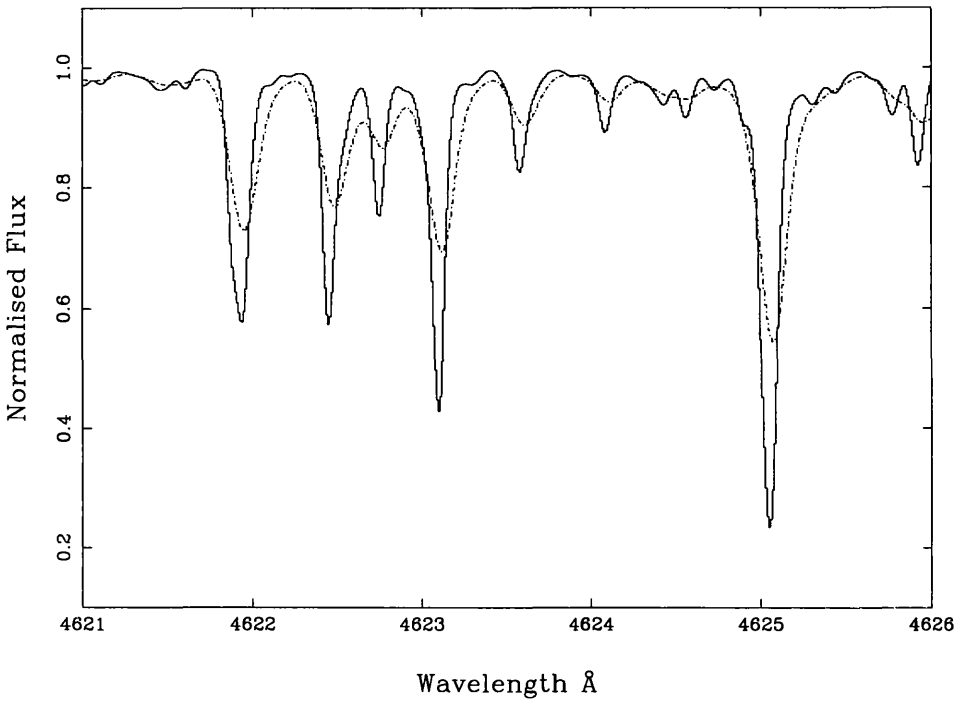

Figure 2.8: Comparison of the convolved solar atlas and the original, unconvolved atlas. Note the pronounced asymmetry. The observational data are the broken line.

distributions (the parameter F), and then calculates the probability that a variance the same as or larger than the largest variance would be produced by chance (the *significance*).

The result from a line-free strip of continuum which was flat-fielded by wide and short-slit flat-fields gave a value for F of 1.35 and a significance of 0.006. This value of the significance implies that the spectra are significantly different, while the closeness of F to 1 implies this is by a relatively small amount. Figure 2.11 shows the effects produced using one spectrum of Vega and different types of flat-field spectrum.

Therefore it is best to use the long-slit but short-slit extraction will suffice if long-slit data are unavailable. This was the case for the stars θ Leo, υ Her, ζ Dra, 21 Aql and τ Her. Adverse or changeable observing conditions can affect the photon count rate and therefore vary the quality of the extracted data more significantly than the adopted flat-field. As the intensities of the frames in the 'red' (4900 Å in this case) varied between 7 000-17 000 counts pixel^{-1} any difference between the different

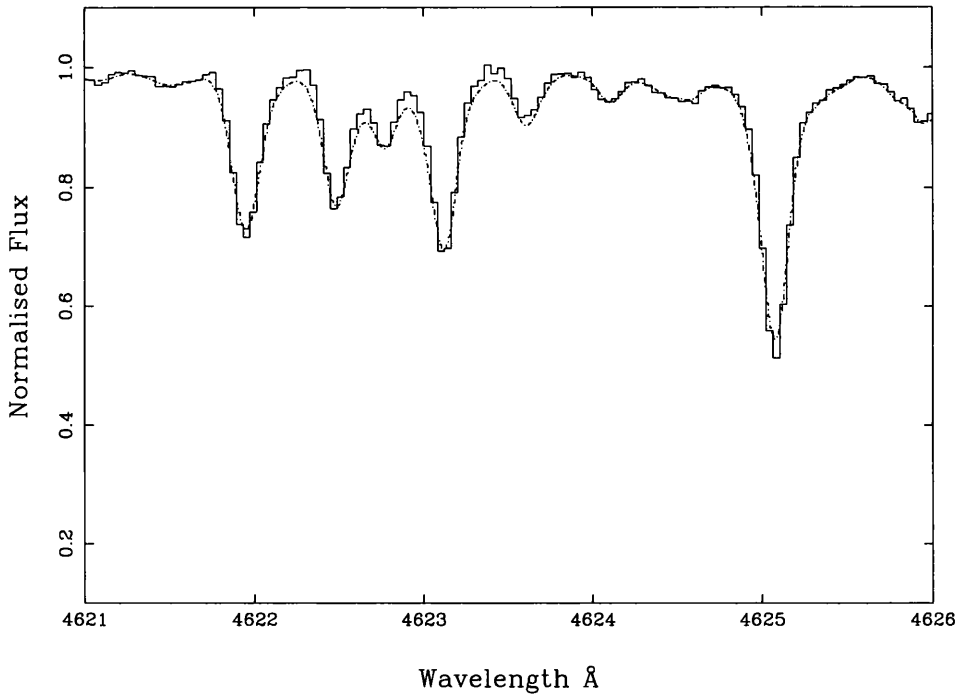

Figure 2.9: Comparison of the observed spectrum with the Kitt Peak Flux Atlas spectrum convolved with the Hamilton ϕ_λ. The observational data are the broken line.

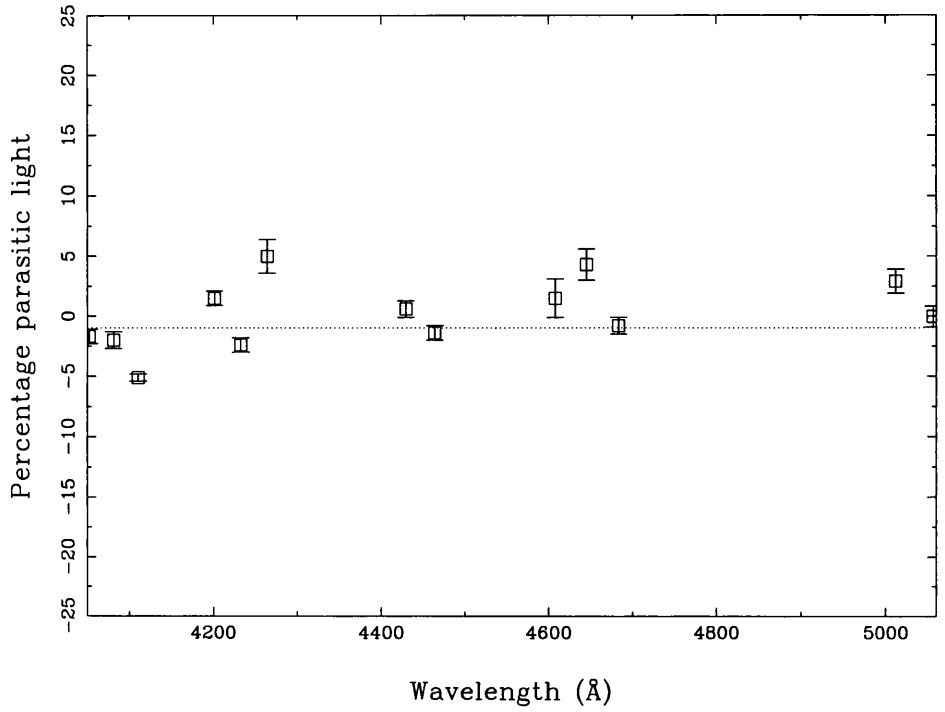

Figure 2.10: The percentage parasitic light found in the solar spectrum taken at Lick. The weighted mean is superposed

types of flat-field was negligible compared to variation in observing conditions.

Wavelength calibration was performed using ECHARC (Shortridge *et al* 1997) where the centres-of-gravity of the lines were used to give an accurate fit to the ESO échelle thorium-argon arc atlas (D'Odorico et al 1986). No evidence for large-scale systematic shifts was found but the possibility should not be excluded that use of a simple quadratic law when fitting the dispersion curve may introduce a slight distortion due to higher-order terms in the wavelength scale. The final root-mean-square deviation from a quadratic fit was 0.007Å per order.

The spectra from LHS and RHS échellograms were combined to obtain a continuous spectrum. The wavelength shifts with respect to the laboratory frame were measured for a number of metal lines covering the range required which are visible in all of the stars. The lines are shown in Table 2.6. A correction radial velocity, v_{corr_i}, was obtained for each of the lines, i, and a weighted mean, v_{corr} calculated.

Line equivalent widths were adopted as weights w_{corr_i} because a weak line has a less accurately determined wavelength. The error σ_{n-1} on the arithmetic mean

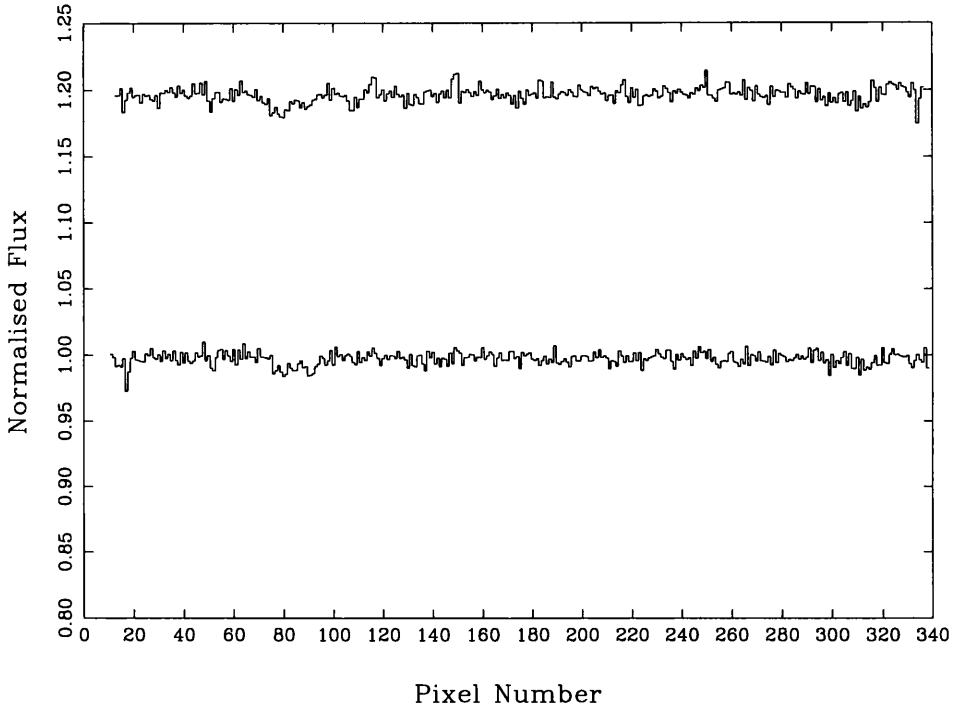

Figure 2.11: The effect of using different flat fields on the same region of spectrum, in this case a part of the spectrum of Vega. The top spectrum was flat fielded with the short-slit flat field; the lower spectrum was flat fielded using the long-slit flat field.

Table 2.6: The lines used in correction for radial velocity

Wavelength	Species
3933.66	Ca II
4128.05	Si II
4130.88	Si II
4351.76	Fe II
4390.58	Mg II
4416.82	Fe II
4481.23	Mg II
4491.40	Fe II
4522.63	Fe II
4558.66	Cr II

v_{corr}, for each star was found to be of the order of 0.5 kms^{-1}. v_{corr} does not represent a *heliocentric* radial velocity as it also includes both possible orbital stellar motion (in the case of spectroscopic binaries) and geocentric motion. Wavelength co-registration was performed by removing this velocity component from each stellar spectrum using VCORR in DIPSO. The spectra were then weighted and merged using the formula

$$Z_\lambda = \frac{wX_\lambda + vY_\lambda}{w + v} \tag{2.4}$$

where w and v are the mean photon counts per pixel for the entire LH and RH data frames respectively, and X_λ and Y_λ are the LH and RH side un-normalised data respectively. Z_λ is the weighted spectrum.

The spectra were then normalised by fitting a hand-drawn spline fit through the continuum using DIPSO. The author was aware that the presence of weak metal lines can lower the apparent level of the continuum but the high resolution nature of the data, the lower density of lines than in late A-stars and the low $v \sin i$ values of some of the programme stars makes this a less important consideration than it was in the work of Smith and Dworetsky (1993) and Smalley and Dworetsky (1993).

Chapter 3

Spectrum analysis and synthesis

3.1 Spectrum analysis

The first stage of analysis was to measure the positions and equivalent widths of spectral lines for the HgMn star υ Her using the software package DIPSO. This star is ideal for the purpose because being at the cool end of the HgMn range it exhibits strong lines of neutral and singly-ionised iron-group elements (e.g. chromium, manganese, titanium and iron) which may not be visible in hotter stars. It also has a low $v \sin i$ (11kms^{-1} Smith 1992) which means spectral lines should be easy to separate. Lines were identified with the aid of Moore (1959) (hereafter referred to as the RMT), Dworetsky (1971), Adelman (1989, 1991) and sometimes Kurucz and Peytremann (1975), Kurucz (1990).

Equivalent widths were then measured for selected lines of all the sample stars using DIPSO; these can be found in Tables 3.1 and 3.2. Effective temperatures and surface gravities were adopted from the work of Smith and Dworetsky (1993) and microturbulence parameters then determined using the method of Magain (1984). Abundances were derived using the spectrum synthesis package UCLSYN (Smith and Dworetsky 1988).

3.1.1 Identification of spectral lines from the spectrum of υ Her

The line wavelengths were measured for the spectrum of υ Her using the XV command in DIPSO. Some ambiguity existed as to the 'true' position of the line centre because of the profile asymmetry, discussed in Section 2.5. For all line wavelength measurements the deepest part of the profile (core) was assumed to represent the central wavelength, which ensured consistency in wavelength measurements. Systematic error in the velocity-corrected wavelength position due to the asymmetric instrumental profile should be common to all wavelength measurements and its presence can be corrected by a linear coordinate transform. No systematic shift was found on comparison of the observed wavelengths to the laboratory wavelengths. The *rms* random error between the measurements and laboratory values was found to be 0.037Å for the whole spectrum and the mean deviation to be consistent with zero.

Wavelength identification proceeded by first identifying the strong well-known lines in the spectrum; the H and K lines of calcium, the hydrogen Balmer lines, Mg II λ4481 and Mn II λ4206. Next the strong iron, chromium and titanium lines were rapidly found from reference to work by Adelman (1989, 1991,1994).

Identifications were then checked against predicted line strength and fellow multiplet members with the aid of the RMT. Where no identification was obvious the work of Iglesias and Velasco (1964) sometimes yielded a manganese line not listed in Moore. Some lines could not be identified in the aforementioned sources; these were checked against the tables of Kurucz and Peytremann (1975). The presence of line blends was indicated by asymmetric profiles, wide profiles or indications from spectrum synthesis techniques that the line was far too strong to be a single line.

Blending species were initially identified with the aid of Kurucz and Peytremann (1975) and spectrum synthesis, then more reliable wavelengths were taken from Adelman (1989,1991,1994) and the RMT. The complete line-list for υ Her, including blends and measured equivalent widths, is presented in Appendix A.

3.1.2 Measuring the equivalent widths of spectral lines

Equivalent widths in υ Her

Equivalent widths of spectral lines in υ Her were measured for as many individual lines as possible using the 'EW' command in DIPSO. This command performs a trapezoidal integration of the area of the spectral line between two user-specified points at a user defined continuum height. In order to obtain estimates for the uncertainty on the equivalent widths two sets of measurements were made with the continuum placed at the upper and lower limits of the rectified continuum points. This takes into account any uncertainty in the continuum placement, under the assumption such uncertainty dominates in the line equivalent widths. Errors due to differences in the two data frames used to compose the spectra were found to be negligible compared to the continuum placement errors. No dependence was found between the magnitude of the equivalent width itself and the uncertainty in the continuum placement ΔW_λ, which makes it difficult to estimate the uncertainty from a single W_λ measurement. This is probably because the spectra contain discontinuous regions of low signal-to-noise where there is no redundancy of data. The signal to noise was found to vary between approximately 200:1 and 100:1; this was based on the standard deviation of the data on either side of a user-normalised continuum. This variation is illustrated in Figure 3.1 and is probably due to variations in weather and exposure times; the signal to noise is also known to depend on the properties of the spectrograph blaze (Misch 1991).

Selecting lines for measurement of equivalent widths

Adelman (1989,1991,1994) takes the approach of measuring equivalent widths for all visible lines which have published atomic data, however crude (e.g., Kurucz and Peytremann 1975) because this will reduce the standard error on the final mean abundance. To obtain the large number of lines necessary to reduce the standard error a sample would not only need to include very weak lines, but also saturated lines and blended lines.

Here, the approach is very different, in that a small sample of relatively strong, unsaturated lines is selected. Candidate lines were selected from lines believed to

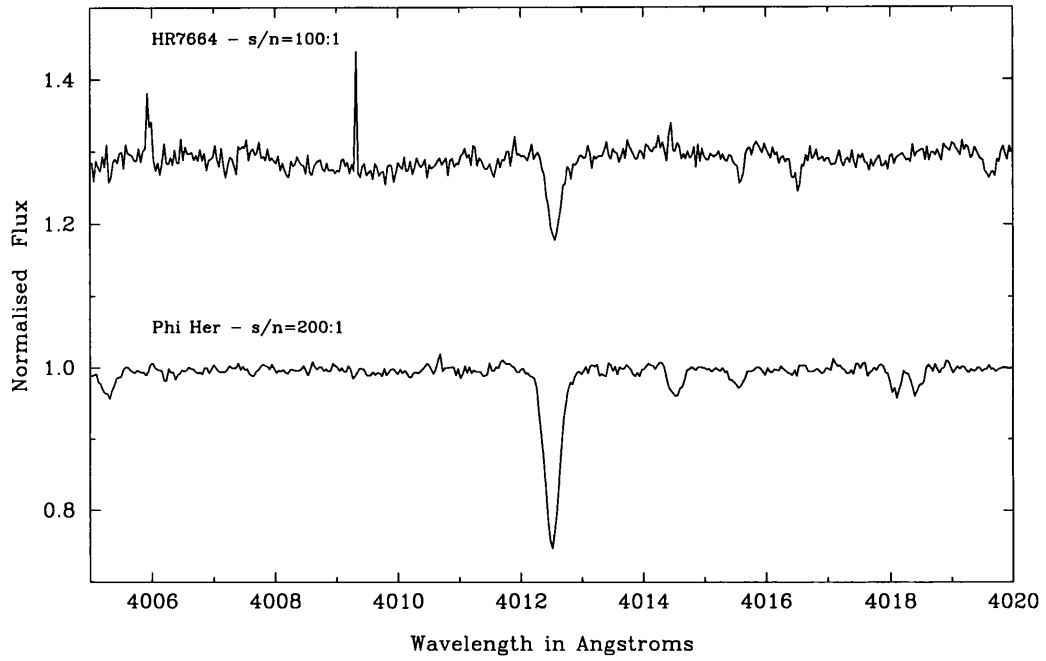

Figure 3.1: The range in signal to noise in the stellar sample. Signal to noise varied between approximately 100:1 and 200:1. The stars used in this illustation are HR7664 (top) and ϕ Her (bottom). The spectra have been re-normalised to allow direct comparison.

be unblended in υ Her. Lines in this list were examined in other program stras and those that appeared to be blended were culled from the list. For some elements, *i.e.* zirconium, lines which were present in other stars and not present in υ Her, were examined in the same way. Lines which were too weak in *upsilon* Her were not used in other stars because a consistent line sample was required.

Higher accuracy $\log gf$ values exist for the stronger lines, strong lines are easy to measure more accurately, and the noise in the spectrum becomes less important, decreasing the fractional error in the measured equivalent widths and hence the final abundances. There are several reasons why it is believed that a study of carefully selected lines is a more valid approach to obtain accurate abundances:

(a) Using very weak lines (of the order of the error on a measured equivalent width) can have a detrimental effect on the dispersion of the abundances derived from these lines and give rise to a broad population standard deviation for that element.

Weak lines may also be affected by weak blends not apparent in the spectrum. It is also important to bear in mind that for a very weak line the fractional uncertainty in the equivalent width $\Delta W_\lambda / W_\lambda$ could be of the order of unity or higher as continuum noise and weak blends will dominate.

(b) Lines which are blended with other elements will also affect the accuracy of the final abundances, by introducing systematic error.

(c) Saturated lines lie on the flat part of the curve of growth and so are very insensitive to variations in abundances. This means any systematic error in the measurement of equivalent widths of saturated lines can lead to large errors in the calculated abundances, as the equivalent width of such a line can only grow by $\log A$. The only known saturated lines in the spectra were the Ca II K and H lines, (which occasionally appeared on the damping portion of the curve of growth in cool stars) the Mg II doublet at λ4481, and the Si II lines at $\lambda\lambda$4128 and 4130, all of which have equivalent widths higher than 60mÅ. These lines were modelled using Stark damping constants taken from Sahal-Bréchot (1969) except for Ca II whose constants came from Roberts and Eckerle (1985). For magnesium, which has several unsaturated lines in the visible region, the saturated doublet was not chosen for inclusion in the

final mean abundance.

It can be concluded that it is best to choose the line sample with care, and the spectrum of υ Her was examined very carefully before the preliminary choices were made.

Many lines are still unidentified, and, had time been permitting, this could have been mitigated by measuring the wavelengths of the unknown lines in other programme stars, in order to investigate which lines are present in υ Her and not present in the other stars. Comparison of line strengths between the stars would then be useful in postulating possible element ID's and even finding new elements in the programme stars. Lines blended in υ Her may not be so in other stars; weak lines may be stronger in other stars. Further work could be done subsequent to this thesis.

It is also important to bear in mind that line blending can be a problem in HgMn stars with rotational velocities which give rise to broadening of spectral lines greater than the FWHM of the instrumental profile (which is $\sim$9kms^{-1}) and the selection of measured equivalent widths should reflect this situation.

Subsequent work in this thesis is therefore based on the initial measurements taken from υ Her. In hindsight, it would perhaps have been better to take detailed measurements from all of the stellar spectra, because an unusual abundance may be missed. However, the approach used in this project is satisfactory for examining the elements present in υ Her which were examined in all of the stars.

The line-list for υ Her was used as a template for selecting suitable lines for measurement in the sample spectra. The selected lines were measured for all of the stellar spectra. These measurements and their uncertainties are given in Table 3.2. In some cases high abundances of elements or even relatively low stellar $v \sin i$ values result in blends not listed in Appendix A.

The spectra of the other sample stars were also searched for the lines of zirconium which did not appear in υ Her. The equivalent widths for normal and HgMn stars and the uncertainty due to continuum placement are presented in Tables 3.1 and 3.2.

Table 3.1: Equivalent widths for normal stars

Line		θ Leo	α Lyr	HR7098	21 Aql	ζ Dra	τ Her	21 Peg
Ti II	3913.46	147±9:	Z	Z	11±8	–	–	54±4
Mn II	3917.23	B	–	–	–	–	–	–
Fe II	3935.94	20±4:	14±3	33±4:	25±8	11 ±6	–	33±6:
Al I	3944.01	97±5	41±3	50±5	5±4	6±4	–	29±1:
Fe II	3945.21	40±16:	7±2	19±3	6±1	11±6	–	12±2
Y II	3950.35	37±11	Z	B	–	–	–	–
V II	3951.97	46±5	12±4	20±3	–	–	–	8±2
Zr II	3958.22	–	–	–	–	–	–	–
Al I	3961.52	103±5	55±7	48±1	–	–	B	–
Cr II	3979.51	36±5	–	18±4	4±2	5±2	–	11±2:
Y II	3982.59	30±2	–	–	–	–	–	–
Zr II	3991.13	34±7	–	4±1	3±1	–	–	–
Zr II	3998.97	B	–	5±2	B	–	–	–
Cr II	4003.28	B	–	–	–	–	–	10±2
V II	4005.71	B	B	17±2	–	–	–	14±3
Ti II	4012.37	102±10	37±4	62±4	4±1	11±5:	–	41±11
Ni II	4015.50	48±2	10±3	24±2	10±2	B	4±2	18±2
Ti II	4025.14	B	B	B	–	–	–	6±1
Ti II	4028.33	70±3	B	B	B	–	–	28±2:
S II	4028.79	–	B	B	B	B	B	B
Mn I	4030.76	59±5:	26±7	–	–	–	–	B
Ga I	4032.99	–	S	–	–	–	–	–
Mn I	4034.48	25±5:	16±6	–	–	–	–	–
V II	4035.63	54±3	15±3:	29±4:	–	–	–	15±2
Mn I	4041.36	12±4	12±3	–	–	–	–	–
Fe II	4044.61	16±3	–	11±1	3±1	3±1	–	9 ±2
Fe I	4045.82	143±9	82±6:	71±4	7±4	–	B	43±6
Zr II	4048.67	B	–	B	–	B	–	–
Ti II	4053.81	73±6	19±3:	B	–	–	–	B
Mn I	4055.54	–	–	–	–	–	–	–

Line		θ Leo	α Lyr	HR7098	21 Aql	ζ Dra	τ Her	21 Peg
Fe I	4063.60	103±7	62±5	57±10	–	6±3	–	32±5
Ni II	4067.05	94±10	20±5	52±3	22±3	32±1	11±3	Z
Fe I	4071.74	94±6	55±5	50±2	–	–	–	Z
Sr II	4077.71	130±6	50±5	65±3	4±2	13±5	–	C
Fe II	4122.64	53±5	18±2	39±4	14±3	17±4:	5±3	26±2
Si II	4128.07	92±13	48±6	99±11	107±3	10 9±8	105±13	95±5
Ba II	4130.65	B	B	B	B	B	B	B
Si II	4130.89	129±11	73±8	112±6	123±13	124±4	107±8	103±12
Cr II	4145.76	B	B	B	B	B	B	B
S II	4153.10	–	–	16±1	18±3	20±6	29±6	6±1
Zr II	4156.24	B	–	–	–	–	–	–
Ti II	4161.52	B	8±3	8±2	–	–	–	B
S II	4162.70	–	–	12±4	24±2	18±2	33±4	–
Ti II	4163.55	94±3:	C	55±2	–	–	–	36±1
Mg I	4167.26	S	S	S	–	–	–	S
Ga I	4172.04	–	–	–	–	–	–	–
Mn II	4206.37	11±3	5±1	6±2	–	–	–	–
Zr II	4208.985	B	–	–	–	–	–	–
Zr II	4211.88	21±4	–	–	–	–	–	–
Sr II	4215.52	112±4	50±5:	55±3	7±2	–	–	26±7
Ca I	4226.73	87±4	S	32±1	–	–	–	9±1
Cr II	4242.38	75±4	–	46±4	B	B	4±2	37±5
Sc II	4246.89	S	69±9	42±3	6±3	–	–	16±2
Ni II	4244.82	8±4:	–	–	B	–	–	4±2
Cr I	4254.35	50±2	20±3:	29±2	–	–	–	16±3:
Fe II	4273.22	56±2	17±3	39±5	11±6	11±3	16±4	28±2
Cr I	4274.80	38±3	17±3	14±4	–	–	–	4±2
Fe II	4278.13	38±3	7±3	18±3	–	10±2	–	11±2
Ti II	4287.89	48±3	19±3	18±3	–	–	–	8±1
Cr I	4289.72	B	B	9±2	–	–	–	4±1
Ti II	4290.22	B	61±5	64±3	5±1	4±2	–	38±2

Line		θ Leo	α Lyr	HR7098	21 Aql	ζ Dra	τ Her	21 Peg
Fe II	4296.57	83±4:	30±3	51±3	22±2	24± 2	10±6	37±2
Ti II	4300.05	126±4	89±4	91±5:	10±2	12 ±3:	5±2	52±2
Ti II	4301.93	Z	Z	Z	–	5±4	–	24±4
Fe II	4303.16	100±8	47±6	66±3	Z	38±4	16 ±5	56±4
Y II	4309.62	B	–	B	–	–	–	–
Ti II	4312.86	93±5	49±5	51±3	6±4	6± 5	–	29±3
Zr II	4317.32	21±4:	–	–	–	–	–	–
Mn II	4326.68	11±2:	–	–	–	–	–	–
Mg I	4351.90	S	B	S	B	B	B	S
Ni II	4362.10	27±2	–	17±2	7±5	B	–	11±1
Mn II	4363.26	B	–	–	–	–	–	–
Mn II	4365.22	–	–	–	–	–	–	–
Fe II	4369.40	43±6	Z	20±1	10±2	5±2	–	26±7
Y II	4374.94	B	B	B	–	–	–	6±3
Zr II	4379.78	B	–	–	–	–	–	–
Fe II	4385.38	94±3	40±2	64±4	35±2:	B	B	51±2
Mg II	4390.58	50±6	24±2	59±7	50±4	52± 2	43±4	56±3
Ti II	4394.06	41±3	11±2	19±2	–	–	–	7±2
Ti II	4395.85	B	6±1	15±3	–	–	–	7±2
Ti II	4395.03	133±8:	77±2	79±3	6±1	7±3	B	55±3
Y II	4398.02	–	–	–	–	–	–	–
Ti II	4399.78	87±4:	B2	44±2	–	–	B	22±1
Ni I	4401.55	–	B2	7±3	–	B	–	4±2
Fe I	4404.75	102±13	56±3	52±5	–	7±3	–	29±2
Fe II	4416.82	93±3	12±3	64±10	35±2	39±3	31±5	51±2
Ti II	4417.72	B	40±3	68±2	–	–	–	23±1
Ti II	4418.34	B	11±1	42±2	–	–	–	5±1
Mg II	4427.99	S	S	S	S	S	S	S
Mg II	4433.99	S	S	S	S	S	S	S
Fe II	4461.77	52±4:	B	B	10±2	10±2	6±2	3±1
Ti II	4464.53	46±2	22±2	22±3	7±1:	B	B	9±1

Line		θ Leo	α Lyr	HR7098	21 Aql	ζ Dra	τ Her	21 Peg
Ti II	4468.54	B	87±3	76±4	–	6±4	–	50±5
P II	4475.26	–	–	–	–	–	–	–
Mn II	4478.64	8±2	–	6±2	–	–	–	–
P II	4483.68	–	–	–	–	–	–	–
Fe II	4491.40	82±2	28±2	56±4	27±3	29±8	12±4	47±6
P II	4499.24	–	–	–	–	–	–	–
Ti II	4501.24	117±1:	64±4	69±4	6±4	5±3	–	43±2
Fe II	4508.28	111±4	59±4	78±5	46±6	42±6	24±10	32±4
Fe II	4515.34	102±4	49±5	70±7	41±7	45±5	27±5	57±6
Fe II	4520.22	92±6	49±5	50±1	33±1	36± 5	–	49±2
Fe II	4522.63	123±6	69±2	77±5	51±4	50±6	28±5	64±2
Fe I	4528.62	B	14±2	17±1	–	–	–	7±4
Fe II	4533.99	170±3:	81±4:	108±4:	22±4:	31±5:	11±4:	B
Ba II	4554.03	90±4	–	30±3	–	–	–	15±2
Fe II	4555.89	112±4	B	Z	36±1	45±5	3 0±10	55±3
Cr II	4558.66	117±6	63±2	75±4	26±2	31 ±3	12±5	65±2
Ti II	4563.76	108±6	64±3	63±4	5±2	4±2	-	39±2
Ti II	4571.97	130±4	80±3	80±2	9±2	10±3	–	56±6
Fe II	4576.33	68±2	30±3	49±2	21±3	15± 5	11±3	35±4
Fe II	4582.835	55±6	17±3	40±3	B	B	–	28±4
Cr II	4588.217	110±8	49±3	65±4	22±2	B	–	55±3
P II	4602.08	–	–	–	–	–	–	–
Fe II	4620.51	45±4	Z	Z	12±4	B	B	26±3
Fe II	4625.91	11±2	–	8±4	6±4	–	–	5±3
P II	4626.70	–	–	–	–	–	–	–
Fe II	4629.336	112±4	B	C	B	39±4	18±6	5±4:
Al II	4663.05	S	S	S	31±3	35±5	–	24±5
Mg I	4702.94	S	S	S	–	–	–	S

B : Line blended and blending species dominates

Z : Spectrum missing or contaminated

C : Cosmic ray contamination

S : Synthesized abundance

– : Line not visible

':' symbol next to a line represents a weakly blended line.

Table 3.2: Equivalent widths for HgMn stars

Line		ϕ Her	υ Her	87 Psc	hr7664	hr7361	hr6997
Ti II	3913.46	72±5:	70±4	74±5	Z	Z	34±7
Mn II	3917.32	21±5	28±6	27±6	Z	73±4:	50±5
Fe II	3935.94	31±3:	20±4	B	43±2	26±4	28±9
Al I	3944.01	B	53±4:	61±4	–	12±2	B
Fe II	3945.21	8±3	11±4	Z	16±2	7±2	B
Y II	3950.35	C	26±3:	21±5	–	20±10	Z
V II	3951.97	2±1	–	Z	–	13±3	B
Zr II	3958.22	29±3	–	Z	–	–	–
Al I	3961.52	–	4±2	–	4±2	12±4	–
Cr II	3979.51	36±3	15±4:	–	–	13±2	Z
Y II	3982.59	Z	6±4	18±4	–	10±2	–
Zr II	3991.13	33±3	–	–	–	–	–
Zr II	3998.97	30±2	–	–	–	–	–
Cr II	4003.28	29±2	10±3	17±5	–	8±2	–
V II	4005.71	20±2	4±3	Z	–	9±3	B
Ti II	4012.37	76±9	47±5:	59±13	30±3	19±3	–
Ni II	4015.50	6±2	–	3±1	5±2	4±4:	B
Ti II	4025.14	34±2	13±1:	17±3	5±3	B	B
Ti II	4028.33	38±3	35±5:	B	14±1	–	B
S II	4028.79	3±1:	5±2:	B	4±1:	–	B
Mn I	4030.76	B	19±2:	21±1	Z	11±3	14±4
Ga I	4032.99	S	S	S	S	S	S
Mn I	4034.48	16±4	11±4:	17±5	C	10±4	7±4
V II	4035.63	B	6±2	5±2	2±1	8±2	5±3
Mn I	4041.36	20±4	18±4:	15±2	C	9±3	13±6
Fe II	4044.61	10±3	7±3	C	25±3	15±4	Z
Fe II	4045.84	B	18±5	B	30±3	33±3	19±7
Zr II	4048.67	B	–	–	–	–	–
Ti II	4053.81	B	38±3:	46±7	9±1	–	B
Mn I	4055.54	9±1	7±3	8±3:	–	7±3:	5±2:

Line		ϕ Her	υ Her	87 Psc	hr7664	hr7361	hr6997
Fe I	4063.60	30±2	13±3	9±2	–	14±2:	B
Ni II	4067.05	19±5	9±2:	11±3	14±2	26±5	18±2
Fe I	4071.74	19±2	10±3:	Z	15±2	7±4	B
Sr II	4077.71	B	45±6:	B	–	5±4	B
Fe II	4122.64	26±3	20±1:	5±2	45±3:	28±4	B
Si II	4128.07	115±8†	123±7†	106±4 †	104±4†	172 ±10†	180±7†
Ba II	4130.65	B	B	B	–	B	B
Si II	4130.89	107±8†	103±10†:	97±6 †	118±9†	157 ±7†	111±6†
Cr II	4145.76	41±2:	14±4:	17±5:	B	5±4:	B
S II	4153.10	8±1	10±4	9±1	6±1	10±3	16±5
Zr II	4156.24	21±3	–	–	–	–	–
Ti II	4161.52	B	8±3	10±4	–	–	B
S II	4162.70	9±1	9±2	12±2	6±1	6±3	20±5
Ti II	4163.64	44±5	51±4	66±3	32±2	16± 5	17±2
Mg II	4167.26	B	–	–	–	–	–
Ga I	4172.04	S	S	S	S	S	S
Mn II	4206.37	56±3	72±2	83±4	15±3	117±2	S
Zr II	4208.985	33±2	–	–	–	–	Z
Zr II	4211.88	18±4	–	–	–	–	4±1
Sr II	4215.52	S	S	4±1	–	23±2:	B
Ca I	4226.73	4±1	4±2	–	–	–	–
Cr II	4242.38	77±5:	70±5:	B	19±3:	22±4:	B
Ni II	4244.82	B	B	–	B	22±4	B
Sc II	4246.89	69±1	8±2	36±5	5±2	40±3	S
Cr I	4254.35	B	8±3	B	–	B	B
Cr I	4274.80	12±4	2±1	–	B	–	–
Fe II	4273.32	B	15±2	10±3	Z	21±2	B
Fe II	4278.13	12±1	9±2:	22±3:	21±2	15±4	B
Ti II	4287.89	33±4:	B	42±4	7±2	35±2:	B
Cr I	4289.72	B	10±3	B	S	17±4	B
Ti II	4290.22	B	54±4	68±10	31±2	10±5	B

Line		ϕ Her	υ Her	87 Psc	hr7664	hr7361	hr6997
Fe II	4296.57	45±5	27±2	12±3	51±2	35±4	–
Ti II	4300.052	Z	86±6:	B	Z	Z	C
Ti II	4301.93	44±3	39±2	47±3	20±2	4±2	–
Fe II	4303.16	56±3	55±4:	34±5	72±3	59±5	
Y II	4309.62	42±2	16±3:	15±5	–	7±2	–
Ti II	4312.86	43±3	48±3	54±3	B	12±3	17±3
Zr II	4317.32	5±1	–	–	–	–	–
Mn II	4326.68	60±2:	88±4:	81±4:	Z	87±3:	102±3:
Mg II	4351.90	B	B	–	–	–	–
Ni II	4362.10	5±2	3±2	2±1	2±1	4±2:	B
Mn II	4363.26	B	25±3	30±3	5±1	49±4	37±4
Mn II	4365.22	19±1	27±3	28±2	6±1	47±4	39±3
Fe II	4369.40	14±4	7±3	4±2	30±2	1 2±4	B
Y II	4374.94	B	50±6:	S	14±3	30±2	B
Fe II	4385.38	42±2	40±3:	B	64±2	51±3	B
Mg II	4390.58	37±3	29±4	29±3	8±4	32±3	17±4
Ti II	4394.06	18±4	18±2	25±3	B	–	B
Ti II	4395.03	65±3	67±4	74±4	49±2	20± 3	B2
Ti II	4395.85	11±1	14±3	25±4	20±2	17±4:	B2
Y II	4398.02	40±4	14±3	B	–	–	–
Ti II	4399.78	37±4	32±4	52±7	C	3±1	3±1
Ni I	4401.55	–	–	–	–	–	–
Fe I	4404.75	B	10±4	–	21±1	–	B
Fe II	4416.82	43±2	35±2	19±5	59±3	47±4	B
Ti II	4417.72	38±2	40±1	B2	20±3	16±2	B
Ti II	4418.34	12±3	11±3	B2	4±1	6±2	B
Mg II	4427.99	S	S	S	S	S	S
Mg II	4433.99	S	S	S	S	S	S
Fe II	4461.77	B	B	B	B	12±4	30±8
Ti II	4464.53	B	19±3	33±4	8±2	6±3	7±3
Ti II	4468.54	65±2	63±2	66±4	40±2	15± 4	B

Line		ϕ Her	υ Her	87 Psc	hr7664	hr7361	hr6997
P II	4475.26	–	5±2	–	15±2	50±2	40±6
Mn II	4478.64	31±2	44±2	39±3	11±2	57±4	55±4
P II	4483.68	–	–	–	6±2	17±4	19±6
Fe II	4491.40	41±2	33±2	11±2	56±2	42±3	–
P II	4499.24	–	–	–	24±1	51±2	35±4
Ti II	4501.24	59±4	59±3	68±4	43±3	13± 4	Z
Fe II	4508.28	58±5	46±4	24±3	70±3	54±4	43±6
Fe II	4515.34	B	45±3	22±4	B	48±4	43 ±5
Fe II	4520.22	44±2	38±4	17±3	Z	42 ±5	35±5
Fe II	4522.63	62±7	53±1	32±5	74±2	62±4	50±5
Fe I	4528.62	–	–	–	–	–	–
Fe II	4533.99	93±13†	B	83±5†:	75±4:	40±4	46±3:
Ba II	4554.03	30±4	11±5	10±3	–	–	–
Fe II	4555.89	50±2	45±5	22±5	67±3	58±5	B
Cr II	4558.66	100±5:	67±3	70±4	20±4	48±5	54±6
Ti II	4563.76	B	57±4	69±4	32±2	11±2	22±3
Ti II	4571.97	73±5	72±2	79±3	49±2	20 ±3	54±6
Fe II	4576.33	30±2	24±1	10±4	45±3	31±5	25±5
Fe II	4582.835	25±4	19±3	B	43±2	27±5	B
Cr II	4588.217	80±4	62±5	64±7	51±4	98±4:	71±7
Fe II	4620.51	23±3	16±2	7±2	–	–	Z
Fe II	4625.91	7±3	4±2	–	18±1	8±2	B
P II	4626.70	–	3±2	–	B	26±4	B
Fe II	4629.336	B	42±3	20±4	75±2	48±4	49±7
Al II	4663.05	S	S	S	S	S	S
Fe II	4576.33	33±5	25±4	11±3	46±3	32±4	23±4
Mg I	4702.94	B	B	–	–	–	–

B : Line blended and blending species dominates

Z : Spectrum missing or contaminated

S : Synthesized

C : Cosmic ray

– : Line not visible

† : Line saturated

':' symbol next to a line represents a weakly blended line.

3.2 Use of spectrum synthesis in abundance analysis

It was decided to use spectrum synthesis techniques to determine the chemical abundances of the program stars. This is because spectrum synthesis provides abundances for individual elements and is useful for determining the exact composition of these stars. Spectrum synthesis also allows a modelled replica of an observed spectrum to be produced, which acts as a visual check against the observational data. This technique also does not rely on previous in-depth analysis of control stars, instead it provides results which stand alone and can then be compared to previous work. The main disadvantage of spectrum synthesis is the reliance on atomic data, but this can be mitigated to some extent by careful selection of these data.

Spectrum synthesis was faciliated with the use of the spectrum synthesis program UCLSYN (Smith and Dworetsky 1988), pre-computed solar-metallicity LTE model atmospheres and the necessary atomic data, which were all used to construct synthetic normal and HgMn star spectra.

3.2.1 Spectrum synthesis

A model atmosphere contains data on stellar parameters such as optical depth, electron pressure and temperature and offers a prediction of how these properties vary radially inside the star. For this thesis a grid was interpolated of model atmospheres covering the late-A/early-B temperature range and based on solar-composition precomputed ATLAS-6 models (Kurucz 1979).

Assumptions

These models assume plane-parallel geometry, chemical homogeneity and time independence. It is also assumed that there is no incident flux from binary companions onto the stellar surface. The models include the line blanketing effect of 9×10^5 metal lines.

Another assumption is the use of solar abundances in the model atmospheres. Adelman (1991) records a helium underabundance in the HgMn stars he studied. Opacity due to neutral hydrogen (Gray 1992) is the most important opacity source in

stars of this temperature, with free-free opacity from ionised helium being much less important, only slightly more contributory to opacity than the metal ions magnesium, aluminium and silicon (which are modelled in UCLSYN). However, the helium deficiency was shown not to affect the abundances.

Auer *et al* (1966) showed analytically that stars with low helium abundances will behave like stars with a lower surface gravity. Smith (1992), further showed that in the temperature and gravity range seen in HgMn stars, only the effect on surface gravity of low helium abundance need be considered. Smith demonstrated that a helium deficiency would give rise to small systematic errors in the surface gravity of the order of 0.1 dex, which are too small to have any effect on the calculated abundances.

Enhancements in the metal ions in mercury manganese stars are selective and the opacity and electron density effects contributed by these elements are far less important than that due to helium, silicon, aluminium and magnesium. The data for elements unaffected by the HgMn phenomenon do not show any systematic difference between HgMn and normal stars, which again indicates a low helium abundance in HgMn stars does not appear to affect the results. The use of solar abundance model atmospheres does not lead to large errors in the derived abundances.

The atmospheres were calculated under the assumption of local thermodynamic equilibrium (LTE). This assumes that all thermodynamic properties at any point in the atmosphere are assumed to be defined by a local, unique temperature and are given by the appropriate relationships for a gas in thermodynamic equilibrium; *i.e.* velocities are Maxwellian, the occupation of atomic energy levels is governed by the Boltzmann equation and the ionisation balance by the Saha equation. The LTE atmospheres were used by the program UCLSYN to produce synthetic spectra.

Constructing a synthetic spectrum

UCLSYN determines the continuous opacity due to hydrogen, helium and metals at every frequency point in the spectrum. These continuous opacity sources are classified as 'absorption' sources and represented by the symbol κ_ν and are mapped onto a grid of equally spaced frequency points. Additional contribution from scat-

tering sources (symbolised by σ_ν) such as Rayleigh and Thompson scattering are also taken into account. However, in a typical early-A or late-B stellar atmosphere the dominant source of continuous opacity is from neutral hydrogen (Böhm-Vitense 1989).

The total continuous opacity κ_ν at frequency ν is given by the sum of all these opacity contributions. UCLSYN requires the total opacity to be expressed as the mass absorption coefficient. The opacity due to a line transition, κ_{L_ν} (again expressed as a mass-absorption coefficient), at frequency ν is then determined by the formula

$$\kappa_{L_\nu} = \frac{\pi e^2}{m_e c} f \frac{H(a,\nu)}{\sqrt{\pi}\Delta\nu_D} \frac{A_k}{\mu m_H} \frac{N_{ijk}}{N_k} \left(1 - e^{h\nu/kT}\right) \tag{3.1}$$

where $\pi e^2 f/m_e c$ is the total absorption of the line, including oscillator strength f, $H(a,\nu)/\sqrt{\pi \triangle \nu_D}$ is the frequency-distribution of the absorption line profile, A_k is the abundance of element k, $1/\mu m_H$ (which can also be written as N_H/ρ) is a conversion factor to ensure the final line-opacity is expressed as the mass-absorption coefficient, N_{ijk}/N_k is the total number-fraction of the element in question capable of absorbing radiation and the last term is the correction factor for stimulated emission.

The source function S_ν is the ratio of the emissivity η_ν and the total opacity κ_ν and is defined as

$$S_\nu = \frac{\eta_\nu}{\kappa_\nu} \tag{3.2}$$

In LTE terms this can be expressed as

$$S_\nu = \left(\frac{\kappa_\nu}{\kappa_\nu + \sigma_\nu} B_\nu + \frac{\sigma_\nu}{\kappa_\nu + \sigma_\nu} J_\nu\right) \tag{3.3}$$

The source function and the flux are dependent quantities and must be calculated simultaneously, which is computationally expensive.

However, two simplifying assumptions can be made. For stars with effective temperatures below 15 000K scattering is negligible, which means that scattering sources can be treated as absorption sources. It is also assumed that LTE holds, which is important because in LTE the radiation field has no effect on the gas, so the rate of change of the specific intensity with respect to optical depth is necessarily zero, making

$$S_\nu = I_\nu = B_\nu \tag{3.4}$$

S_ν can then instead be taken directly from the Planck function, *i.e.*,

$$S_\nu(\tau_0) = B_\nu(T[\tau_0]) \tag{3.5}$$

making calculations more straightforward (Optical depth scale is defined with $\lambda_0 =$ 500nm).

The total flux is then calculated from a quadrature sum of equation 3.6 using the method of Norton's 18-point quadrature

$$F_\nu = 2\pi \int_0^\infty S_\nu(\tau_\nu) E_2(\tau_\nu) \frac{d\tau_\nu}{\mu} \tag{3.6}$$

where E_2 is the second exponential integral, τ_ν the monochromatic optical depth and S_ν the source function. The continuous and line opacity are both implicitly present in the monochromatic optical depth scale and the exponential integral E_2 which is a function of τ_ν.

A sum of line and continuous source functions is substituted into Equation 3.6 to obtain a synthetic spectrum. The same calculation is performed for continuous opacity alone. The two resulting spectra are then divided to give a normalised synthetic spectrum. The wing of a Balmer line, for example, can be treated as a region of slowly varying continuous flux, which can be advantageous if studying lines in the wing.

Chapter 4

The data required for abundance analysis through spectrum synthesis

In order to use the spectrum synthesis technique and to calculate the abundances of the 13 stars, data from equivalent widths, instrumental profiles, line profiles, temperatures and gravities and rotational velocities were all required. Equivalent widths were previously determined; acquisition of the other data is discussed here.

4.1 Effective temperatures and surface gravities

Effective temperatures and surface gravities are needed to select the correct model atmospheres in order to minimise systematic error in the abundances. Photometric databases are useful in determining stellar atmospheric parameters. The programme stars' $T_{\rm eff}$ and $\log g$ values were determined by Smith and Dworetsky (1993) with the aid of a variety of photometric data, in this case Hauck and Mermilliod (1980), (1990) for the Strömgren system and Hauck and North (1982) for the Geneva photometric system.

The best-fit values for these stellar parameters can be further constrained by determining the stellar surface gravity using Balmer-profiles in a technique detailed

Table 4.1: The effective temperatures and surface gravities of the programme stars, listed in temperature order, adopted from Smith and Dworetsky (1993). The errors on effective temperature are estimated to be ± 250K, those on $\log g$ to be ±0.25 dex.

HD	HR	Star	$T_{\rm eff}$/K	log g
97633	4359	θ Leo	9350	3.67
172167	7001	α Lyr	9500	3.90
174567	7098	–	10180	3.55
209459	8404	21 Peg	10440	3.50
145389	6023	ϕ Her	11670	4.00
144206	5982	υ Her	12000	3.78
155763	6396	ζ Dra	12900	3.92
179761	7287	21 Aql	13060	3.50
7374	364	87 Psc	13150	4.02
190229	7664	–	13190	3.59
182308	7361	–	13650	3.51
172044	6997	–	14520	3.89
147394	6092	τ Her	15010	3.93

in Gray (1992). Here observed Hγ profiles are compared with theoretical profiles representing a certain $T_{\rm eff}$ and $\log g$. Information on $\log g$ is concentrated in the line wings, which must be calibrated accurately. However, in this thesis data set there are no spectrophotometric data and the Balmer line wings are several times as broad as the free spectral range of an échelle order in A- and B-type stars, making a fit impossible.

In addition, no new Strömgren data were available at the time of writing this thesis so the surface gravities and effective temperatures determined by Smith and Dworetsky (1993) were adopted for the programme stars. These are reproduced in Table 4.1.

4.2 Measurement of microturbulence

4.2.1 Microturbulence

Mictroturbulence (ξ) is an additional velocity term which represents motions in the stellar atmosphere on a scale less than the photon mean free path. This is taken into account before abundances are calculated because it can introduce systematic error by desaturating the line profile in the stellar atmosphere. The error on the abundance increases and the abundance itself is too high.

Microturbulence can be defined as an additional velocity term to the Maxwellian velocity distribution;

$$v_{kinetic} = \sqrt{\frac{2kT}{m} + \xi^2} \tag{4.1}$$

The concept of microturbulence originated in early model atmosphere calculations where it was found that strong lines gave higher abundances than those obtained from weak lines (Gray 1992). Introduction of this term into a curve of growth analysis had the result of desaturating the strong spectral lines and removing systematic differences in the abundances, but it was found weak lines were not obviously affected.

4.2.2 Measurement of microturbulence

The microturbulence can be determined from a plot of line equivalent width *vs* calculated abundance and is best determined from a selection of weak and strong lines to give a good indication of the plot gradient. Use of blended lines will increase the microturbulence by making the lines appear stronger and so they must be avoided to prevent systematic error in the microturbulence and therefore the final abundance. Magain (1984) recommended a plot of *synthetic* equivalent width *vs* abundance to remove systematic error resulting from random errors in the measurements. UCLSYN computes the synthetic equivalent width W'_λ for a mean abundance taken from the abundances calculated for the equivalent width measurements of all the lines. The microturbulence is then determined by finding a null correlation between the $\log A$ and W'_λ. Singly ionised iron was used for the calculations because this ion satisfied the requirements of a mixture of numerous weak and strong lines, unblended lines,

and well documented atomic data.

4.2.3 The microturbulence problem

Determining ξ is a complex problem with no straightforward solution. It can be seen that different elements will give different results. Three stars were chosen for an investigation into the different microturbulence fits for different species, θ Leo, ϕ Her and HR6997. Table 4.2 shows the results. The fits were performed for chromium, iron, titanium, yttrium and zirconium. Where the microturbulence is denoted by 'Im' there is no solution at $\xi^2 \geq 0\,\mathrm{kms}^{-1}$ and the microturbulence is imaginary. Where '–' is seen, there are either too few lines for analysis or only weak lines in the spectrum of the star.

For the cool star θ Leo, ξ is most certainly non-zero, but for ϕ Her ξ is zero for iron but non zero for the other elements. A contributory factor to this anomaly may be that most other elements have 4-6 lines available and suitable for analysis and that iron has more suitable lines. This does not explain why titanium, with more lines than iron, gives a non-zero microturbulence. HR6997 has very few unblended lines and these appeared to be insensitive to microturbulence.

This implies that the ξ parameter is more difficult to determine than might first be supposed. The different fits to ξ for ϕ Her, between different species, may be because some species could be formed at a different depth in the atmosphere than the iron lines. This means that it may be incorrect to simply adopt an iron microturbulence for zirconium. The solution to this question is a difficult one and the straightforward approach was to adopt the Fe II ξ for this analysis, bearing in mind the difficulties encountered in this investigation.

4.2.4 Results for iron

Table 4.3 shows the results from the best-fits to the microturbulence on a series of weak and strong iron lines, shown in Table 4.2, already measured in the programme stars.

Table 4.2: Microturbulence fits in kms^{-1} for three programme stars using several different elements

Species	θ Leo	ϕ Her	HR6997
Cr II	2.2	1.8	–
Fe II	2.0	0.0	Im
Ti II	3.1	0.8	Im
Y II	–	–	–
Zr II	–	2.3	–

Table 4.3: Iron lines used in υ Her microturbulence analysis

Species	Wavelength/ Å	W_λ/mÅ
Fe II	4044.01	7
Fe II	4369.40	7
Fe II	4416.82	37
Fe II	4508.28	46
Fe II	4515.34	45
Fe II	4520.22	35
Fe II	4522.63	56
Fe II	4555.89	49
Fe II	4576.33	71
Fe II	4620.51	15

Figure 4.1: Microturbulence fits at optimal values of ξ using Fe II for the 13 programme stars. 87 Psc, HR6997 and τ Her do not show null correlation at zero microturbulence.

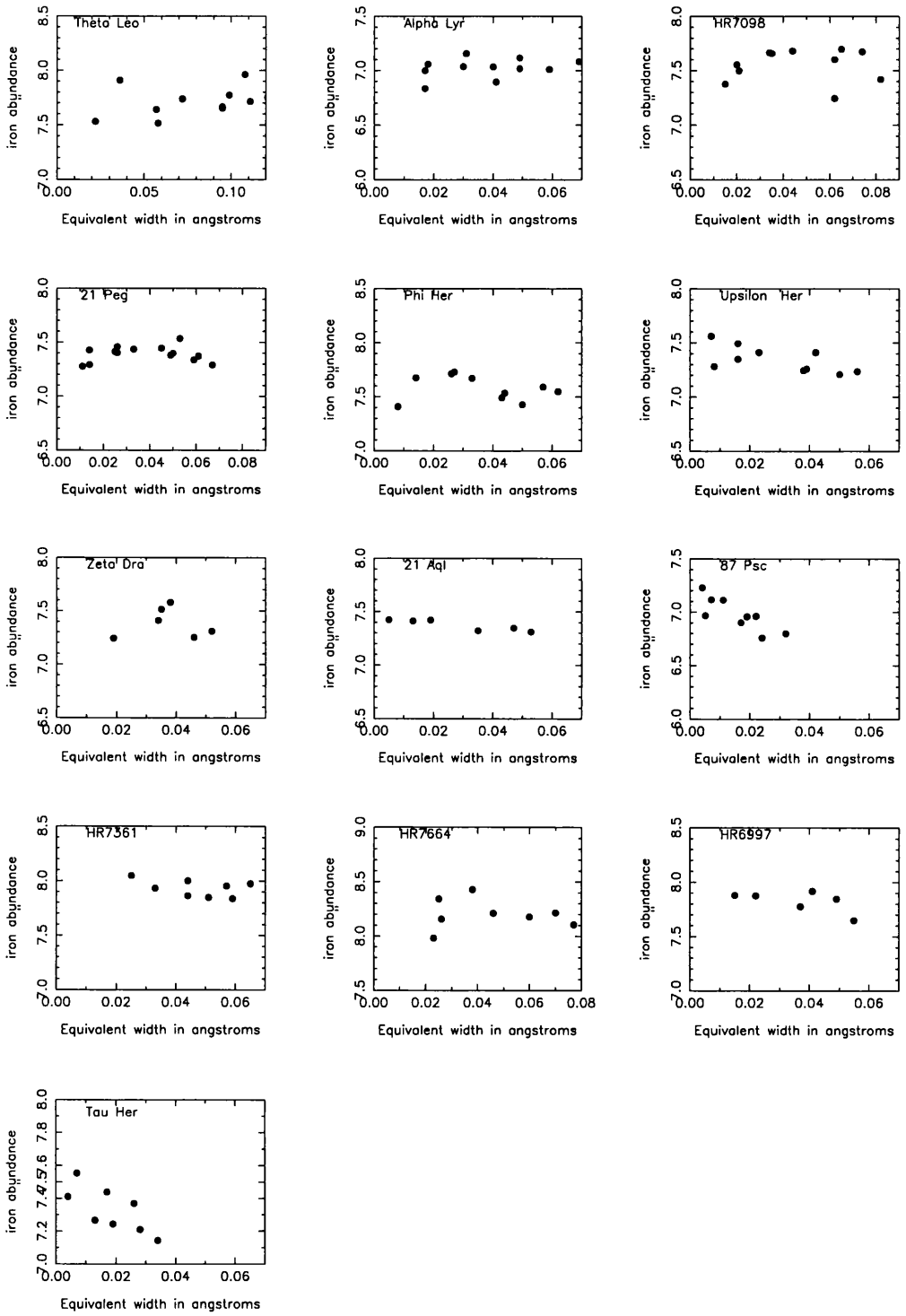

Table 4.4: The adopted microturbulence parameters of the program stars. The stars are shown in $T_{\rm eff}$ order.

HD	HR	Star	$T_{\rm eff}$/K	ξ kms^{-1}
97633	4359	θ Leo	9350	2.0
172167	7001	α Lyr	9500	1.2
174567	7098	–	10180	1.0
209459	8404	21 Peg	10440	0.3
145389	6023	ϕ Her	11670	0.0
144206	5982	υ Her	12000	0.0
155763	6396	ζ Dra	12900	0.0
179761	7287	21 Aql	13060	0.0
7374	364	87 Psc	13150	–
190229	7664	–	13190	0.0
182308	7361	–	13650	0.0
172044	6997	–	14520	–
147394	6092	τ Her	15010	–

4.2.5 Discussion

The main-sequence stars in this programme with $T_{\rm eff}$ greater than 11 000K show no measurable microturbulence; this is taken to imply that their atmospheres are stable and that they show no surface convection zones, unlike cooler stars, which have measurable microturbulence parameters. This would imply that use of sophisticated models may remove the need to use this parameter when modelling stars with $T_{\rm eff}$ greater than 11 000K, and the values measured for cooler stars may be due to a real phenomenon. In some cases there are very few strong Fe II lines present in the spectrum. This is seen in hotter HgMn stars with a sub-solar iron abundance. Only very weak lines, which are not sensitive to microturbulence, are available and therefore the microturbulence in 87 Psc (low abundance), HR6997 and τ Her (hot stars) is indeterminate. Indeed, a plot of abundance *vs* synthetic equivalent width requires an imaginary microturbulence to obtain a null-correlation. ξ was set to zero in these stars for the purposes of the analysis but not explicitly stated in Table 4.4.

4.3 Rotational velocities

Rotational velocities were adopted from those listed by Smith and Dworetsky (1993) and are reproduced in Table 4.5.

4.4 Instrumental profile

It is important to know the profile of the instrumental response of the Hamilton Échelle Spectrograph and its FWHM because this makes an accurate model of the data possible, which can then be compared directly to observations. The response of the instrument was examined during data reduction and the results can be seen in Section 2.5. The combination of a quadratic variation in FWHM and the non-linear variation of the profile asymmetry made modelling ϕ_λ a very difficult task. Instead ϕ_λ was measured for arc lines from 16 orders and a set of four 'mean profiles' was constructed for four wavelength ranges where the quadratic variation does not exceed experimental uncertainty (Figures 2.6, 2.7); this was best achieved over the wavelength ranges $\lambda\lambda$3900-4100, 4100-4300, 4300-4650 and 4650-4900. The profiles

Table 4.5: Rotational velocities taken from Smith and Dworetsky (1993)

HD	HR	Star	$v \sin i$ km s^{-1}
97633	4359	θ Leo	23
147394	6092	τ Her	32
155763	6396	ζ Dra	34
172167	7001	α Lyr	23
179761	7287	21 Aql	19
174567	7098	-	11
209459	8404	21 Peg	4
7374	364	87 Psc	21
144206	5982	υ Her	11
145389	6023	ϕ Her	10
172044	6997	-	34
182308	7361	-	9
190229	7664	-	8

were tested in preliminary spectrum syntheses, and found to give an excellent visual match between observations and synthetic spectrum.

4.5 Atomic data

The atomic data required to calculate κ_{L_ν} came from a variety of sources. Natural damping constants were all calculated using the following classical formula (Mihalas 1978);

$$\Gamma_c = \frac{8\pi^2 e^2}{3 m_e c \lambda^2} \tag{4.2}$$

Van der Waals damping was neglected because pressure-broadening by neutral hydrogen (H) atoms can be assumed to be insignificant in early A and B stars due to the ionisation of H. Stark damping constants for the strong lines of silicon, and strontium were taken from Sahal-Bréchot (1969). The Stark damping constants for the Ca II K line were taken from Roberts and Eckerle (1985).

The adopted oscillator strengths, their sources and their accuracy (where known)

are listed in Table 4.6 for all the lines used in this thesis. The first column in Table 4.6 contains the element and ionisation stage, the second lists the multiplet number where such data is available. Column 3 gives the lower excitation potential of the transition, and the fourth column lists the oscillator strength, the reference for which can be found in column 5. Where the accuracy is known it is listed in column 6.

Critical compilations containing oscillator strengths ($\log gf$ values) are used when possible, *e.g.*, Martin, Fuhr and Wiese (1988), Fuhr, Martin and Wiese (1988), Wiese and Martin (1980), Wiese, Smith and Miles (1969). The semi-empirical line-list developed by Kurucz and Peytremann (1975), Kurucz (1990) is another source of $\log gf$ values. This list consists of data usually used in large-scale stellar-atmosphere calculations but was only used in this project if other literature sources were unavailable.

Where the critical compilations did not list modern data for a certain element, literature sources were chosen from Adelman and Lanz (1988) and are listed in Table 4.7. If data from this source did not contain appropriate data, a literature search was undertaken to find suitable oscillator strengths. Modern compilations were not found for Ni II, Mg II and Cr II, and only the list from Warner (1967) and the corrections made by Smith (1976) had atomic data for these three species. As that work is known to be inaccurate, and indeed preliminary abundance calculations for nickel in the spectra of normal stars did not give encouraging results (usually at least 1 dex below solar abundance), the Warner atomic data were replaced by those of Kurucz and Peytremann (1975).

Table 4.6: Atomic data.

Element	λ	RMT[1]	χ_{low}/eV	$\log gf$	reference	Accuracy
Ti II	3913.46	34	1.1156	-0.53	MFW 88	D
Mn II	3917.32	–	6.913	-1.147	KX	–
Fe II	3935.94	173	5.569	-1.86	FMW 88	C
Ca II	3933.68	1	0.00	1.40	WM 69	A
Mn II	3941.23	–	5.437	-2.62	KX	C
Al I	3944.01	1	0.000	-0.644	MOR 91	A–
Fe II	3945.21	3	1.6952	-4.125	FMW 88	D
Y II	3950.35	6	0.10	-0.49	HAN 82	–
V II	3951.97	–	1.4764	-0.74	MFW 88	–
Zr II	3958.22	16	0.52	-0.26	GRE 81	–
Al I	3961.52	1	0.0139	-0.345	MOR 91	A-
Cr II	3979.51	–	5.670	-0.731	KX	–
Y II	3982.59	6	0.130	-0.50	HAN 82	–
Zr II	3991.13	30	-0.75	-0.30	GRE 81	–
Zr II	3998.97	16	0.56	-0.67	GRE 81	–
Cr II	4003.28	–	6.484	-0.601	KX	–
V II	4005.71	32	1.8171	-0.46	MFW 88	D
Ti II	4012.37	11	0.5739	-1.61	MFW 88	C
Ni II	4015.50	12	4.010	-2.42	KX	–
Ti II	4025.14	11	0.6073	-1.98	MFW 88	D–
S II	4028.79	45	15.944	-0.00	WM 69	D–
Ti II	4028.33	87	1.8916	-1.00	MFW 88	D
Mn I	4030.75	2	0.000	-0.470	KX	–
S II†	4032.81	–	16.24	0.24	WM 69	–
Fe II†	4032.99	–	3.65	-3.61	KX	–
Ga I	4032.99	1	0.000	-0.61	WM 80	C
Mn I†	4033.06	–	0.00	-0.618	MFW 88	–
Mn I	4034.48	2	0.000	-0.811	MFW 88	C+
V II	4035.63	32	1.793	-0.96	KX	–
Mn I	4041.36	5	2.114	+0.285	MFW 88	C+

Element	λ	RMT[1]	χ_{low}/eV	$\log gf$	reference	Accuracy
Fe II	4044.01	172	5.550	-2.37	FMW 88	C
Fe I	4045.84	43	1.485	0.280	FMW 88	C
Zr II	4048.67	43	0.80	-0.48	GRE 81	–
Ti II	4053.81	87	1.8928	-1.21	MFW 88	D
Mn I	4055.55	5	2.143	-0.070	MFW 88	C+
Mn I	4059.39	29	3.073	-0.69	MFW 88	E–
Fe I	4063.60	43	1.557	+0.070	KX	–
Ni II	4067.05	11	4.030	-1.29	KX	–
Fe I	4071.74	43	1.608	-0.022	KX	–
Sr II	4077.71	1	0.00	0.21	PS 81	–
Fe II	4122.64	28	2.583	-3.380	FMW 88	C
Si II	4128.07	3	9.839	0.310	WM 69	C
Ba II	4130.65	–	2.721	0.44	WM 80	B
Si II	4130.89	3	9.839	0.462	WM 69	C
Cr II	4145.76	–	5.319	-1.164	KX	–
S II	4153.10	44	15.889	+0.62	WM 69	D–
Zr II	4156.24	29	0.71	-0.71	GRE 81	–
Ti II	4161.52	21	1.0841	-2.36	MFW 88	D
S II	4162.70	44	15.944	+0.78	WM 69	D–
Ti II	4163.46	102	2.5903	-0.40	MFW 88	D
Mg I	4167.26	–	4.349	-0.710	WM 80	C
Cr II†	4171.90	–	2.5977	-0.56	MFW 88	–
Ti II†	4171.91	–	3.105	-2.38	KX	–
Ga I	4172.04	1	0.102	-0.324	WM 80	C
Mn II	4206.37	72	5.397	-1.566	KX	–
Zr II	4208.985	41	0.71	-0.46	BIE 81	–
Zr II	4211.88	15	0.53	-0.65	GRE 81	–
Sr II	4215.52	1	0.00	-0.18	PS 81	–
Ca I	4226.73	2	0.0000	0.244	WM 69	B+
Cr II	4242.38	–	3.871	-0.590	KX	–
Sc II	4246.89	7	0.3150	0.32	MFW 88	D

Element	λ	RMT[1]	χ_{low}/eV	$\log gf$	reference	Accuracy
Ni II	4244.82	9	4.0324	-3.109	KX	–
Cr I	4254.35	1	0.0000	-0.114	MFW 88	B
Fe II	4273.22	27	2.7044	-3.34	FMW 88	D
Cr I	4274.80	1	0.0000	-0.231	MFW 88	B
Fe II	4278.13	32	2.6920	-3.68	HEB 83	–
Ti II	4287.89	20	0.799	-2.02	MFW 88	D–
Cr I	4289.72	1	0.000	-0.503	MFW 88	B
Ti II	4290.22	21	1.0800	-2.010	MFW 88	D–
Fe II	4296.57	28	2.704	-3.010	FMW 88	C
Ti II	4300.052	41	1.1801	-1.12	MFW 88	D–
Ti II	4301.93	41	1.160	-1.22	MFW 88	D–
Fe II	4303.16	27	2.7044	-2.49	FMW 88	C
Y II	4309.62	5	0.18	-0.74	PN86	–
Ti II	4312.86	41	1.180	-1.16	MFW 88	D–
Zr II	4317.32	40	0.71	-1.38	BIE 81	–
Mn II	4326.68	–	5.398	-1.254	KX	–
Mg I	4351.90	14	4.346	-0.520	WM 80	D
Ni II	4362.10	9	4.029	-2.723	KX	–
Mn II	4363.26	–	5.567	-1.909	KX	–
Mn II	4365.22	–	6.573	-1.350	KX	–
Fe II	4369.40	33	2.778	-3.670	FMW 88	C
Y II	4374.94	13	0.41	0.16	HAN 82	–
Fe II	4385.38	27	2.778	-2.570	FMW 88	C
Mg II	4390.58	10	9.999	-0.530	KX	–
Ti II	4394.06	51	1.2214	-1.59	MFW 88	D–
Ti II	4395.03	19	1.0841	-0.66	MFW 88	D–
Ti II	4395.85	61	1.2430	-2.17	MFW 88	D–
Y II	4398.02	5	0.13	-1.24	PN 86	–
Ti II	4399.78	51	1.2369	-1.27	MFW 88	D–
Ni I	4401.55	86	3.193	+0.080	KX	–
Fe I	4404.75	41	2.759	-1.92	FMW 88	C

Element	λ	RMT[1]	χ_{low}/eV	$\log gf$	reference	Accuracy
Fe II	4416.82	27	2.779	-2.60	FMW 88	C
Ti II	4417.72	40	1.1650	-1.43	MFW 88	D–
Ti II	4418.34	51	1.2369	-2.46	MFW 88	D–
Mg II	4427.99	9	9.996	-1.201	WM 80	C+
Mg II	4433.99	9	9.999	-0.900	WM 80	C+
Ti II	4464.53	40	1.1610	-2.08	MFW 88	D-
Ti II	4468.54	31	1.1305	-0.60	MFW 88	D-
P II	4475.26	24	13.080	+0.44	WM 69	D
P II	4475.26	24	13.080	+0.44	WM 69	D
Mn II	4478.64	–	6.045	-0.950	KX	–
P II	4483.68	–	13.050	-0.78	WM 69	D–
Fe II	4491.40	37	2.856	-2.70	FMW 88	C
P II	4499.24	11	13.380	-0.47	WM 69	D
Ti II	4501.24	31	1.116	-0.750	MFW 88	D–
Fe II	4508.28	38	2.856	-2.21	FMW 88	C
Fe II	4515.34	37	2.844	-2.48	FMW 88	C
Fe II	4520.22	37	2.807	-2.60	FMW 88	C
Fe II	4522.63	38	2.844	-2.03	FMW 88	B
Fe I	4528.62	68	2.1760	-0.822	FMW 88	B+
Fe II	4534.166	37	2.8555	-3.47	FMW 88	D
Ba II	4554.03	1	0.000	0.163	WM 80	A
Fe II	4555.89	37	2.828	-2.29	FMW 88	C
Cr II	4558.66	–	4.073	-0.660	KX	–
Ti II	4563.76	50	1.2214	-0.96	MFW 88	D–
Ti II	4571.97	82	1.5718	-0.53	MFW 88	D–
Fe II	4576.33	38	2.844	-3.04	FMW 88	C
Fe II	4582.853	37	2.8441	-3.04	FMW 88	C
Cr II	4588.217	–	4.071	-0.630	KX	–
P II	4602.08	15	12.8534	0.74	WM 69	D
Fe II	4620.51	38	2.828	-3.28	FMW 88	C
Fe II	4625.91	37	2.8441	-0.310	FMW 88	C

Element	λ	RMT[1]	χ_{low}/eV	$\log gf$	reference	Accuracy
P II	4626.70	–	12.810	-0.310	WM 69	D–
Fe II	4629.336	37	2.8067	-2.37	FMW 88	D
Al II	4663.05	2	10.5981	-0.284	WM 69	D
Mg I	4702.94	11	4.346	-0.370	WM 80	–

†: Lines used for blend synthesis in Ga I analysis. Not used for abundance analysis.

Table 4.7: Sources of atomic data

Element	Abbreviation	Full reference
Al I	MOR 91	Morton, D.C., (1991)
Al II	WM 69	Wiese, Smith and Miles (1969)
Ba	WM 80	Wiese and Martin (1980)
Ca I	WM 69	Wiese, Smith and Miles (1969)
Ca II	WM 69	Wiese, Smith and Miles (1969)
Cr I	MFW 88	Martin, Fuhr and Wiese (1988)
Cr II	KX	Kurucz and Peytremann (1975)
Fe I	KX	Kurucz and Peytremann (1975)
Fe II	FMW 88/HEB 83	Fuhr, Martin and Wiese (1988), Heber (1983)
Ga I	WM 80	Wiese and Martin (1980)
Mg I	WM 80	Wiese and Martin (1980)
Mg II	WM 80	Wiese and Martin (1980)
Mn I	MFW 88	Martin, Fuhr and Wiese (1988)
Mn II	KX	Kurucz and Peytremann (1975)
Ni	KX	Kurucz and Peytremann (1975)
P	WM 69	Wiese, Smith and Miles (1969)
S	WM 69	Wiese, Smith and Miles (1969)
Sc	MFW 88	Martin, Fuhr and Wiese (1988)
Si	WM 69	Wiese, Smith and Miles (1969)
Sr	PS 81	Pirronello, Strazzulla (1981)
Ti	MFW 88	Martin, Fuhr and Wiese (1988)
V	MFW 88	Martin,Fuhr and Wiese (1988)
Y	PN 86/ HAN 82	Pitts and Newsom (1986), Hannaford *et al* (1982)
Zr	GRE 81/ BIE 81	Grevesse (1981), Biemont *et al* (1981)

Chapter 5

Metal abundance analysis

5.1 The line abundance

Two comparative techniques are used in the spectrum synthesis package UCLSYN to calculate abundances. The first technique involves iteration, whereby the synthetic equivalent width is altered until it matches the observed equivalent width, thereby giving an abundance; the second technique is the determination of abundances from direct comparison between synthetic and observational spectra.

5.1.1 Deriving abundances from equivalent width measurements

UCLSYN was used in 'exact curve-of-growth' mode in order to determine the abundance of a single unblended line from a measured equivalent width. Each line's curve-of-growth is in effect computed exactly from the model atmosphere and atomic parameters supplied. An unbroadened synthetic profile is calculated for a spectral line using an initial abundance and integrated over a half-profile to produce a synthetic equivalent half-width and the result then doubled. If the synthetic and observed equivalent widths do not match then the abundance is adjusted, and a new equivalent width calculated. Iteration proceeds until an abundance is found at which theoretical and observed equivalent widths match.

5.1.2 Deriving abundances from comparison between synthetic and observed spectra

Visual fitting from spectrum synthesis is most useful when dealing with species where there are only a few visible lines in the optical region or when these lines are blended. The line profile is calculated at a user-specified abundance. Instrumental broadening can be achieved by convolving the synthetic spectrum with the instrumental profile, and rotational broadening is performed by calculating the quadratic limb-darkening function and then convolving the resultant rotational profile through the spectrum.

The synthetic spectra are interpolated onto a uniformly spaced wavelength grid and the necessary rotational and instrumental broadening parameters are convolved through the spectrum. The spectrum can then be compared with the observational data by superposition and a family of synthetic spectral lines covering a narrow range of abundances obtained, from which an unweighted mean abundance can be obtained. The error on the mean fit to the abundance can be determined from the two extreme values of the family of fits.

The line abundances for the normal and mercury-manganese star sample are given in Appendix B in Tables B.1 and B.2.

5.1.3 The total error

The total error on the calculated abundance for a line depends on errors in equivalent width measurement, the stellar effective temperature, stellar $\log g$, line $\log gf$, and stellar microturbulence. The errors in the Stark damping parameters may also become important in strong saturated lines, but they were neglected in this thesis as the lines used in this project were not saturated.

The total error for a single line is calculated by quadratically propagating the individual components, assuming mutual independence between the variables. It is correct to assume the variables are independent of one another in a single line, because the surface gravity of a star cannot, for example, depend upon the measured equivalent width or the oscillator strength of a spectral line. The approach used here is in line with that of Smith (1993, his paper II), except that in this project the frac-

tional error on the equivalent width is usually estimated directly from measurements and not assumed to be within 10%.

The errors in the effective temperature and surface gravities were adopted from Smith and Dworetsky (1993) and take the values of ±250K and ±0.25 dex respectively. The errors in the $\log gf$ values came from the literature except in the case of those taken from Kurucz and Peytremann (1975), where an estimate for the error was adopted as ±50%. The error in the equivalent width was estimated from direct measurement of the uncertainty in the continuum placement.

Tests in UCLSYN imply that microturbulence may not be an independent variable but may instead depend in a complicated way on effective temperature and gravity. A small perturbation of the stellar effective temperature can alter the strength of weak and strong lines in a way which may be a complicated function of the excitation potential and oscillator strength of each line. The presence of line blends can also alter the microturbulence, with stronger lines giving rise to higher abundances. A single random error of $\pm 0.5 \mathrm{kms}^{-1}$ was estimated for each microturbulence value in an attempt to account for these errors. Smith (*priv. comm*) informs me that UCLSYN takes the error in ξ into account using a 'one-sided error' when $\xi \leq \Delta\xi$ by calculating a single-tailed Gaussian distribution from the given error on the microturbulence (usually σ=0.5kms^{-1}), then assumes this distribution is symmetrical about zero when calculating the total error on the abundance.

The total error on synthetic spectral lines was derived by quadratically propagating the errors on the individual components; surface gravity, effective temperature and oscillator strength. In this case, however, the equivalent widths were assumed to have an error of 20%, which is a reasonable estimate given that many measured lines have errors of this magnitude.

5.2 The mean abundance

The mean abundance of each species was calculated without taking the strengths of the individual lines into account. At first thought it would make sense to weight each line abundance by the line equivalent width because this would give the stronger lines more weight, thereby reducing random error in the measurements; however,

this may not be a valid approach as stronger lines on the flat part of the curve-of-growth have a larger uncertainty in their abundances. It was therefore decided to calculate the line abundances without use of weighting factors.

5.2.1 The standard deviation on the mean abundance

The error on the mean abundance is not as straightforward a calculation as it is for the error on the line abundance. The work of Smith (1993) defines two estimates for the error on the mean abundance and his approach has been followed in this project.

The sample standard deviation, σ_s, is a weighted error based on the dispersion of the individual line abundances about the mean abundance, calculated using

$$\sigma_s = \sqrt{\frac{\Sigma_k w_k (A_k - \bar{A})^2}{\Sigma_k w_k} \frac{N}{N-1}} \tag{5.1}$$

where A_k is the logarithmic abundance of line k, A is the weighted mean abundance, w_k is the weighting factor $1/\sigma_k^2$ and N is the number of lines in the sample. $N/(N-1)$ is included to give an unbiased estimate for σ_s.

The second estimate, the model standard deviation σ_m, is obtained by taking the non-independence of some of the variables into account. The errors on the equivalent widths are assumed to be random from one line to the next, but the abundance errors in the effective temperatures, surface gravities and microturbulence are clearly correlated for any given star. Oscillator strengths from the same multiplet also give rise to systematic errors.

The systematic nature of these errors can be modelled by taking their covariance into account. The covariance is given by

$$\mathrm{cov}(A_k, A_l) = \sigma_i \sigma_j \left(\frac{dA_k}{dx_{i,k}}\right)\left(\frac{dA_l}{dx_{j,l}}\right)\mathrm{cov}(x_{i,k}, x_{j,l}) \tag{5.2}$$

where $x_{i,k}$ and $x_{j,l}$ are different model parameters (i.e. temperature, gravity, equivalent width) i and j for the different lines k and l respectively. The covariance between independent variables (e.g. $i \neq j$) will be zero, but that between non-independent variables ($i = j$) will be non-zero. This situation can be envisioned as a matrix where the diagonal terms of the matrix are given by the variances of each

line, and the covariances are given by the non-diagonal terms of the matrix. The non-diagonal terms are zero where the variables are independent.

UCLSYN is used to calculate the model standard deviation taking covariance into account, using

$$\sigma_m = \sqrt{\frac{\sum_k \sum_l w_k w_l \mathrm{cov}(A_k, A_l)}{(\sum_l^k w_k)^2}} \tag{5.3}$$

where w_k and w_l are the weighting factors as in Equation 5.2 and A_k and A_l the relevant abundances.

5.3 The results

The abundances were initially obtained from a combination of line profile synthesis and/or calculations based on equivalent width measurements. The line abundances can be found in Tables B.1 and B.2; lines from more than one ionisation stage were included for the sake of completeness and to allow detection of possible effects of nLTE in subordinate ionisation stages, giving rise to differing abundances.

The unweighted mean abundances were then calculated for the elements, and, in the case of magnesium, calcium, aluminium, manganese, iron, nickel and chromium, the abundances of the neutral and first ionisation stages. For these latter ions, a further mean elemental abundance was determined, which was weighted by the number of lines analysed for each species. Here σ_m and σ_s are calculated the same way as for a single species. Were the equivalent widths and atomic data exactly known, σ_s would reduce to zero, but σ_m would still take its calculated value. Alongside the mean abundances s, the standard error on the mean, given by $\sigma_s/\sqrt{N}$, is also listed.

In each section which follows a brief description is given of how the analysis proceeded.

5.3.1 Magnesium

Magnesium exhibits three strong singlet lines of neutral and three doublets of ionised magnesium in the optical region with wavelengths at $\lambda\lambda$4167, 4351, 4702 and $\lambda\lambda$4390, 4428, 4434 as well as the strong Mg II doublet at λ4481. Five of the six lines analysed are blended with other elements and the blends are shown in Table 5.1.

Table 5.1: Blending species for selected magnesium lines

Line	Blending Species
Mg I λ4167.26	Fe II,4167.30
Mg I λ4351.77	Fe II,4351.77
Mg I λ4702.94	Mn II,4702.74
Mg II λ4390.58	–
Mg II λ4427.99	Ti II,4427.88
Mg II λ4433.99	Fe I,4433.78; Mn II,4434.07

The line at λ4390 is not blended and its measured W_λ was used to obtain a single abundance and external error in EXACT mode in UCLSYN. The remaining five lines were synthesised, together with their blending components. The abundances of the blending elements were determined previously and used as constraints when determining the magnesium abundance. However, lines which were heavily blended were not synthesised.

The mean magnesium abundances are presented in Table 5.2.

Table 5.2: Magnesium abundances

Star	Mg I	σ_m	σ_s	Mg II	σ_m	σ_s	Mg	σ_m	σ_s
θ Leo	7.38±0.02	0.22	0.03	7.55±0.04	0.20	0.05	7.47±0.04	014	0.09
α Lyr	7.01±0.03	0.26	0.05	6.97±0.04	0.17	0.07	7.02±0.05	0.13	0.05
HR7098	7.62±0.02	0.26	0.03	7.62±0.05	0.16	0.08	7.62±0.01	0.11	0.06
21 Peg	7.36±0.04	0.26	0.08	7.56±0.06	0.15	0.10	7.46±0.05	0.10	0.14
ζ Dra	–	–	–	7.59±0.04	0.13	0.08	7.56±0.04	0.13	0.08
21 Aql	–	–	–	7.57±0.03	0.13	0.07	7.57±0.03	0.13	0.07
τ Her	–	–	–	7.66±0.03	0.14	0.06	7.66±0.03	0.14	0.06
ϕ Her	–	–	–	7.42±0.09	0.17	0.11	7.42±0.09	0.17	0.11
υ Her	–	–	–	7.26±0.04	0.14	0.09	7.26±0.04	0.14	0.09
87 Psc	–	–	–	7.06±0.04	0.14	0.09	7.06±0.04	0.14	0.09
HR7664	–	–	–	6.65±0.09	0.13	0.11	6.65±0.09	0.13	0.11
HR7361	–	–	–	7.26±0.10	0.19	0.12	7.26±0.01	0.19	0.12
HR6997	–	–	–	7.03±0.01	0.16	0.03	7.03±0.01	0.16	0.03

Table 5.3: Mean abundances for aluminium

Star	Al I	σ_m	σ_s	Al II	σ_{tot}	Al	σ_m	σ_s
θ Leo	6.53±0.27	0.36	0.39	6.65	–	6.61±0.03	0.24	0.06
α Lyr	5.79±0.03	0.26	0.05	5.60	0.20	5.70±0.06	0.16	0.09
hr7098	6.35±0.07	0.20	0.11	6.47	0.23	6.39±0.06	0.15	0.07
21 Peg	6.25	0.27	–	6.34	0.37	6.30±0.05	0.15	0.06
ζ Dra	6.27	0.32	–	6.41	0.26	6.34±0.07	0.15	0.10
21 Aql	6.35	0.26	–	6.30	0.20	6.23±0.13	0.15	0.18
τ Her	–	–	–	–	–	–	–	–
ϕ Her	–	–	–	5.65	0.30	5.65	0.30	–
υ Her	–	–	–	$\leq$4.88	–	$\leq$4.88	–	–
87 Psc	–	–	–	5.71	0.35	5.71	0.35	–
HR7664	–	–	–	$\leq$4.98	–	$\leq$ 4.98	–	–
HR7361	–	–	–	$\leq$4.98	–	$\leq$ 4.98	–	–
HR6997	–	–	–	5.20	0.28	5.20	0.28	–

5.3.2 Aluminium

Aluminium has three observable lines, two of these from Al I, available in the optical region studied in this thesis. The Al I line at λ3944 is weak in hot stars and is often blended with manganese whereas the other multiplet 1 line at λ3962, which is in the Balmer Hϵ wing, has a comparable W_λ but is not blended. The Al II line at λ4663 appears to be blended with a line, provisionally identified as Fe II, in the spectra of θ Leo, α Lyr and 21 Aql. The Al II line was therefore synthesised including this line, which was modelled from the Kurucz line-list. The oscillator strength for this iron line appears to be too weak as the abundance required to model the iron line needs to be exaggerated by $\sim$0.5 dex in all three stars. Plots of the syntheses are shown in Figures 5.1, 5.2 and 5.3. The remaining abundances for Al I and Al II in other stars were calculated directly from the measured W_λ. Upper limits were calculated where the lines are weak or invisible and the aluminium abundance is apparently below the solar value. The mean abundances for aluminium are shown in Table 5.3.

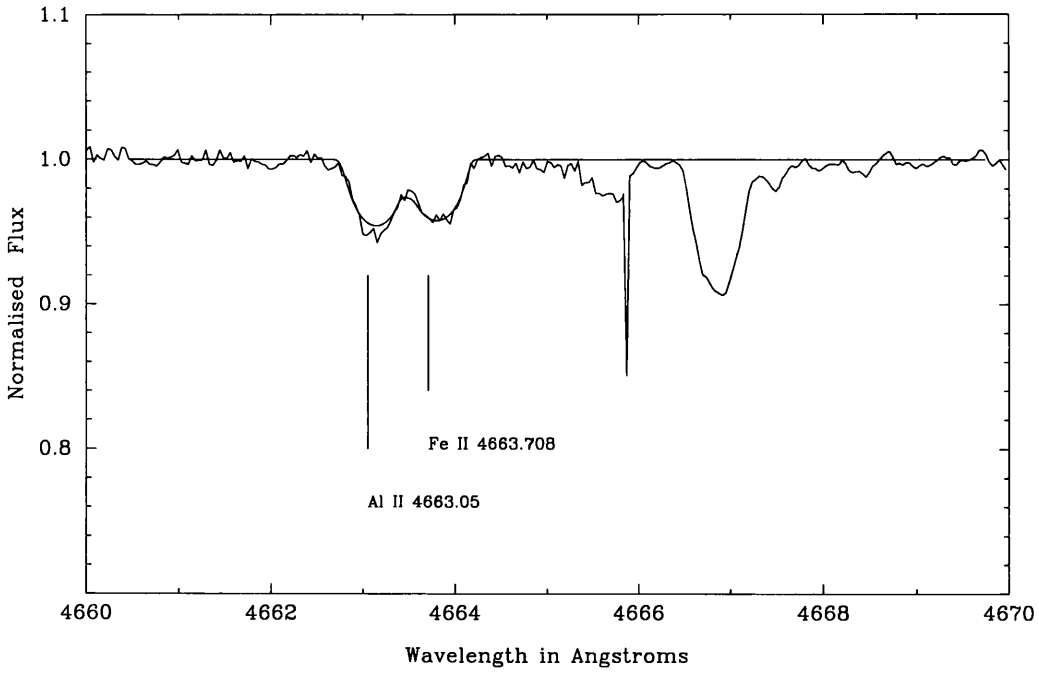

Figure 5.1: Synthesis of Al II and a possible Fe II line for θ Leo

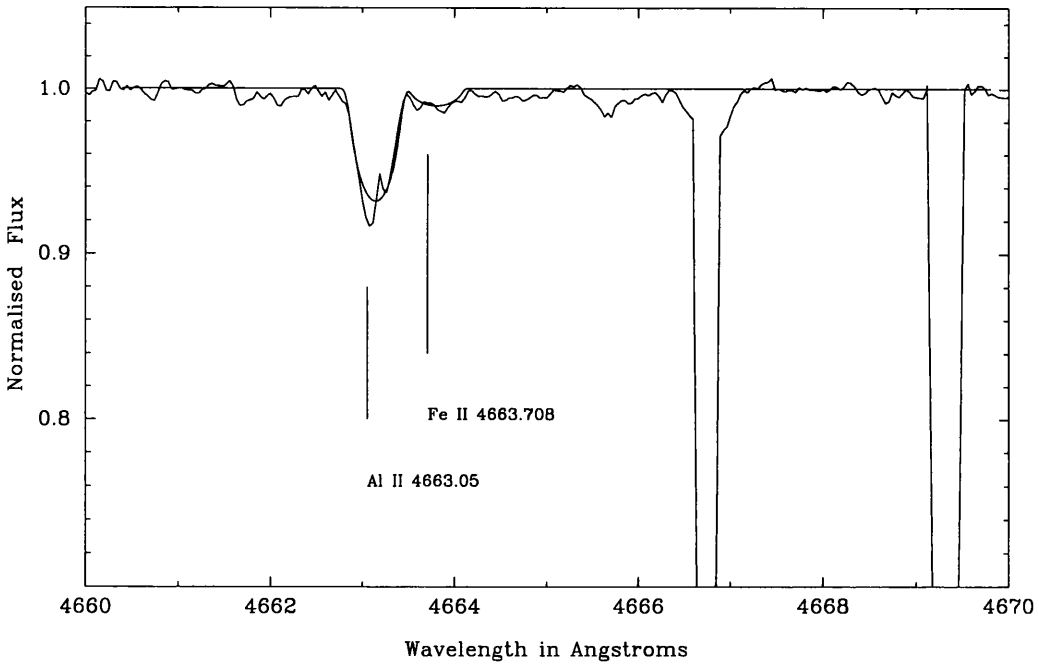

Figure 5.2: Synthesis of Al II and a possible Fe II line for 21 Aql

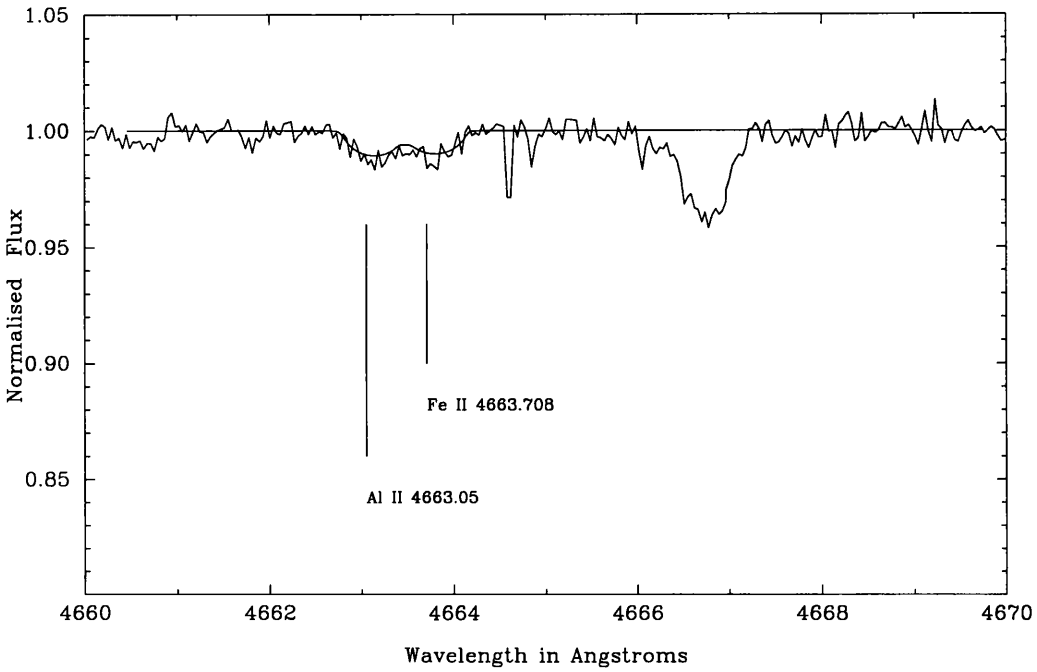

Figure 5.3: Synthesis of Al II and a possible Fe II line for Vega

5.3.3 Silicon

Silicon exhibits two strong lines from multiplet 3 in the first ionisation stage at $\lambda\lambda$ 4128 and 4130. Both lines are saturated and exhibit Stark damping wings and often other elements are found in the line wings making synthesis necessary. Stark damping parameters (Sahal-Bréchot 1969) were taken into account when synthesising the line profiles. The weak doublet at λ4621 is often not visible so was not used in this study. The λ4128 line was not used in HR6997 as it was contaminated with three lines in the line wing and an additional cosmic ray event. The blending components were thought to be Mn II 4128.14, Fe II 4128.74 and Fe II 4128.87 on the RHS of the silicon line.

HgMn stars and normal stars both show abundances consistent with solar values and a close internal consistency between the two lines although HR7361 shows a slight overabundance. Results are shown in Table 5.4.

Table 5.4: Silicon abundances

Star	Si	σ_m	σ_s
θ Leo	7.67±0.12	0.24	0.17
α Lyr	7.17±0.10	0.20	0.14
HR7098	7.56±0.01	0.14	0.01
21 Peg	7.47±0.03	0.26	0.04
ζ Drac	7.63±0.01	0.27	0.01
21 Aql	7.41±0.04	0.26	0.06
τ Her	7.43±0.07	0.24	0.09

Star	Si	σ_m/σ_{tot}	σ_s
ϕ Her	7.58±0.13	0.23	0.18
υ Her	7.52±0.03	0.24	0.05
87 Psc	7.36±0.14	0.23	0.21
HR7664	7.45±0.03	0.11	0.04
HR7361	7.95±0.13	0.24	0.18
HR6997	7.40	0.37	–

Table 5.5: Phosphorus abundances

Star	P	σ_m	σ_s
θ Leo	–	–	–
α Lyr	–	–	–
HR7098	–	–	–
21 Peg	–	–	–
ζ Drac	–	–	–
21 Aql	–	–	–
τ Her	–	–	–

Star	P	σ_m/σ_{tot}	σ_s
ϕ Her	–	–	
υ Her	6.27	0.26	–
87 Psc	5.91	0.36	–
HR7664	7.20±0.03	0.14	0.05
HR7361	7.81±0.04	0.12	0.07
HR6997	7.41±0.01	0.17	0.06

5.3.4 Phosphorus

Four lines of phosphorus (P II) were available in the optical region, $\lambda\lambda$ 4475, 4483, 4499 and 4626Å. Phosphorus lines are very obvious in the majority of HgMn stars studied in this project and the lines are much stronger in hotter stars. The normal stars did not show lines of phosphorus at any $T_{\rm eff}$ so no lower-limit calculations were made for these stars. This is consistent with solar system abundances as shown by Figure 7.4. The HgMn stars were analysed with no difficulty from measured equivalent widths and the resulting abundances were consistent for all four visible lines, which indicates that the phosphorus lines used here are all unblended. The final mean abundances are given in Table 5.5.

5.3.5 Sulphur

The lines chosen for analysis in this thesis were the strong S II lines seen at $\lambda\lambda$ 4153 and 4162. Another line at λ4028 was weak and always blended with the Ti II line at λ4028.33 and the Mn I line at λ4028.59 and therefore was not used, but no problems with blending were encountered with the other two sulphur lines so no spectrum synthesis was necessary when analysing this element. Table 5.6 shows the mean abundance. Usually there was good consistency between the abundances determined from the two lines but HR7361, υ Her and ζ Dra show differences of up to 0.6 dex between the abundances, which is curious as the other stars do not show this. The lines are weak so this could due to measurement errors and noise.

Table 5.6: Mean sulphur abundances

Star	S	σ_m/σ_{tot}	σ_s	Star	S	σ_m/σ_{tot}	σ_s
θ Leo	$\leq$7.28	–	–	ϕ Her	7.16	0.30	–
α Lyr	$\leq$7.36	–	–	υ Her	7.08±0.13	0.24	0.19
HR7098	6.75	0.35	–	87 Psc	6.91±0.03	0.22	0.04
21 Peg	7.27	0.16	–	HR7664	6.40±0.10	0.23	0.14
ζ Drac	7.44±0.14	0.27	0.20	HR7361	6.49±0.28	0.20	0.40
21 Aql	7.29±0.04	0.25	0.06	HR6997	6.99±0.01	0.22	0.01
τ Her	7.41±0.04	0.22	0.06				

5.3.6 Calcium

There are three lines of calcium available in the optical region.

The Ca I line at λ4226 is often weak (*i.e.*, below 10mÅ) but it has reliable atomic data (Wiese et al 1969 B+) and is not blended or subject to saturation. The singly-ionised K and H lines at λ3933 and 3968 respectively are both strong and obvious in the spectra of all the sample stars, but problems can be associated with the analysis of each line. The Ca-H line is blended with the Balmer $H\epsilon$ line and was not analysed, but the strong Ca-K line was analysed using synthesis techniques as abundances for the hotter stars could not be determined using Ca I alone.

The first step for Ca II was to ensure that a Stark damping constant was known for the line and this came from Roberts and Eckerle (1985). The line then was synthesised using an initial solar abundance, which was then varied until a fit to the line wings was achieved, as it was found that a good fit to the line core was difficult to achieve. This situation is unlikely to be due to interstellar contamination, as the observed line core became progressively deeper with respect to the synthetic line at cooler temperatures.

Dworetsky (*priv. comm*) suggests this behaviour may be due to line-forming taking place in higher layers of the star (above $\log\tau$=-4) which is not taken into account by the stellar atmosphere. This is borne out by the presence of a mismatch in cooler stars where the K-line is strongest. A layer of calcium at a lower optical depth could account for this. Hotter stars also show a profile asymmetry, clearest in HR6997, which is *plausibly* caused by interstellar blending. Despite these problems the fits obtained were satisfactory and do not prevent the determination of $\log A$ with reasonable accuracy. Results shown in Table 5.7.

Table 5.7: Calcium abundances

Star	Ca I	σ_{tot}	σ_s	Ca II	σ_{tot}*	σ_s	Ca	σ_m	σ_s
θ Leo	6.18	0.71	–	6.35	0.45	–	6.27±0.13	0.42	0.18
α Lyr	5.90	0.42	–	5.78	0.45	–	5.84±0.01	0.38	0.01
HR7098	6.65	0.53	–	6.42	0.49	–	6.53±0.06	0.43	0.08
21 Peg	5.99	0.23	–	6.15	0.49	–	6.08±0.01	0.42	0.01
ζDrac	–	–	–	6.50	0.42	–	6.50	0.42	–
21 Aql	$\leq$6.50	–	–	6.60	0.46	–	6.60	0.46	–
τ Her	$\leq$6.50	–	–	6.50	0.47	–	6.50	0.47	–
ϕ Her	6.40	0.38	–	6.60	0.42	–	6.50±0.15	0.32	0.21
υHer	–	–	–	6.70	0.43	–	6.70	0.43	–
87 Psc	–	–	–	6.70	0.43	–	6.70	0.43	–
HR7664	–	–	–	6.70	0.46	–	6.70	0.46	–
HR7361	–	–	–	7.10	0.49	–	7.10	0.49	–
HR6997	–	–	–	7.10	0.45	–	7.10	0.45	–

* assuming error on synthetic line of 20%

5.3.7 Scandium

Scandium exhibits a single line of doubly ionised scandium at λ4246. Results from this single line are shown in Table 5.8. This line is the strongest scandium line at this temperature, but it is often weak or not visible in many of the stars. There appears to be some interference with the scandium line profile in HR7361, so blending from an unknown line should not be ruled out. HR6997 shows no scandium line in its spectrum and no blending species is shown in the RMT or Kurucz (1992) close to the Sc II line.

Table 5.8: Scandium abundances

Star	Sc	σ_{tot}	Star	Sc	σ_{tot}
θ Leo	2.87	0.33	ϕ Her	4.16	0.52
α Lyr	2.84	0.39	υ Her	2.91	0.27
HR7098	2.76	0.27	87 Psc	4.35	0.24
21 Peg	2.32	0.26	HR7664	3.17	0.16
ζ Drac	3.04	0.28	HR7361	4.61	0.24
21 Aql	3.12	0.38	HR6997	$\leq$3.00	–
τ Her	$\leq$3.46	–			

5.3.8 Titanium

Titanium is very well represented in the spectra of the programme stars, and a total of 23 strong lines were selected for analysis. Occasionally the lines at λ4417 and 4418 were blended with one another in spectra of stars with high $v \sin i$ values. Some titanium lines were not seen in hotter stars. The internal consistency between lines was generally good and the mean results are shown in Table 5.9.

5.3.9 Vanadium

Vanadium has a few weak lines available at $\lambda\lambda$ 3951, 4005 and 4035 but atomic data are not available from a single source for these lines. The $\log gf$ sources do not coincide so a rationalisation of the $\log gf$ values by converting them to the same

Table 5.9: Titanium abundances

Star	Ti	σ_m/σ_{tot}	σ_s
θ Leo	5.25±0.05	0.18	0.18
α Lyr	4.80±0.05	0.20	0.17
HR7098	5.33±0.05	0.20	0.13
21 Peg	4.81±0.04	0.13	0.19
ζ Drac	4.64±0.07	0.14	0.18
21 Aql	4.69±0.06	0.17	0.19
τ Her	4.90	0.27	–

Star	Ti	σ_m	σ_s
ϕ Her	5.47±0.10	0.14	0.37
υ Her	5.93±0.04	0.15	0.10
87 Psc	6.73±0.07	0.15	0.16
HR7664	5.85±0.08	0.10	0.31
HR7361	5.61±0.10	0.16	0.38
HR6997	5.62±0.12	0.15	0.33

reference frame is not possible. Some systematic errors between line abundances are to be expected for vanadium, giving rise to poor internal consistency and an apparently large random error. The analyses performed in this thesis appear to be the most extensive for this element. Results are shown in Table 5.10.

Table 5.10: Vanadium abundances

Star	V	σ_m/σ_{tot}	σ_s
θ Leo	4.35±0.08	0.20	0.12
α Lyr	4.44	0.27	–
HR7098	4.12±0.11	0.17	0.19
21 Peg	3.91±0.03	0.20	0.04
ζ Drac	$\leq$3.95	–	–
21 Aql	$\leq$4.01	–	–
τ Her	$\leq$4.59	–	–

Star	V	σ_m/σ_{tot}	σ_s
ϕ Her	3.43±0.06	0.50	0.09
υ Her	3.92	0.29	–
87 Psc	4.28±0.13	0.20	0.18
HR7664	4.16±0.15	0.15	0.21
HR7361	4.94	0.17	–
HR6997	4.99	0.30	–

5.3.10 Chromium

Five unblended lines of Cr II at $\lambda\lambda$ 3979, 4242, 4558, 4588 and 4003 and three unblended lines of Cr I at $\lambda\lambda$ 4254, 4274 and 4289 were used in the analysis, but as in vanadium the oscillator strength source that was available differed between the two chromium ionisation stages; again no attempt was made to reduce the data to the same $\log gf$ scale because there were no common lines to the two sources (the

neutral chromium values are likely to be of high quality). This could in turn give rise to a systematic error between the two stages and an unknown systematic error in the final mean abundance.

The internal consistency between lines is variable from star to star. The normal stars show a chromium abundance consistent with the solar abundance of 5.7 dex with some scatter (Figure 7.10). Mean abundances are shown in Table 5.11.

Table 5.11: Chromium abundances

Star	Cr I	σ_m	σ_s/σ_{tot}	Cr II	σ_m/σ_{tot}	σ_s	Cr	σ_m/σ_{tot}	σ_s
θ Leo	5.84±0.04	0.30	0.05	6.07±0.03	0.22	0.06	5.99±0.05	0.19	0.12
α Lyr	5.37±0.02	0.28	0.03	5.64±0.05	0.18	0.09	5.48±0.07	0.17	0.16
HR7098	5.94±0.07	0.28	0.04	5.79±0.05	0.18	0.05	5.85±0.05	0.15	0.12
21 Peg	5.80±0.08	0.26	0.12	5.71±0.06	0.13	0.10	5.74±0.06	0.09	0.16
ζ Drac	–	–	–	5.43±0.03	0.16	0.05	5.43±0.03	0.16	0.05
21 Aql	–	–	–	5.31±0.02	0.16	0.04	5.31±0.02	0.16	0.04
τ Her	–	–	–	5.51±0.14	0.19	0.20	5.51±0.14	0.19	0.20
ϕ Her	6.80	0.31	–	6.66±0.07	0.15	0.14	6.65±0.07	0.13	0.15
υ Her	–	–	–	6.04±0.11	0.14	0.19	6.04±0.11	0.14	0.19
87 Psc	–	–	–	6.50±0.09	0.18	0.15	6.50±0.09	0.18	0.15
HR7664	–	–	–	5.08	0.23	–	5.08	0.23	–
HR7361	–	–	–	6.10±0.00	0.10	0.00	6.10±0.00	0.10	0.00
HR6997	–	–	–	5.67±0.19	0.19	0.27	5.67±0.19	0.19	0.27

5.3.11 Manganese

Three strong lines of neutral manganese were chosen for the analysis at $\lambda\lambda$ 4030, 4034 and 4041. These are the strongest lines and are only visible in the normal stars of low effective temperature.

Four Mn II lines were also selected on the grounds of their strength and apparent freedom from blendings; these were at $\lambda\lambda$3917, 4363, 4365 and 4478. 4326 was always blended so abundances derived from this were marked 'B' in appendices B1 and B2. 4206 had hyperfine structure (see section 7.25). The consistency between manganese lines is good, but the manganese stars ϕ Her, υ Her, HR7361, HR6997 and 87 Psc exhibited an anomalously strong line at λ4206, whereas HR7664, with a low Mn abundance compared to the other HgMn stars, did not. Further discussion of this

phenomenon can be found in Chapter 7. The mean abundances are shown in Table 5.12.

Table 5.12: Manganese abundances

Star	Mn I	σ_m/σ_{tot}	σ_s	Mn II	σ_m/σ_{tot}	σ_s	Mn	σ_m/σ_{tot}	σ_s
θ Leo	5.39	0.33	–	5.75	0.37	–	5.57±0.17	0.24	0.25
α Lyr	5.38±0.03	0.26	0.05	–	–	–	5.38±0.03	0.26	0.05
HR7098	–	–	–	5.64±0.01	0.25	0.02	5.64±0.01	0.25	0.02
21 Peg	–	–	–	–	–	–	–	–	–
ζ Drac	–	–	–	–	–	–	–	–	–
21 Aql	–	–	–	–	–	–	–	–	–
τ Her	–	–	–	–	–	–	–	–	–
ϕ Her	7.01±0.05	0.22	0.09	6.86±0.01	0.16	0.09	6.95±0 .04	0.12	0.09
υ Her	7.03±0.01	0.29	0.02	7.12±0.03	0.18	0.06	7.09±0 .03	0.16	0.06
87 Psc	7.77±0.03	0.22	0.05	7.33±0.05	0.20	0.10	7.52±0.09	0.15	0.23
HR7664	Z	–	–	6.38±0.02	0.08	0.03	6.38±0.02	0.08	0.03
HR7361	7.98±0.07	0.29	0.12	8.04±0.06	0.14	0.09	8.01±0.04	0.14	0.10
HR6997	8.27±0.03	0.27	0.06	8.05±0.05	0.12	0.10	8.02±0.05	0.12	0.16

5.3.12 Iron

22 strong unblended lines were selected for Fe II from the spectrum of υ Her. Iron is an important element with many lines of neutral and singly ionised atoms. Five Fe I lines were also available; these are seen in cooler stars. Spectrum synthesis was not necessary for this element due to the large choice of apparently single lines, but it was surprising that the internal consistency of the iron lines is poor in some cases, despite good ξ fits, suggesting the possible presence of blends in some stars. Mean abundances are shown in Table 5.13. There is generally good agreement between the ionisation stages, as the $\log gf$ source (Fuhr *et al* 1988) was used for the lines and neutral and singly ionised iron is plentiful in this temperature range.

5.3.13 Nickel

Four nickel lines are available in the spectra of normal and HgMn stars. The Ni I line at λ4401 is very weak or not present in the normal star sample and not seen at all in the HgMn star sample but three of the least-blended Ni II lines at $\lambda\lambda$4015, 4067

Table 5.13: Iron abundances

Star	Fe I	σ_m	σ_s	Fe II	σ_m	σ_s	Fe	σ_m	σ_s
θ Leo	7.71±0.07	0.40	0.10	7.65±0.04	0.20	0.18	7.67±0.03	0.20	0.14
α Lyr	7.32	0.22	–	6.95±0.02	0.18	0.07	6.97±0.02	0.20	0.07
HR7098	7.61±0.03	0.24	0.15	7.59±0.04	0.19	0.16	7.59±0.00	0.17	0.01
21 Peg	7.36±0.07	0.20	0.15	7.61±0.06	0.18	0.16	7.58±0.02	0.10	0.09
ζ Drac	7.46±0.04	0.20	0.14	7.43±0.04	0.09	0.16	7.44± 0.02	0.08	0.15
21 Aql	7.32	0.35	–	7.45±0.05	0.10	0.18	7.43±0.04	0.10	0.16
τ Her	–	–	–	7.33±0.06	0.11	0.20	7.33±0.06	0.11	0.20
ϕ Her	7.16±0.02	0.14	0.04	7.53±0.04	0.09	0.13	7.52±0 .03	0.09	0.01
υ Her	7.39±0.01	0.15	0.03	7.32±0.03	0.0.09	0.13	7.33±0.01	0.11	0.03
87 Psc	7.34±0.32	0.26	0.45	6.98±0.09	0.08	0.24	7.02±0 .08	0.08	0.34
HR7664	8.40±0.05	0.27	0.10	8.26±0.06	0.10	0.23	8.30±0.04	0.09	0.19
HR7361	17.90±0.00	0.34	0.01	7.62±0.07	0.10	0.30	7.70±0.04	0.09	0.19
HR6997	–	–	–	7.85±0.05	0.11	0.13	7.85±0.05	0.11	0.13

and 4362 were used in this work; λ4015 and λ4362 were not usually blended and λ4067 was only used for analysis when it was unblended. The $\log gf$ values provided by Kurucz and Peytremann (1975) were used instead of those from Warner (1967) (corrected by Smith 1976) in line with the recommendations of Adelman (1989) and preliminary analysis which gave a poor consistency between lines.

Furthermore, the normal stars appeared to be systematically rich in nickel using Warner/Smith $\log gf$ values. No spectrum synthesis was necessary when analysing nickel as only clean lines were analysed. Results are shown in Table 5.14.

5.3.14 Gallium

Gallium is present in two ionisation stages in the programme stars, but the aim was to analyse the neutral gallium lines at λ4032 and 4172. It was hoped it would be possible to compare the mean abundance derived from these lines with the ongoing work of Smith (1996, in prep) for singly ionised lines, based on the same extracted Lick échelle data and IUE data but these data were not available at the submission

Table 5.14: Nickel abundances

Star	Ni I	σ_m	σ_s	Ni II	σ_m	σ_s	Ni	σ_m	σ_s
θ Leo	–	–	–	5.62±0.08	0.21	0.14	5.62±0.08	0.21	0.14
α Lyr	–	–	–	5.89±0.09	0.19	0.13	5.89±0.09	0.13	0.09
HR7098	6.43	0.32	–	6.26±0.31	0.16	0.53	6.30±0.24	0.15	0.50
21 Peg	6.59	0.20	–	6.32±0.05	0.20	0.08	6.41±0.13	0.19	0.15
ζ Drac	–	–	–	5.16	0.24	–	5.16	0.24	–
21 Aql	–	–	–	6.03±0.06	0.17	0.10	6.07±0.06	0.17	0.10
τ Her	–	–	–	5.98±0.04	0.20	0.05	5.98±0.04	0.20	0.05
ϕ Her	–	–	–	6.02±0.06	0.20	0.11	6.02±0.06	0.20	0.11
υ Her	–	–	–	4.35±0.17	0.21	0.24	4.35±0.17	0.21	0.24
87 Psc	–	–	–	5.72±0.04	0.18	0.07	5.72±0.04	0.18	0.07
HR7664	–	–	–	5.74±0.03	0.13	0.04	5.74±0.03	0.13	0.04
HR7361	–	–	–	6.18	0.15	–	6.18	0.15	–
HR6997	–	–	–	6.13	0.24	–	6.13	0.24	–

time of this thesis.

No modern $\log gf$ values were found for Ga II. It could be possible in future to obtain astrophysical $\log gf$ values for these lines using the abundances for Ga II derived by Smith (1994). Bidelman and Corliss (1962) also found hyperfine structure in the transitions of Ga II, making this element difficult to study unless this structure is adequately modelled.

Ga I is strong in HgMn stars but there are several strong blending components also present at the position of both gallium lines, at λ4032 and λ4172. λ4172 is particularly contaminated.

It was necessary to synthesise the gallium lines in order to obtain an abundance. The abundances of the blending species are derived from other, unblended lines of the same species seen elsewhere in the spectrum. The wavelength of the blended line is fixed using surrounding lines as a reference point. The blend is then synthesised by increasing or decreasing the blending species until they fit the profile well. The galliun blended component is then introduced and the abundance obtained from the final fit for all the lines. When gallium is not overabundant, as is the case in normal

Table 5.15: Gallium abundances for normal stars

Species	Line	θ Leo	α Lyr	HR7098	21 Peg	ζ Dra	21 Aql	τ Her
Ti II	4171.91	5.4	4.6	5.3	4.8	5.5	4.7	4.8
Cr II	4171.90	5.9	5.5	5.9	5.5	5.5	5.3	5.5
Ga I	4172.04	$\leq$4.5	$\leq$3.0	$\leq$4.0	$\leq$4.50	–	–	–
S II	4032.81	$\leq$7.3	$\leq$7.4	7.6	7.1	7.4	7.3	7.4
Ga I	4032.99	$\leq$4.0	$\leq$3.0	$\leq$3.0	$\leq$4.0	$\leq$4.5	–	–
Fe II	4032.99	7.7	7.0	7.5	7.4	7.6	7.5	7.3
Mn I	4033.06	5.3	$\leq$5.3	5.7	5.3	$\leq$5.8	$\leq$5.8	–

Table 5.16: Gallium abundances for HgMn stars

Species	Line	ϕ Her	υ Her	87 Psc	HR7664	HR7361	HR6997
Ti II	4171.91	6.2	6.5	7.1	5.9	5.5	5.6
Cr II	4171.90	6.8	6.0	6.7	5.1	6.1	5.7
Ga I	4172.04	5.8	6.0	6.5	6.1	6.8	–
S II	4032.81	7.2	7.0	7.0	6.8	6.1	7.2
GaI	4032.99	6.0	6.1	–	–	–	–
Fe II	4032.99	7.8	7.7	7.6	8.3	8.0	8.0
Mn I	4033.06	7.0	7.0	7.5	6.4	8.4	8.2

stars, it is usually only possible to obtain an upper limit; however, for the HgMn stars, $\log A$ turned out to be $\geq$5 dex and so it was possible to obtain both a fit to the lines and an error estimate based on σ_{tot} for each line.

The synthesised abundances of the gallium blending species and gallium are shown in Tables 5.15 and 5.16 along with mean abundances for gallium in Table 5.17.

5.3.15 Strontium

Two strong lines of Sr II at $\lambda\lambda$ 4077 and 4215 were analysed, both of which are saturated and occasionally blended. The lines were synthesised when blended in ϕ Her, υ Her and HR6997 and Stark damping was also taken into account when

Table 5.17: Gallium abundances

Star	Ga I	σ_m	σ_s
θ Leo	–	–	–
α Lyr	–	–	–
HR7098	–	–	–
21 Peg	–	–	–
ζ Drac	–	–	–
21 Aql	–	–	–
τ Her	–	–	–

Star	Ga I	σ_m/σ_{tot}	σ_s
ϕ Her	5.90±0.10	0.19	0.07
υ Her	6.05±0.05	0.18	0.07
87 Psc	6.50	0.18	–
HR7664	6.10	0.25	–
HR7361	6.80	0.22	–
HR6997	–	–	–

calculating the abundances, which are shown in Table 5.18.

5.3.16 Yttrium

Yttrium has five lines available, of which $\lambda\lambda$3950, 3982, 4309 and 4398 are unblended. This element shows strong overabundances in HgMn stars, of which ϕ Her is apparently the strongest, with an overabundance of 2.7 dex compared to the solar value (Anders and Grevesse 1989). See Table 5.19 for the results.

5.3.17 Zirconium

Zirconium was only identified with certainty in the spectrum of ϕ Her, where there is an overabundance well over a factor of ten greater than that seen in the Sun. The normal star θ Leo shows several lines at the correct wavelengths for zirconium; which lends great weight to the identification of zirconium in this star, and on analysis of these lines an overabundance was yielded. Weak zirconium lines at λ3991 and 3998 were also seen in HR7098 and 21 Peg and these yielded a solar abundance (Anders and Grevesse 1989) when analysed. The remainder of the normal and HgMn stars, including υ Her, did not show zirconium in their spectra. The results are shown in Table 5.20.

Table 5.18: Strontium abundances

Star	Sr	σ_m/σ_{tot}	σ_s
θ Leo	3.59±0.08	0.52	0.11
α Lyr	2.16±0.02	0.37	0.02
HR7098	3.50±0.16	0.36	0.22
21 Peg	2.91	0.47	–
ζ Drac	2.66±0.09	0.18	0.13
21 Aql	2.79±0.08	0.21	0.12
τ Her	–	–	–

Star	Sr	σ_m/σ_{tot}	σ_s
ϕ Her	3.96±0.08	0.26	0.11
υ Her	3.89±0.02	0.24	0.03
87 Psc	2.68±0.06	0.18	0.08
HR7664	–	–	–
HR7361	3.04	0.28	–
HR6997	3.73	0.26	–

5.3.18 Barium

Two lines of singly ionised barium are available in the optical region: $\lambda\lambda$4554 and 4130; the former was chosen for the analysis because the other optical barium line at λ4130 was usually not visible and is always severely blended with Si II λ4130.

The abundances were calculated from the measured equivalent widths which are tabulated in Tables 3.1 and 3.2. Barium is only visible at solar abundances in normal stars with effective temperatures below approxmately 13 000K, and these stars show a systematic overabundance. Upper limits were determined for HgMn stars which did not show the barium line at λ4554.

Table 5.21 shows the abundances; the solar abundance is at 2.06 dex (Anders and Grevesse 1989).

Table 5.19: Yttrium abundances

Star	Y	σ_m/σ_{tot}	σ_s
θ Leo	2.77±0.05	0.36	0.06
α Lyr	2.17±0.06	0.50	0.10
HR7098	2.62±0.04	0.23	0.05
21 Peg	2.30	0.64	–
ζ Drac	–	–	–
21 Aql	–	–	–
τ Her	–	–	–

Star	Y	σ_m	σ_s
ϕ Her	4.77	0.26	–
υ Her	3.68	0.34	–
87 Psc	4.66±0.06	0.16	0.13
HR7664	4.02±0.09	0.16	0.13
HR7361	4.68±0.04	0.14	0.06
HR6997	–	–	–

Table 5.20: Zirconium abundances

Star	Zr	σ_m	σ_s
θ Leo	3.21±0.06	0.22	0.08
α Lyr	–	–	–
HR7098	2.65	0.17	–
21 Peg	$\leq$2.52	–	–
ζ Drac	–	–	–
21 Aql	–	–	–
τ Her	–	–	–

Star	Zr	σ_m	σ_s
ϕ Her	4.75	0.16	–
υ Her	–	–	–
87 Psc	–	–	–
HR7664	–	–	–
HR7361	–	–	–
HR6997	–	–	–

Table 5.21: Barium abundances

Star	Ba	σ_{tot}
θ Leo	3.34	0.59
α Lyr	2.21	0.39
HR7098	3.00	0.58
21 Peg	2.76	0.56
ζ Drac	–	–
21 Aql	–	–
τ Her	–	–

Star	Ba	σ_{tot}
ϕ Her	4.07	0.32
υ Her	3.35	0.40
87 Psc	3.66	0.30
HR7664	$\leq$3.08	–
HR7361	$\leq$3.21	–
HR6997	$\leq$3.40	–

Chapter 6

Comparison to the literature

The abundance patterns for each star taken from this thesis and from the literature can be found in the sections which follow. These results are examined star-by-star as the sample size of HgMn stars is too small for a statistical analysis of element behaviour to be performed. Instead, comparison is made between the work here and that detailed in the literature for each star. This is particularly important for the normal stars as they can be used as a check for the presence of systematic errors in the spectra of HgMn stars.

6.1 The normal stars

6.1.1 θ Leo (A2V)

Myron Smith (1974) undertook the first analysis of this star, which at the time was the A2V spectral standard (Cowley et al 1969). Smith was interested in stars at the border of the Am-star domain; using an early ATLAS model he discovered the metal-rich spectrum of θ Leo was enhanced in iron, strontium and calcium and that abundances from the first and second ionisation stages of iron gave different results.

A decade later the work of Adelman (1986) also showed overabundances in strontium (0.8 dex) and zirconium (0.5 dex), though a normal abundance was obtained for the remaining optical lines of the other elements he studied. One peculiarity of Adelman's work was that lines from the first and second ionisation stages of man-

ganese gave different abundances when a mean value was calculated. This is much like the different abundances of Fe II and Fe I seen by Smith (1992) for this star.

In 1989 and 1990 Lemke published an in-depth analysis of six elements for a selection of A-type stars which included θ Leo. Lemke found that, as in θ Leo, strontium was overabundant (in this case 1.1 dex) in many stars of the normal star sample as was barium (1 dex). This result was further enhanced when calculations were repeated in conditions of nLTE where Lemke found a discrepancy between Fe I and Fe II which was mirrored by the work of Smith; this became more pronounced in the calculations performed under the assumption of nLTE.

K.C. Smith (1992) next looked at θ Leo and based this work on UV data from the IUE which included nine of the seventeen elements studied in this project. Smith detected a possible enhancement in the abundances of gallium (0.7 dex). Chromium (0.3 dex) and nickel (0.5 dex) on the other hand, were slightly underabundant in the UV.

This work finds θ Leo effectively solar in the abundance patterns seen for most elements. The exception to this is seen in the elements barium (1.2 dex), strontium (0.7 dex) and zirconium (0.4 dex), which are overabundant. Again, neutral and singly ionised iron give slightly different abundances.

The work of Adelman and M.A. Smith and that presented here all describe overabundances in barium, strontium and zirconium and confirms θ Leo as a mild metallic-lined A- star. There is also general agreement between the results of K.C. Smith and that seen in this project but it was not possible to confirm or reject the gallium overabundances of K.C. Smith as Ga I lines were not visible in this star. Smith's results for magnesium were definitely higher than in this work, while Lemke's results for this star were not significantly different in LTE from my work or that of Adelman except in the case of strontium, which was more enhanced in Lemke's paper.

6.1.2 α Lyr (A0Va)

Hunger (1955) published the first analysis of Vega. He devised a number of model atmospheres for different stellar effective temperatures, but finally settled on a $T_{\rm eff}$

of 9500K. Smith (1974) analysed Vega in the same work as θ Leo; he stated he had found a solar abundance, but close inspection of his results reveal abundance anomalies much like those commonly derived for Vega nowadays; iron is underabundant, phosphorus high and nickel low in abundance. Dreiling and Bell (1980) then looked at the spectrum of Vega in some detail and derived their own model atmosphere. They also obtained a low iron abundance, and suggested this could be due to a systematic error from nLTE effects of unknown origin in the spectrum. This hypothesis overlooked the inference that A-stars with solar iron abundances calculated under LTE would then all be overabundant!

Sadakane and Nishimura (1981) found aluminium and silicon to be deficient. Iron-peak and heavier elements were found to be underabundant by $\sim$0.4 dex. A small increase of calcium, strontium and barium abundances were seen in an nLTE analysis of the same data set in unpublished work by Borsenberger and Praderie and mentioned in Sadakane and Nishimura (1981) but the elements were still underabundant.

Adelman and Gulliver's (1990) work provided a lower microturbulence ($1.3 \mathrm{kms}^{-1}$) than previous work and obtained a mean underabundance of metals of 0.6 dex, which made Vega slightly more metal poor than shown by the abundances found by Dreiling and Bell and Sadakane and Nishimura. Adelman attributes this fact to 'better data'.

Lemke (1989,1990) found iron, barium, strontium and calcium to be underabundant. These elements were again slightly more enhanced in nLTE calculations. He also found a discrepancy between the abundances of the different species of iron when calculated under nLTE; this was not so noticeable under LTE. This is surprising as correctly allowing for the effects of nLTE *should improve* the agreement between different ionisation stages not decrease it.

Smith and Dworetsky's (1993) and Smith's (1993) work in the UV presented underabundances in this star of nickel, silicon, iron, manganese (0.4 dex) and aluminium and confirmed the low metallicity in this star.

Finally, in this work α Lyr was not found to show a solar distribution of abundances; in accordance with the previous work it is confirmed that this star is un-

derabundant in the elements nickel (0.3 dex), silicon (0.4 dex), strontium (0.7 dex), manganese (0.5 dex), aluminium (0.6 dex) and iron (0.6 dex).

This work confirms Adelman and Gulliver's work that Vega is a metal deficient star with a microturbulence of $1.2 kms^{-1}$. The possibility that Vega is a rapidly-rotating pole-on star is discussed in Chapter 1. This is important as this may help explain why a narrow lined star such as Vega does not show Am-star abundance patterns. Lemke's (1990) LTE results for Vega seem much lower than the abundances derived here.

6.1.3 HR7098 (A0Vs)

Smith (1992) appears to have performed the first abundance analysis of this star and to have studied it in both the UV and the optical region. Chromium was found to be solar in the optical region, but was overabundant by 0.7 dex in the UV; iron was solar in the UV and in the optical region. In the optical region Smith found a difference between Ni I and Ni II of over 1 dex. Titanium was only very slightly overabundant (0.25 dex) in the optical region. Of the remaining elements, aluminium and manganese were of solar abundance; although manganese is apparently overabundant in the UV.

The aluminium, gallium, magnesium, silicon and zirconium abundances in this work are essentially solar and barium exhibits an overabundance (0.9 dex), although the line is so weak there is a large error on the abundance. Strontium, vanadium, nickel and yttrium were also found to be overabundant but sulphur (-0.45 dex) and scandium (-0.35 dex) show lower abundances than the Sun (Anders and Grevesse 1989).

Lemke's work on A-stars is echoed in this star by the overabundance of strontium which matches the results obtained for his sample of normal A-stars, although he did not include HR7098 in his work. The results presented here generally agree with the UV abundances of Smith (1992) although Smith's abundance for magnesium is 0.3 dex higher than in this thesis.

6.1.4 21 Peg (B9.5V)

Cowley (1980) classified this star as a superficially-normal star by examining its spectrum and finding strong lines of chromium, iron, scandium, titanium and vanadium. Sadakane's (1981) analysis of 21 Peg then found an underabundance in aluminium (0.4 dex), calcium, iron (0.5), magnesium (0.25 dex) and nickel (0.3 dex), an overabundance in manganese (0.55 dex) and yttrium (0.67 dex) and a solar abundance for chromium and nickel.

A decade later Smith (1992) studied 21 Peg's UV spectrum and found abundances for aluminium, chromium, iron, magnesium, silicon and nickel which differ by less than 0.1 dex from the solar abundance. Manganese was slightly enhanced by 0.2 dex.

The aluminium abundance in this work for 21 Peg has also been found to be solar, although calcium (-0.3 dex) and scandium (-0.8 dex) are possibly underabundant. Unlike the three cooler stars in this sample strontium is not obviously overabundant; and unlike α Lyr, yttrium is solar.

The aluminium abundance from this work and that of Smith is solar, but that obtained by Sadakane is 0.4 dex underabundant. Sadakane's nickel and silicon abundance enhancements (0.21 and 0.13 dex respectively) are also much smaller than that obtained by Smith and in this work; however calcium, chromium, scandium and strontium are solar in all three works and agree extremely well. The marginal enhancement of yttrium (0.2 dex) seen in this work is much more exaggerated in the work of Sadakane (1981) (0.6 dex). Basically this star shows a Vega-like underabundance of the key elements calcium, silicon and nickel and an enhancement of yttrium. However, the abundances of manganese and iron do not follow the abundance patterns seen in the cooler star.

6.1.5 ζ Dra (B6 III)

Pagel (1974) first studied silicon; this was followed in 1983 by the work of Sadakane et al (1983) who studied aluminium abundances and found a possible underabundance of 0.2 dex.

No further work was done on the abundances of ζ Dra until 1992, where Smith's results in the UV for ζ Dra show a general underabundance for the elements he studied, especially in iron. However, silicon and aluminium were found to be of solar abundance.

This work found the abundances of aluminium, silicon and magnesium in ζ Dra to be consistent with solar abundances and nickel and chromium underabundant with respect to the Sun. No obvious overabundance was seen in strontium or barium, which is unlike the cooler stars studied by Lemke (1989,1990).

This star is the only case where Smith's magnesium abundance is lower than that presented in this thesis. A solar value for magnesium was obtained here but Smith obtained a 0.6 dex underabundance. Apart from aluminium, silicon and manganese, all of which have abundances within 0.1 dex of the respective solar abundances, ζ Dra is anomalously underabundant in the work of Smith, iron (-1.0 dex) being particularly affected. The only exception to this rule seems to be the nickel abundance (0.7 dex), where Smith obtained a higher nickel abundance than seen in this work. A possible explanation for these anomalous results is discussed later in this chapter.

6.1.6 21 Aql (B8II-III)

The first abundance analysis of this star appears to have been undertaken by Adelman (1991), who found that 21 Aql was slightly underabundant in aluminium (-0.3 dex), iron (0.25 dex), chromium (0.3 dex), nickel (0.4 dex) and titanium (0.6 dex). Calcium was the only element found by Adelman to have a solar abundance.

Smith (1993) published an overabundance for magnesium in this star and found most other abundances to be solar, with the exception of aluminium which appears underabundant and manganese (Smith and Dworetsky 1993) which shows a curious overabundance of 0.8 dex.

In this project 21 Aql was found to show a slight underabundance in aluminium (0.17 dex) and titanium but a solar abundance was found for strontium, much as in 21 Peg. The remaining elements in the spectrum were solar in abundance. Barium was not seen in this star so it was not possible to obtain an abundance. Manganese

was not visible in this work and was certainly not overabundant.

None of the workers detected barium lines so the behaviour of this element in hot stars could not be judged. Manganese only appears overabundant in the work of Smith and magnesium is also curiously overabundant.

6.1.7 τ Her (B5IV)

τ Her is the hottest star in this sample and is a fairly rapid rotator, which means few unblended lines are available for study. The star was analysed initially by Adelman (1991) who found underabundant sulphur (0.2 dex), aluminium (0.2 dex), nickel (negligible) and iron (0.3 dex) and high abundances of titanium (+0.6 dex).

Smith (1992) looked at this star in the UV and found a magnesium overabundance of 0.4 dex. Aluminium (-0.3 dex) and nickel (-0.3 dex) were again proved to be underabundant but iron and chromium appeared to be of solar abundance.

According to the results obtained here sulphur is possibly overabundant by 0.2 dex, nickel was found to be possibly underabundant by the same amount and chromium solar. Iron (-0.2 dex) was slightly underabundant and titanium solar.

The results in this thesis for this star are all found within $1\sigma_m$ of the solar abundances, in contrast to Adelman's low abundances for this star. Smith's work coincides more with this project than Adelman except in the case of magnesium which is found to be 0.4 dex more overabundant than the solar-consistent abundance obtained here. Both Smith and Adelman obtained lower abundances in sulphur in τ Her than for the other normal stars.

6.2 The HgMn stars

6.2.1 ϕ Her (B9pMn)

ϕ Her seems to be a popular HgMn star for analysis. Searle and Sargent (1964) first included this star in their survey and found that magnesium and silicon were of normal abundance, A paper by Zimmerman et al (1970) deals with an in-depth study of this star (referred to as a 'manganese star') and the results reflect the HgMn

star pattern of enhanced manganese, strontium and yttrium as well as enhanced zirconium and a slight deficiency in chromium. However, the results from individual species showed discrepancy between the abundances of the same element. Cr I and II differ by over 1 dex and Fe I and II are 0.5 dex apart. The other species show consistent abundances.

Heacox (1979) included ϕ Her in a study of the abundances of HgMn stars using early Kurucz model atmospheres. Silicon, titanium, iron and chromium are often nearly solar in HgMn stars but here there were very strong overabundances. Manganese and strontium are typically overabundant and scandium was found to be overabundant by 1.7 dex. Sadakane's study found aluminium to be underabundant by 1.1 dex.

Guthrie (1984) studied a sample of HgMn stars. For ϕ Her he found an overabundance of 0.7 dex for chromium, a slight overabundance for phosphorous and an enhancement of over 1 dex for titanium. Yttrium was highly enhanced, by 2 dex, and zironium was found to be $\sim$1.5 dex above the solar abundance. Nickel was so underabundant only an upper limit could be obtained and iron gave a solar abundance. Adelman (1988) studied ϕ Her and found that there is a difference of 0.5 dex between the abundances of Mg I and Mg II but that the abundances for different ionisation stages for other elements match well.

Smith (1992) found an underabundance of 0.8 dex in aluminium, a high abundance of chromium and a solar abundance for magnesium. Manganese was mildly overabundant and the abundance of gallium was found to be 5.5 dex, $\sim$1000$\times$ the solar concentration.

Redfors and Cowley (1993) looked at the spectrum of Y III and Zr III in the UV and found evidence of departure from LTE ionisation balance in yttrium as the third yttrium spectrum gave a higher abundance than the spectrum of the first ionisation stage.

This work found strong overabundances of barium, chromium, gallium, manganese, strontium, zirconium and vanadium while scandium was slightly underabundant.

All authors found a clear overabundance of zirconium. Silicon's low abundance

obtained by Adelman was not replicated by other authors; Adelman also provided the lowest scandium and magnesium abundance but Smith's abundance of gallium was the lowest. Heacox showed a consistent overabundance in all the elements except gallium, nickel, calcium and yttrium; normal elements are exaggerated and normally overabundant elements are sometimes found to be increased by a factor of 10.

6.2.2 υ Her (B9III)

Adelman and Fuhr (1985) first found an overabundance of gallium for this star of 3.8 dex and a strong underabundance of nickel of 1.9 dex. The elements scandium, silicon, iron and calcium were found to be within 0.2 dex of the solar abundance but magnesium was underabundant by 0.3 dex and chromium was overabundant by 0.3 dex. Yttrium (1.6 dex), strontium (1.0 dex), phosphorus (0.8 dex), and manganese (1.7 dex) were all found to be overabundant.

Heacox (1979) found an enhancement of all the elements he studied except magnesium, which had a clear 1 dex underabundance and nickel which appeared solar, whilst Guthrie (1984) found that chromium was solar, titanium (0.7 dex), gallium (4.0 dex) and manganese (1.5 dex) overabundant whilst iron (-0.3 dex) and magnesium (-0.7 dex) were underabundant. Smith found an underabundance of aluminium (1.0 dex), nickel (0.7 dex), iron (0.4 dex) and magnesium (0.3 dex).

The results from this project show barium (1.3), chromium (0.3 dex), gallium (4.3 dex), strontium (1.0 dex), manganese (1.7 dex), yttrium (1.6 dex) to be overabundant, whilst scandium, silicon and vanadium and silicon are solar.

Heacox's results seem much higher than mine or Smith's, but Smith and Heacox match in magnesium abundance. Generally Heacox's results are enhanced with respect to other work except for nickel which is solar, magnesium which is underabundant and gallium which is similar in abundance to all published work. Yttrium was only seen in the optical work of Smith (1992).

However, Smith does seem to give lower abundances than Heacox for strontium and titanium, but they match again for silicon, sulphur and scandium. This would imply that Heacox's work has a systematic difference in some elements, especially as Heacox shows systematic enhancement with respect to this work in all elements

except silicon. This is discussed in more detail later.

6.2.3 87 Psc (B8III)

Heacox (1979) found that calcium (0.7 dex), chromium (1.4 dex), gallium (2.7 dex), manganese (3.2 dex), scandium (1.4 dex) and titanium (2.2 dex) were overabundant whilst silicon and nickel (both 0.5 dex) and iron (0.4 dex) are underabundant. Smith (1992) performed a UV and an optical analysis for this star and so obtained additional results for yttrium (2.5 dex), scandium (1.4 dex) and titanium (2.2 dex). Overabundances were found in gallium (2.7 dex), manganese (2.0 dex), silicon and yttrium (1.65 dex) whilst iron gave a curiously low abundance of 6.4 dex. A solar abundance was found for chromium. This work found underabundances in magnesium, nickel, iron, silicon and strontium whilst vanadium, yttrium, manganese, phosphorus and chromium were overabundant.

There were large differences between Smith and Heacox's work of +1.2 dex for Mn, +0.3 dex for nickel, +0.8 dex for iron, +1.2 dex for chromium, and +0.5 dex for titanium, Heacox always having the larger abundance. Other elements show similarities between the two pieces of work. As an additional comment, this work found chromium to be overabundant but Smith found a solar abundance; however both this work and Smith obtained a very low iron abundance.

6.2.4 HR7664 (B9pHgMn)

This star was first analysed by Heacox (1979). He found chromium, nickel, scandium, silicon, strontium and calcium to be solar but large enhancements of iron, gallium, manganese, phosphorus and titantium. Magnesium was found to be underabundant. Guthrie (1984) looked at this star next and found a less enhanced overabundance for manganese and iron but the other elements were enhanced by a similar degree to Heacox (1979). Adelman (1988) found chromium only slightly underabundant but sulphur was extremely so, by 0.7 dex, as was scandium. Yttrium, vanadium and strontium were all enhanced and nickel and magnesium underabundant. Smith and Dworetsky's (1993) work gave results which were consistent with previous work except for nickel which was underabundant by 0.7 dex.

This work found chromium to be underabundant, as was nickel, magnesium and sulphur. Yttrium, scandium, phosphorous, manganese and gallium were overabundant and silicon of solar abundance.

The previous and current work on this star seems to be in agreement except in the case of Heacox whose iron and manganese abundances were $\sim$ 1 dex and 2 dex enhanced respectively. This work provides a new result for vanadium of 4.16 dex and good agreement in this star with the literature.

6.2.5 HR7361 (B9 pHgMn)

This star, near the hot boundary of the HgMn class, was first analysed by Heacox (1979), who found that calcium, iron, gallium, manganese, phosphorus and titanium were overabundant, as seems to be the case in most HgMn stars, magnesium was underabundant and nickel and silicon solar. Guthrie (1984) obtained a normal abundance for iron, titanium and chromium. Manganese, gallium, phosphorous, scandium and yttrium were underabundant. The concurrent work of Adelman (1992) and Smith and Dworetsky (1993), Smith (1994) gave different results for the elements gallium and magnesium, those for gallium being lower in the work of Smith and magnesium also being lower by 0.4 dex when compared to Adelman. Phosphorus, scandium, silicon, nickel and manganese followed the patterns of the previous work. Smith looked at HR7361 in the optical region and the UV, and found differences for the elements chromium, iron, magnesium and manganese.

The results from this project gave enhanced abundances for chromium, gallium, manganese, phosphorus, scandium, vanadium and yttrium. Sulphur was very underabundant, as was magnesium, whilst nickel gave a solar abundance.

6.2.6 HR6997 (B8II-III pHg)

This star is a fairly fast-rotating hot HgMn star. It was first analysed by Heacox (1979) who found a strong iron enhancement and further overabundances in manganese, phosphorous and calcium. It was not possible for Heacox to examine the abundances of titanium, vanadium and yttrium in this star.

Smith and Dworetsky (1993) looked at this star in the UV and the optical region; it was found that manganese was enhanced in both studies, but the UV abundance was slightly lower. Titanium and phosphorous abundances were enhanced, magnesium was underabundant and iron of normal abundance. No other abundances were obtained by these authors.

This work found aluminium to be 1.2 dex underabundant, chromium 0.6 dex underabundant and magnesium 0.6 dex underabundant, this being less enhanced as that found by Smith in the optical region. This work also presents new abundances for strontium and vanadium.

6.3 Summary

Of the normal stars, Vega and 21 Peg seem to be the most consistently metal-deficient, although some elements are deficient in one or two stars. Some elements show consistent abundance patterns; aluminium, for example, is consistently solar or just below solar abundance and silicon is consistently of solar abundance. The abundance of iron varies a great deal among the stars and this variation does not appear to be temperature-dependent.

The magnesium abundances derived by Smith are systematically high with respect to other work. For all sample stars there is a non-zero mean deviation, D, which was found to be

$$D = 0.26 \pm 0.21\text{dex} \tag{6.1}$$

between the abundances of magnesium derived by Smith and that from other work in the literature, excluding the abundances published by Heacox (1979), which is not a statistically significant result. The curious overabundance of manganese in 21 Aql recorded by Smith is not reproduced in the literature or by this thesis. ζ Dra appears to have provided Smith with systematically low abundances in all elements except nickel and aluminium.

Lemke's assertion that cool stars are overabundant in barium and strontium is borne out in the abundances of two of the normal stars, θ Leo and HR7098. The results from this project seem to confirm the modern view that there does not seem to be a standard 'normal' solar-abundance A or B-type star.

The generally good agreement with the literature for normal stars confirms the correctness of the methodology used in this thesis and lends credence to the abundances found for the HgMn star sample.

The HgMn stars studied here all have the manganese overabundance in common but each star is individually very different. One result of interest is the consistently high titanium abundance in the sample examined here. The mean deviation, D between the abundances from the entire HgMn star sample and the literature is constistant with zero; *i.e.*

$$D = 0.01 \pm 0.20\text{dex} \tag{6.2}$$

There does not seem to be an archetype for an HgMn star.

Chapter 7

Discussion

This chapter is divided into three sections. Section 7.1, 'Trends', highlights possible links between factors which may govern the emergence of the HgMn phenomenon and the calculated abundances. The effect of modelling errors and line formation at different depths in the stellar atmosphere are also considered. Section 7.2, 'Anomalies', discusses any unusual results seen in the data and in Section 7.3 published theoretical predictions are compared to the results and an explanation proposed to account for some aspects of the HgMn phenomenon.

7.1 Trends

7.1.1 Abundance trends with effective temperature

Magnesium

Figure 7.1 illustrates how the abundance of magnesium varies with effective temperature. Magnesium shows an underabundance in HgMn stars which appears more pronounced among the four hotter HgMn stars. Of the normal stars only Vega, being an apparently metal-weak star, shows an underabundance, but the normal stars generally exhibit abundances consistent with solar values. In the plot HgMn stars are represented by filled circles while normal stars are open squares. The solar abundance is shown in all the figures in this subsection with a dashed line (Anders and Grevesse 1989).

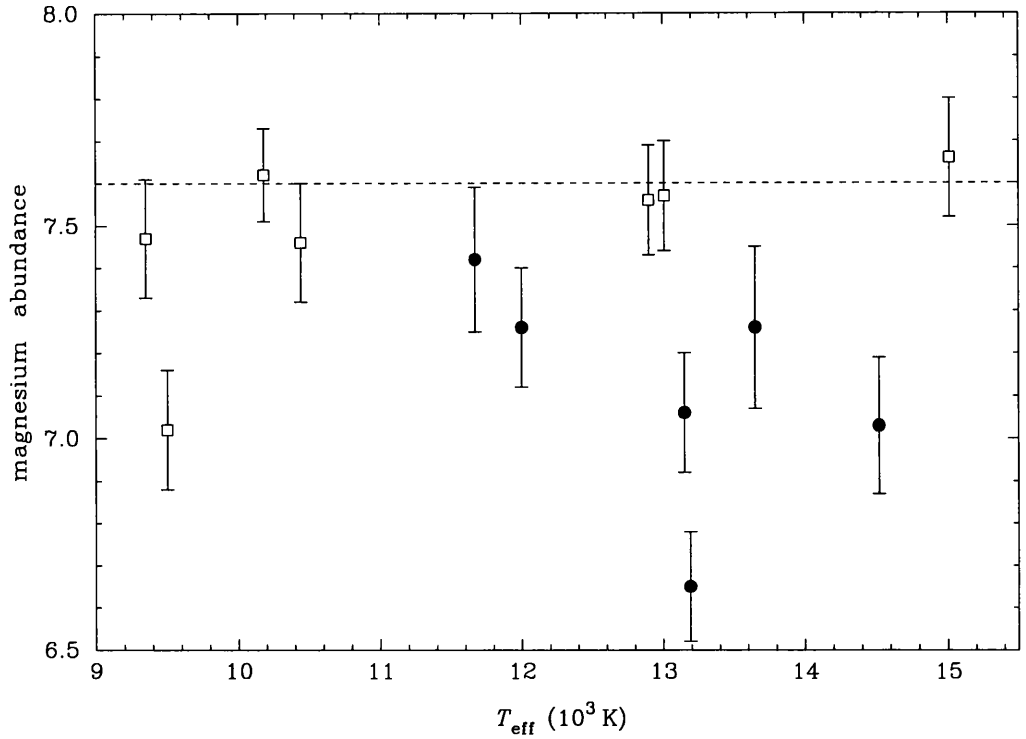

Figure 7.1: Magnesium abundance vs. effective temperature.

Aluminium

Figure 7.2 shows the mean aluminium abundances for the sample stars plotted against stellar effective temperature. Normal stars show abundances fairly consistent with solar values (Anders and Grevesse 1989). Vega is conspicuously underabundant. The HgMn stars show a systematic underabundance for aluminium when compared to the normal stars, indeed often only upper limits can be obtained for aluminium abundances in HgMn stars.

Silicon

Figure 7.3 illustrates silicon abundance *vs* effective temperature. There is scatter in the silicon abundance around the solar value (Anders and Grevesse 1989) in both HgMn and normal stars. No temperature-dependent trends are obvious. Once again, Vega has a lower abundance than the other normal stars, although the result is statistically marginal.

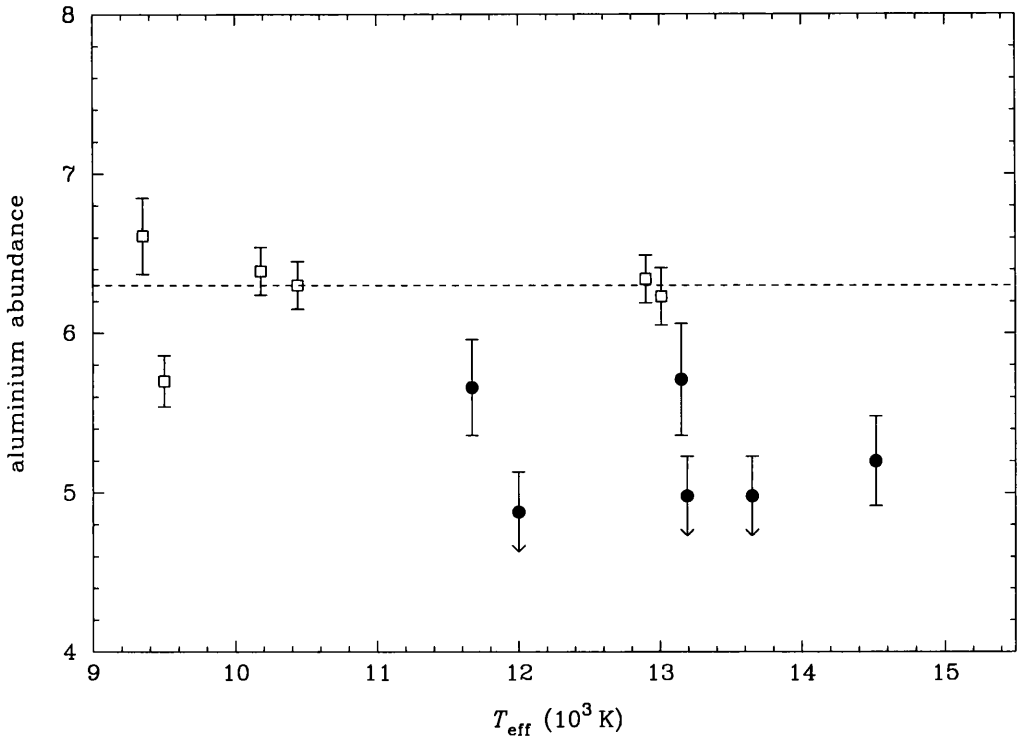

Figure 7.2: Aluminium abundance vs. effective temperature

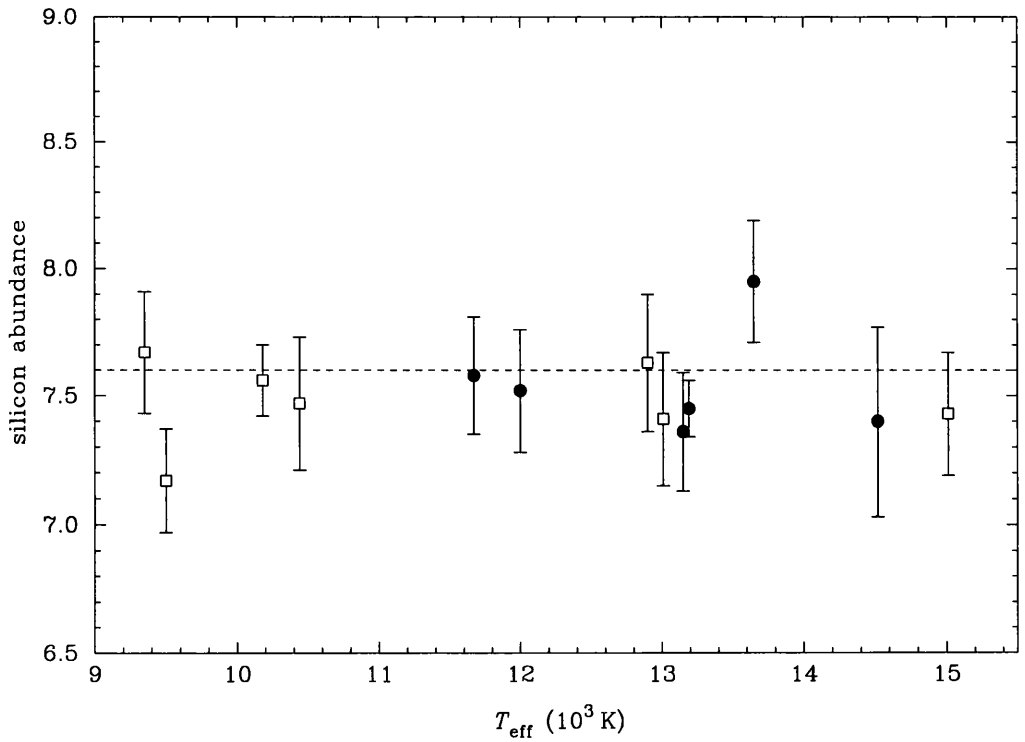

Figure 7.3: Silicon abundance vs. effective temperature

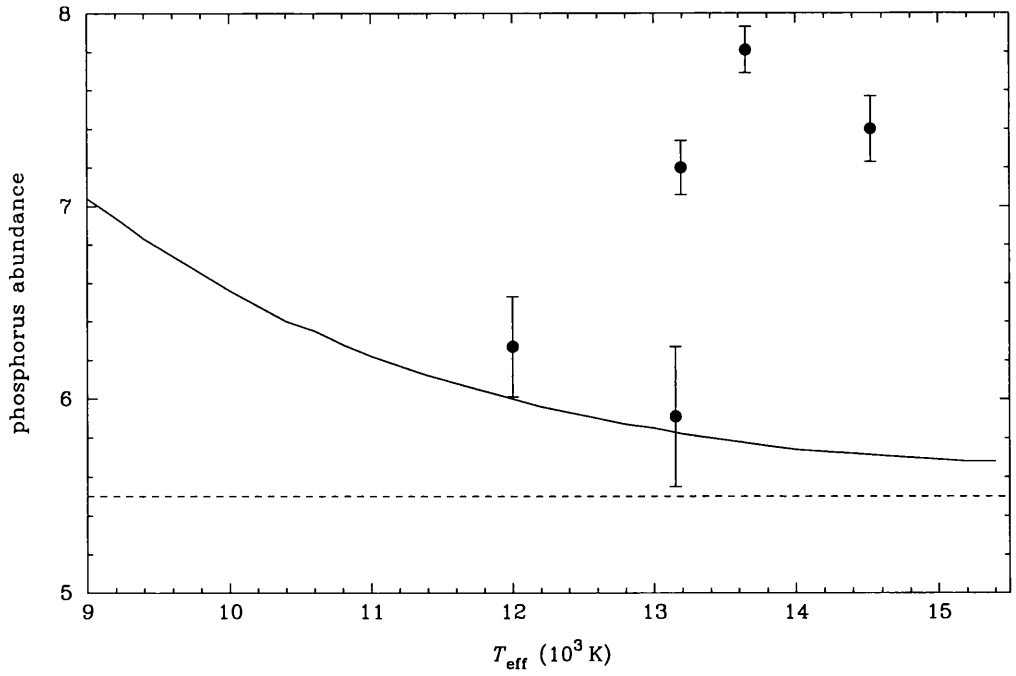

Figure 7.4: Phosphorus abundance vs. effective temperature. The solid line represents the upper limit for line visibility

Phosphorus

A possible relationship between phosphorus abundance and effective temperature is illustrated in Figure 7.4. The solid curve represents the abundance limits above which lines are visible at each $T_{\rm eff}$ (3mÅ). A $T_{\rm eff}$ trend may be present in the P abundances of HgMn stars but the sample size is small. However, the good internal consistency between the abundances from the phosphorus lines (see Tables B.1 and B.2) supports the view that these high P abundances for HgMn stars are real. When synthesis was performed at solar abundance on the spectra of normal stars no lines were predicted and none were seen in the observed spectra.

Sulphur

The abundances derived for sulphur are shown in Figure 7.5. The sample HgMn stars HR7664 and HR7361 show a marked underabundance slightly reminiscent of the underabundance in magnesium which is seen in HR7664 alone. Apart from these two stars the remaining HgMn stars are also underabundant. This underabundance is seen in both sulphur lines and as the sulphur abundance of HR7664 is $3\sigma_m$ below

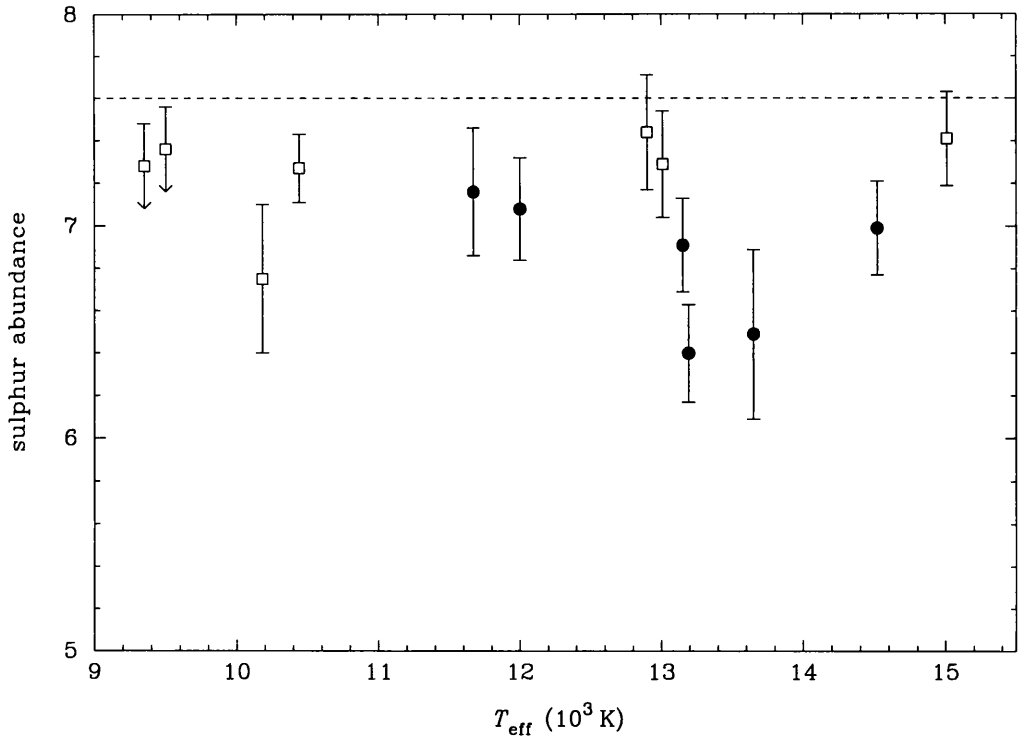

Figure 7.5: Sulphur abundance vs. effective temperature.

the solar value (Anders and Grevesse 1989) and HR7361 $2.5\sigma_m$ below the solar abundance, weight is lent to the significance of these results.

The normal star HR7098 is also apparently low in sulphur but as this result is from only a single sulphur line at λ4153 it is not possible to check the consistency between the sulphur lines for this star. All normal stars show a slight (0.2 dex) underabundance. This may be caused by a systematic error in the $\log gf$ values for sulphur.

Calcium

Calcium consistently shows solar abundances in normal stars, with the exception of Vega, which is ~0.8 dex underabundant. In HgMn stars there seems to be a trend towards higher abundances at higher temperatures. Figure 7.6 illustrates this. More work on calcium in hot stars is required, and it is worth considering that the difficulty in fitting synthetic spectra to the profiles of cooler stars may artificially bias the results between the cool and hotter stars.

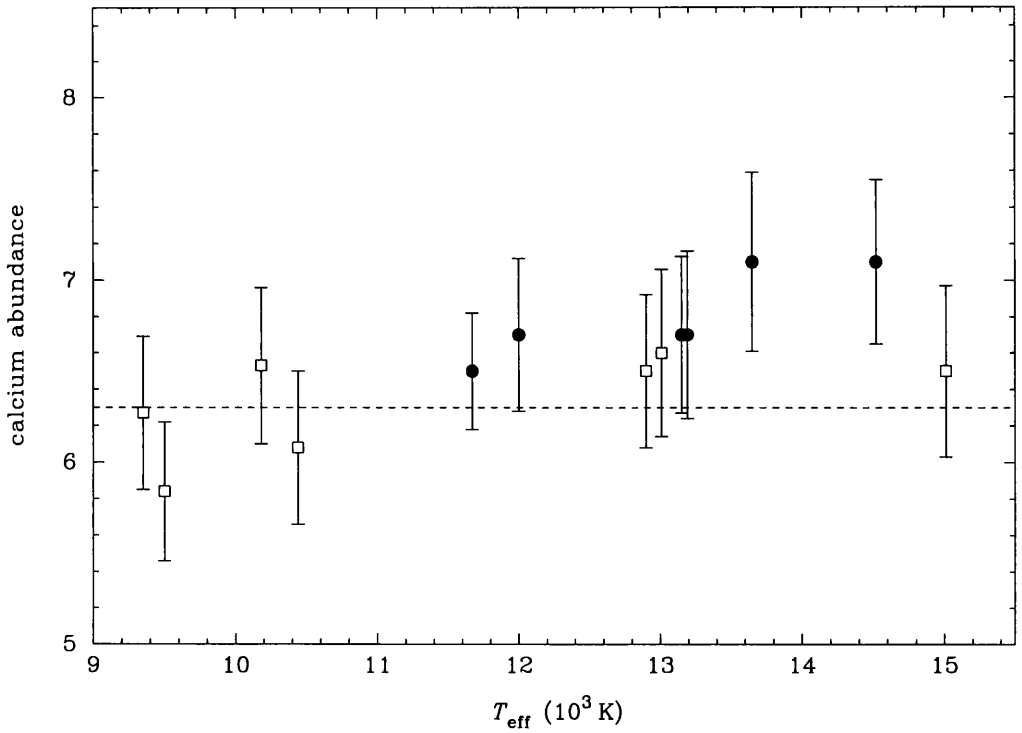

Figure 7.6: Calcium abundance vs. effective temperature

Scandium

Scandium abundances are shown in Figure 7.7.

The abundances for normal stars appear to cluster around 2.91 dex, the solar abundance (Anders and Grevesse 1989), whilst three HgMn stars, ϕ Her, 87 Psc and HR7361 have, in this sample, a 1 dex enhancement of scandium. HR7361 shows an overabundance as high as 1.7 dex, $7\sigma_m$ from the solar value, the highest of any HgMn star. The remaining HgMn stars show a solar abundance. There seems to be a dichotomy between normal and CP stars.

Titanium

The normal stars generally show a variable abundance which is close to the solar value (Anders and Grevesse 1989) but θ Leo is mildly overabundant. It is interesting to note that the abundances of titanium in HgMn stars are all enhanced in this sample. At 13 000K, 87 Psc and HR7664 show a possible peak in titanium abundance (see Figure 7.8).

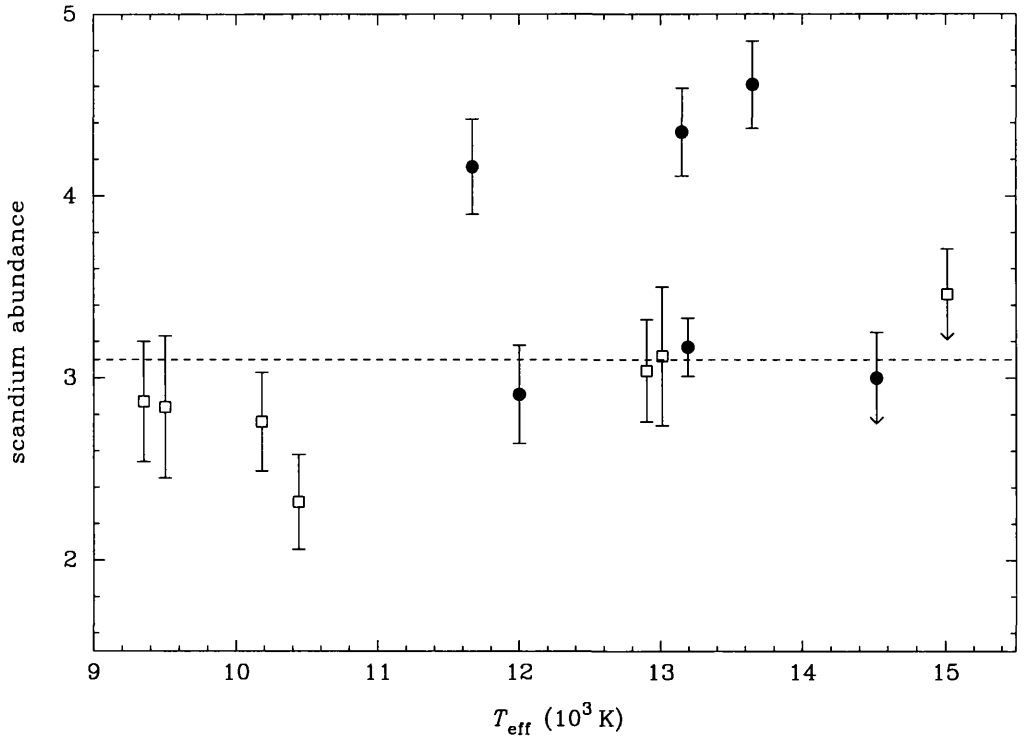

Figure 7.7: Scandium abundance vs. effective temperature

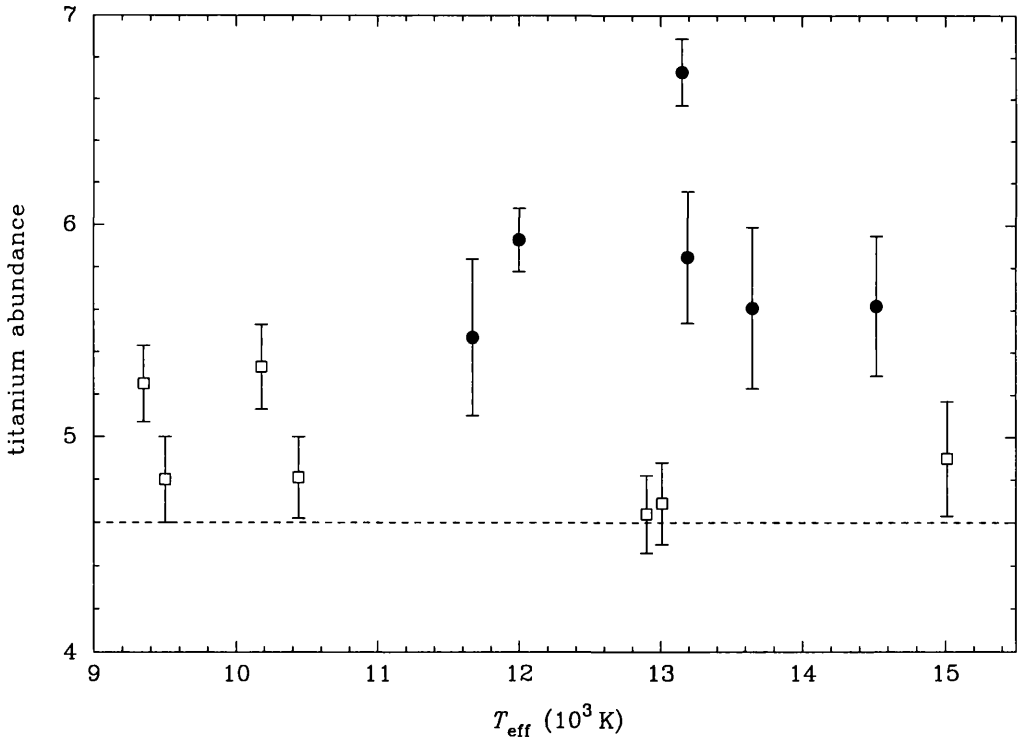

Figure 7.8: Titanium abundance vs. effective temperature.

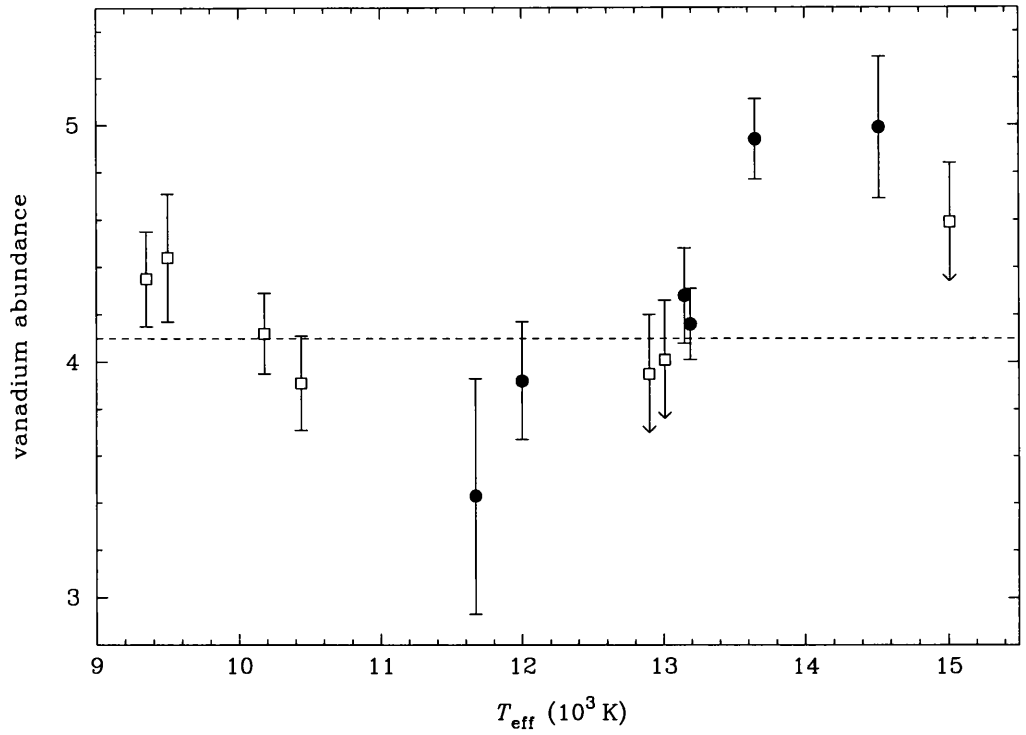

Figure 7.9: Vanadium abundance vs. effective temperature

Vanadium

The abundances of HgMn stars show a curious distribution, an almost linear trend in abundance, starting at an underabundance for cool stars and progressing to an overabundance for hotter HgMn stars. To my knowledge, comprehensive analyses on vanadium have not been performed on all of these programme stars and this is the first published work for many of the sample. It would be interesting to see these results confirmed by other workers. Normal stars show solar abundances where vanadium spectra are visible. The results are shown in Figure 7.9.

Chromium

Both HgMn and normal stars show a wide variation in abundances which is not always accountable by random error. Some HgMn star abundances are significantly higher than those seen in the normal stars and the Sun (Anders and Grevesse 1989) (Figure 7.10). No temperature-dependent trends are obvious.

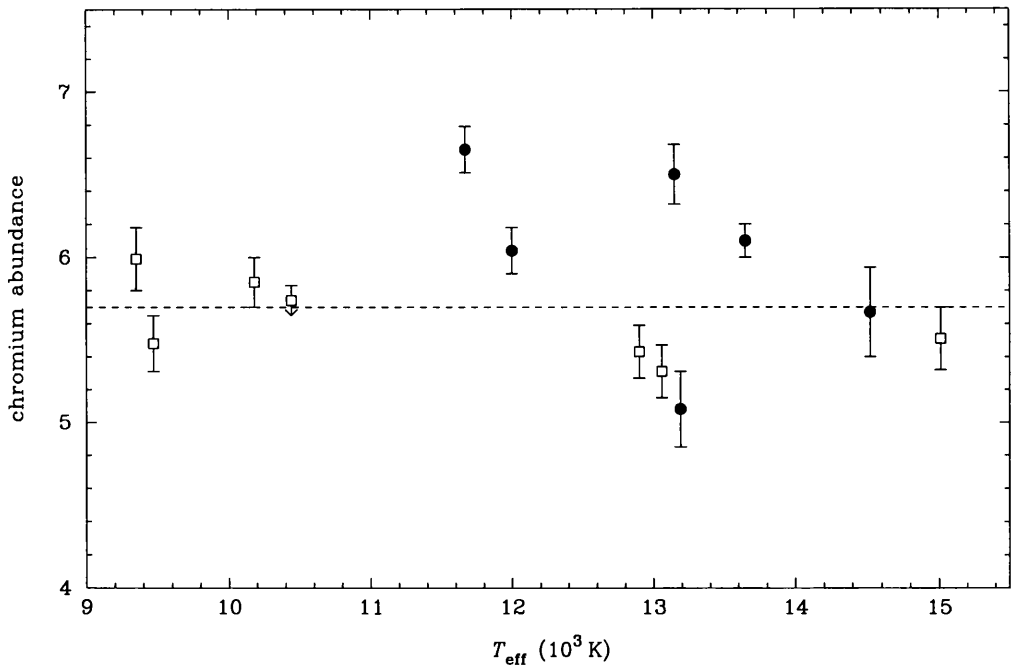

Figure 7.10: Chromium abundance vs. effective temperature

Manganese

The mean abundances were calculated, excluding λ4206, and are plotted against effective temperature and solar abundance (Anders and Grevesse 1989) in Figure 7.11. A temperature dependent trend can be seen in the HgMn stars (although with six sample stars, 'trend' may be too strong a word), but HR7664 curiously shows a lower abundance than the others, as further evinced by the lack of an over-strong λ4206 line in this star.

Iron

The normal stars and HgMn stars show a wide range of abundances scattered about the solar value (7.5 dex, Jaschek and Jaschek 1995). The normal stars show a consistently solar abundance, with some scatter, except for Vega, which is 0.6 dex underabundant. The HgMn stars show a wide range of abundances which do not appear to be temperature dependent; HR7664 is 0.6 dex overabundant whereas 87 Psc is 0.5 dex underabundant and both stars are almost the same effective temperature (Figure 7.12).

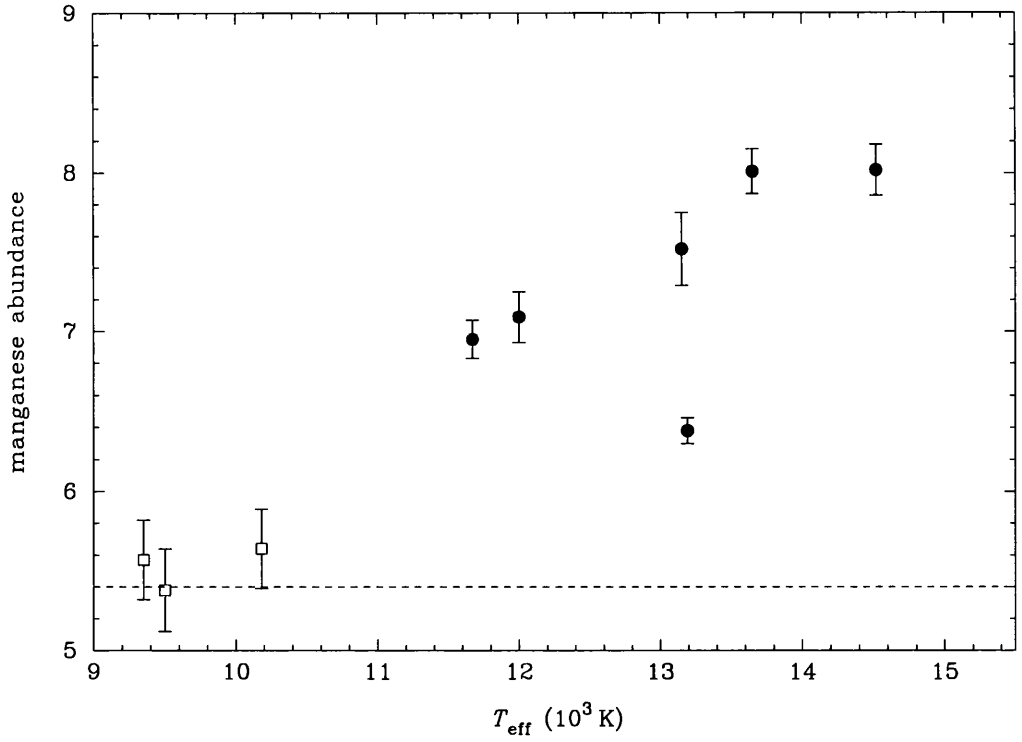

Figure 7.11: Manganese abundance vs. effective temperature

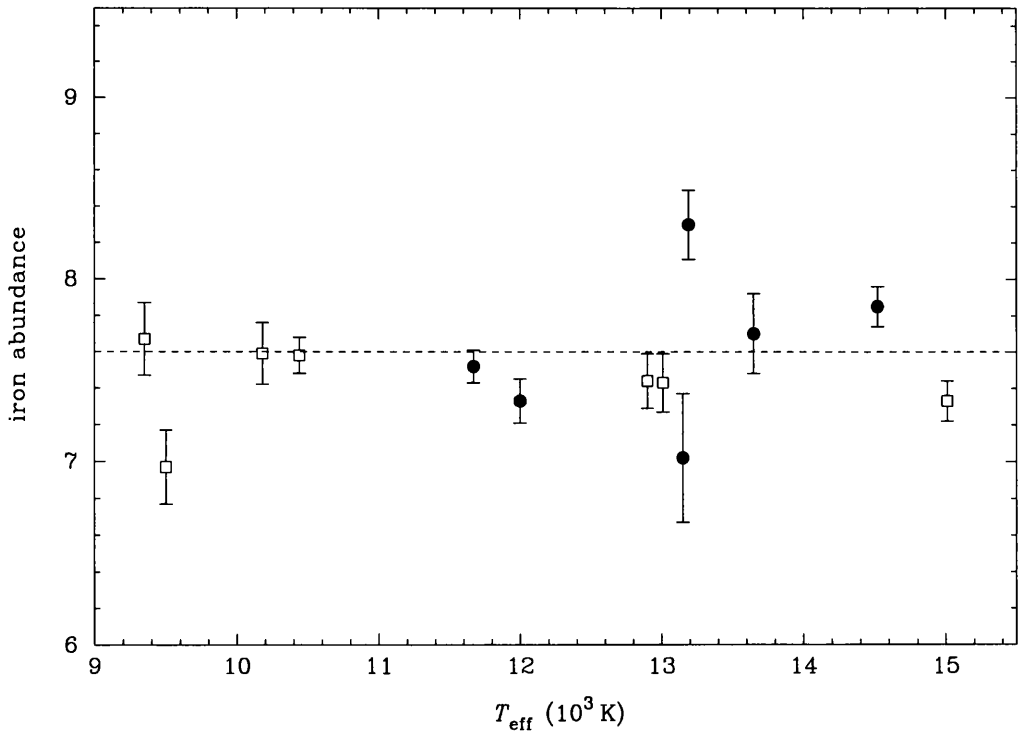

Figure 7.12: Iron abundance vs. effective temperature

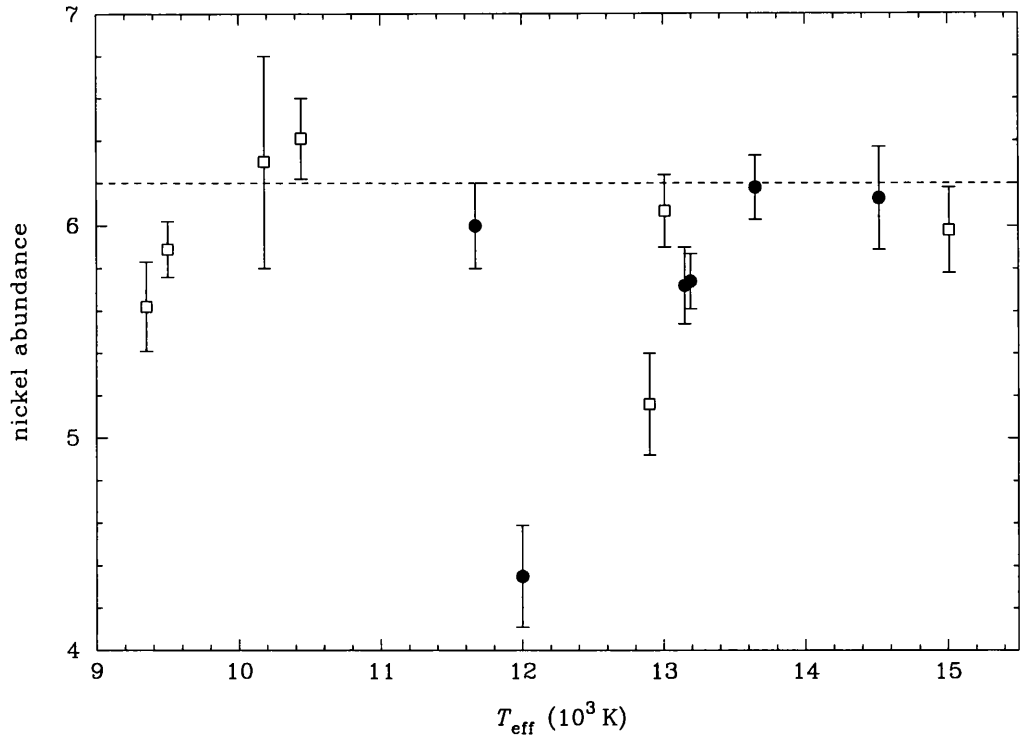

Figure 7.13: Nickel abundance vs. effective temperature

Nickel

Figure 7.13 shows nickel abundances consistent with the solar abundances in both HgMn and normal stars. The exception is υ Her, which is underabundant by 2 dex. The normal star ζ Dra, also in the temperature range (12 000–13 000K) shows a mild underabundance. More results are needed from other stars in this temperature range for these results to be related to the temperatures of the stars.

Gallium

Normal stars did not show evidence of gallium at solar abundance syntheses and so could not have their abundances determined but some upper limits were calculated. HgMn stars show extreme overabundances, (at least 12 σ_s above the solar abundance from Anders and Grevesse 1989) but there is not an obvious correlation with effective temperature (Figure 7.14).

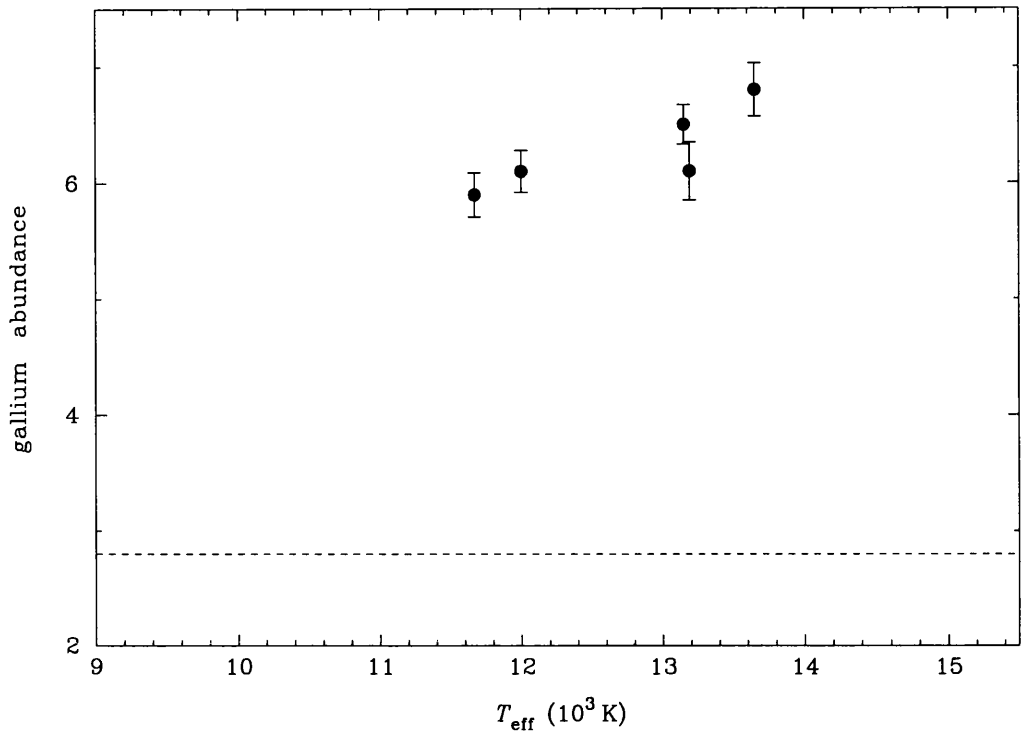

Figure 7.14: Gallium abundances vs effective temperature (from Ga I only)

Strontium

Strontium is overabundant in cooler HgMn stars but otherwise shows normal abundances in normal stars and the hotter HgMn stars. A consistent but scattered solar abundance (Anders and Grevesse 1989) was observed in the cooler normal star sample; this is very likely to be due to measurement errors for weak lines. (Figure 7.15).

Yttrium

Yttrium abundances were obtained from weak lines. An enhancement of yttrium can be seen in Figure 7.16 for HgMn stars. Excluding ϕ Her, there is a possible increase in abundance with effective temperature, but this may be due to selection effects from the small sample. What is clear, however, is the existence of an overabundance of $\sim$ 2.0 dex. By contrast, the normal stars show a typically solar abundance, and this is illustrated in Figure 7.16.

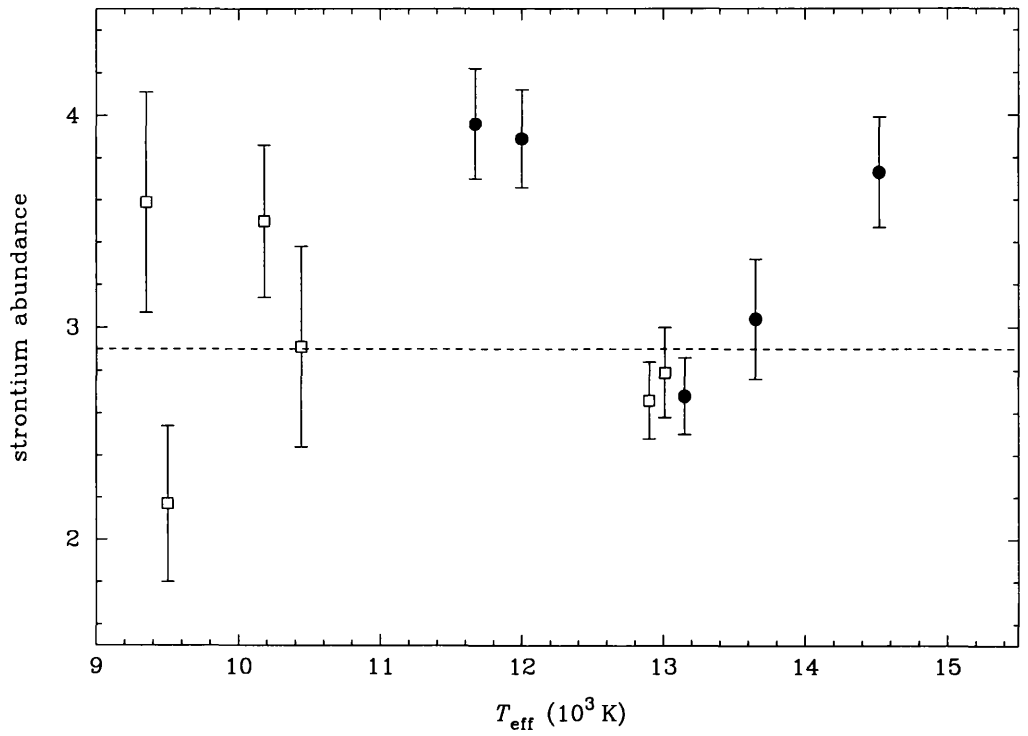

Figure 7.15: Strontium abundance vs. effective temperature

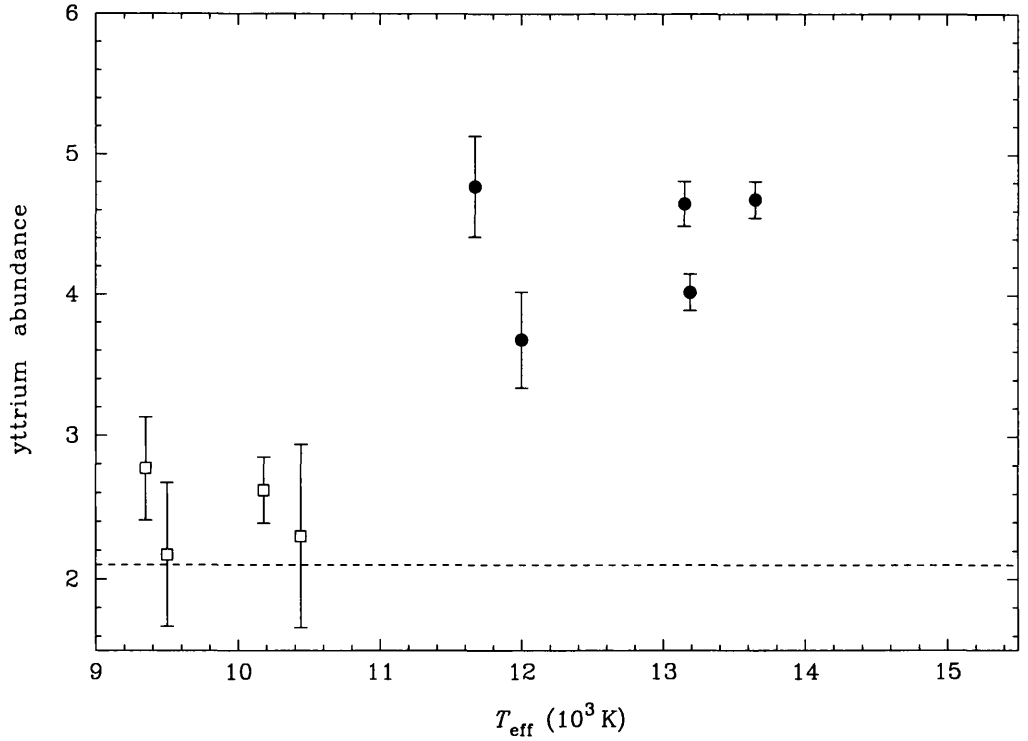

Figure 7.16: Yttrium abundance vs. effective temperature

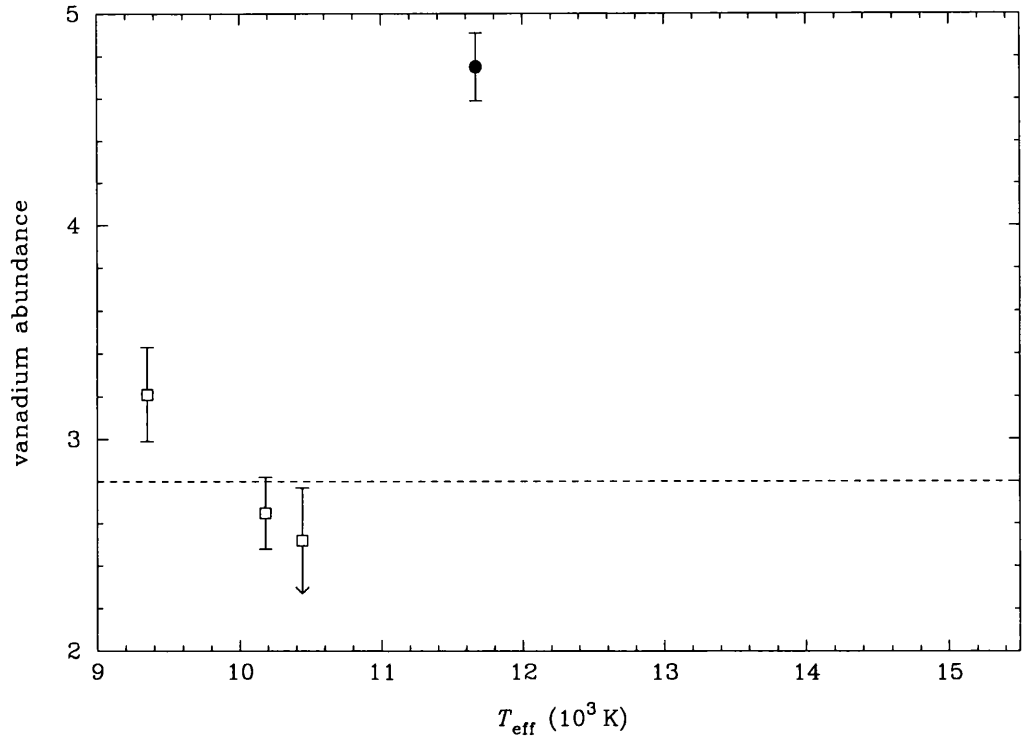

Figure 7.17: Zirconium abundance vs. effective temperature

Zirconium

Figure 7.17 illustrates the zirconium abundances with respect to the Sun for ϕ Her. No zirconium lines were seen in other HgMn stars but some normal stars showed abundances consistent with solar values.

Barium

The three HgMn stars which do exhibit the line at λ4554 all have abundances 0.5-1.0 dex above the solar abundance but the upper abundance limits derived for the hot HgMn stars do not indicate any exaggerated overabundance in these stars. The normal stars also show a possible overabundance. The results can be seen in Figure 7.18.

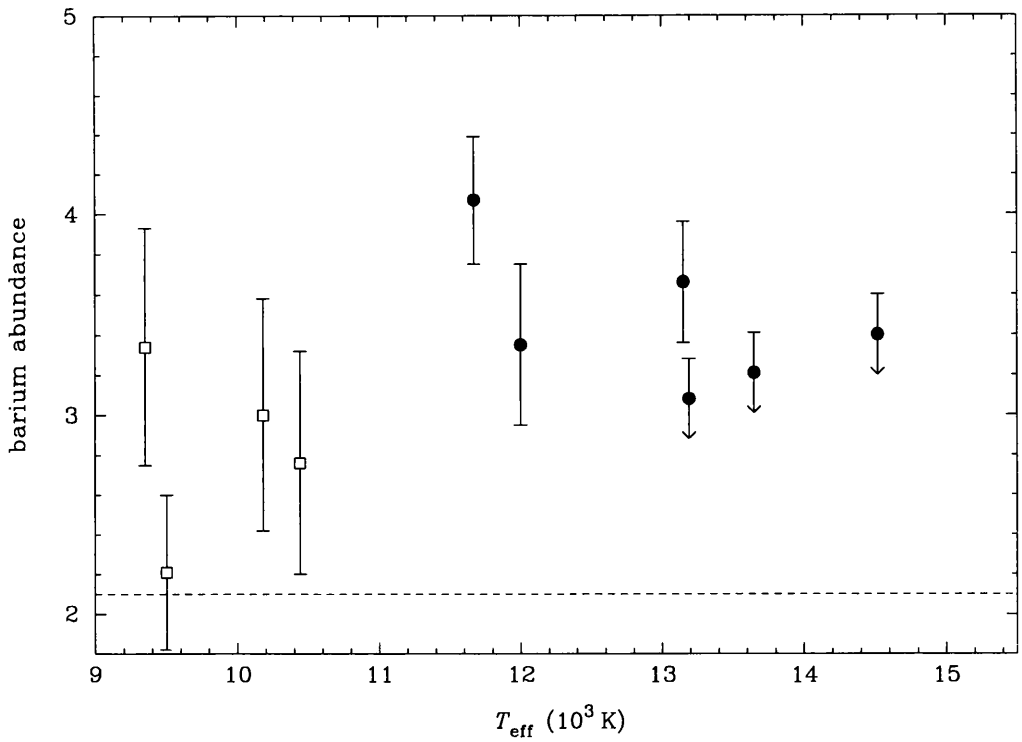

Figure 7.18: Barium abundance vs. effective temperature

7.1.2 Abundance trends with surface gravity

Surface gravity is a key indicator of stellar age: as stars expand during their main sequence lifetime, the surface gravity decreases with age. It might be expected that the apparently lower surface gravity stars in this sample are older, but there is also the possibility they are less massive stars. This possibility was excluded by examining $\log g$ and $T_{\rm eff}$ values (tabulated in Table 4.1); no relationship was seen, so the low gravity stars may indeed be older. The main disadvantage of using surface gravities as an indicator of age in these stars is the high tolerance in the calculated values of $\log g$, which were determined with great care by Smith and Dworetsky (1993), and are adequate when determining abundances (the uncertainties were taken into account in the abundance calculations). This uncertainty makes it difficult to see patterns when searching for age related trends in a small sample.

No obvious trend between surface gravity and abundance was seen in most of the elements for the thesis sample (Table 7.1 and Table 7.2), but a larger sample may allow more progress to be made as more precise values of $\log g$ do not appear to be currently available.

Table 7.1: Stellar abundance with respect to surface gravity for HgMn stars, listed in $\log g$ order

Star	HR7361	HR7664	υ Her	HR6997	ϕ Her	87 Psc
log g	3.51	3.59	3.78	3.89	4.00	4.02
Mg	7.26	6.65	7.26	7.03	7.42	7.06
Al	$\leq$4.98	$\leq$4.98	$\leq$4.88	5.20	5.65	5.71
Si	7.95	7.45	7.52	7.40	7.58	7.36
P	7.81	7.20	6.27	7.41	–	5.91
S	6.49	6.40	7.08	6.99	7.16	6.91
Ca	7.10	6.70	6.70	7.10	6.50	6.70
Sc	4.61	3.17	2.91	$\leq$3.00	4.16	4.35
Ti	5.61	5.85	5.93	5.62	5.47	6.73
V	4.94	4.16	3.92	4.99	3.43	4.28
Cr	6.10	5.08	6.04	5.67	6.65	6.50
Mn	8.01	6.38	7.09	8.02	6.95	7.52
Fe	7.70	8.30	7.33	7.85	7.52	7.02
Ni	6.18	5.74	4.35	6.13	6.02	5.72
Ga	6.80	6.10	6.05	–	5.9	6.5
Sr	3.04	–	3.89	3.73	3.96	2.68
Y	4.68	4.02	3.68	–	4.77	4.66
Zr	–	–	–	–	4.75	–
Ba	–	–	3.35	–	4.07	3.66

Open cluster associations are useful for determining stellar age but HgMn members were not chosen for this project because they were too faint for satisfactory spectra to be obtained in the time allotted for observing.

7.1.3 Error-independent abundance ratios

It is possible that the temperature dependent trends seen in HgMn stars are simply an artifact of the model atmospheres used in this thesis. In order to account for or at least be aware of this effect, four elements commonly found in HgMn stars (barium, strontium, gallium and manganese) were compared.

It was important to make the conditions under which these lines were simulated

Table 7.2: Stellar abundance with respect to surface gravity for normal stars

Star	21 Aql	21 Peg	HR7098	θ Leo	α Lyr	ζ Dra	τ Her
log g	3.50	3.50	3.55	3.67	3.90	3.92	3.93
Mg	7.57	7.46	7.62	7.47	7.02	7.56	7.66
Al	6.23	6.30	6.39	6.61	5.70	6.34	–
Si	7.41	7.47	7.56	7.67	7.17	7.63	7.43
P	–	–	–	–	–	–	–
S	7.29	7.27	6.75	$\leq$7.28	$\leq$7.36	7.44	7.41
Ca	6.60	6.08	6.53	6.27	5.84	6.50	6.50
Sc	3.12	2.32	2.76	2.87	2.84	3.04	$\leq$3.46
Ti	4.69	4.81	5.33	5.25	4.80	4.64	4.90
V	–	3.91	4.12	4.35	4.44	$\leq$3.95	–
Cr	5.31	5.74	5.85	5.99	5.48	5.43	5.51
Mn	–	–	5.64	5.57	5.38	–	–
Fe	7.43	7.58	7.59	7.67	6.97	7.44	7.33
Ni	6.07	6.41	6.30	5.62	5.89	5.16	5.98
Ga	–	–	–	–	–	–	–
Sr	2.79	2.91	3.50	3.59	2.16	2.66	–
Y	–	2.30	2.62	2.77	2.17	–	–
Zr	–	–	–	–	–	–	–
Ba	–	2.76	3.00	3.34	2.21	–	–

Table 7.3: Abundance ratios for HgMn stars

Ratio	ϕ Her	υ Her	87 Psc	HR7664	HR7361	HR6997
Mn I 4030: Ga I 4032	1.17	1.15	1.18	Z	1.15	1.19
Mn I 4030: Ga I 4172	1.03	1.17	1.15	Z	1.27	1.45
Mn I 4034: Ga I 4032	1.17	1.16	1.20	C	1.20	1.19
Mn I 4034: Ga I 4172	1.03	1.18	1.17	C	1.33	1.44
Mn I 4030: Sr II 4032	1.80	1.79	2.93	Z	2.57	2.54
Mn I 4030: Sr II 4032	1.73	1.80	2.81	Z	B	B
Mn I 4034: Sr II 4032	1.79	1.80	2.99	C	2.67	2.53
Mn I 4034: Sr II 4032	1.72	1.82	2.86	C	B	B
Mn I 4030: Ba I 4554	1.89	2.09	2.10	Z	$\geq$2.44	$\geq$2.42
Mn I 4030: Ba I 4554	1.71	2.10	2.13	C	$\geq$2.53	$\geq$2.41
Ga I 4032: Ba II 4554	1.47	1.81	1.78	$\geq$2.01	$\geq$2.12	$\geq$2.03
Ga I 4172: Ba II 4554	1.67	1.79	1.83	$\geq$1.65	$\geq$1.90	$\geq$1.67
Ba II 4554: Sr II 4077	1.03	1.04	1.40	–	$\geq$1.05	$\geq$1.05
Ba II 4554: Sr II 4215	1.00	1.05	1.34	–	B	B
Ga I 4032: Sr II 4077	1.54	1.55	2.48	–	2.23	2.13
Ga I 4032: Sr II 4215	1.48	1.57	2.48	–	B	B
Ga I 4172: Sr II 4077	1.74	1.53	2.55	–	2.00	1.76
Ga I 4172: Sr II 4215	1.68	1.55	2.44	–	B	B

identical, in order to remove the effect of the model atmosphere. This meant it was necessary to choose lines from different elements that formed at the same excitation potential. The excitation potential was chosen to be 0.00eV, because the ground state has no uncertainty (other than broadening mechanisms) in its value, and so it would be identical for all the stars.

Each of the seven selected lines was compared against the other, and the results are given in Table 7.3 and Table 7.4 for HgMn and normal stars. It was important that the trends seen in the abundances also appeared in the ratios, because this meant that the trends seen were genuine and not due to systematic error.

The ratios show that when manganese is high in abundance, so is gallium, which matches the results from the abundances alone. Manganese shows a high ratio with respect to barium and strontium, which implies that manganese is high in abundance

Table 7.4: Abundance ratios for normal stars

Ratio	θ Leo	α Lyr	HR7098	87 Psc	ζ Dra	21 Aql	τ Her
Mn I 4030: Ga I 4032	–	–	–	–	–	–	–
Mn I 4030: Ga I 4172	–	–	–	–	–	–	–
Mn I 4034: Ga I 4032	–	–	–	–	–	–	–
Mn I 4034: Ga I 4172	–	–	–	–	–	–	–
Mn I 4030: Sr II 4032	B	–	–	B	–	–	–
Mn I 4030: Sr II 4032	B	–	–	B	–	–	–
Mn I 4034: Sr II 4032	B	–	–	–	–	–	–
Mn I 4034: Sr II 4032	B	–	–	–	–	–	–
Mn I 4030: Ba I 4554	B	–	–	–	–	–	–
Mn I 4030: Ba I 4554	B	–	–	–	–	–	–
Ga I 4032: Ba II 4554	–	–	–	–	–	–	–
Ga I 4172: Ba II 4554	–	–	–	–	–	–	–
Ba II 4554: Sr II 4077	1.11	–	1.22	C	–	–	–
Ba II 4554: Sr II 4215	1.06	–	B	1.05	–	–	–
Ga I 4032: Sr II 4077	–	–	–	–	–	–	–
Ga I 4032: Sr II 4215	–	–	–	–	–	–	–
Ga I 4172: Sr II 4077	–	–	–	–	–	–	–
Ga I 4172: Sr II 4215	–	–	–	–	–	–	–

because of a genuine mechanism and not through errors in the model atmosphere. Gallium also shows an enhancement with respect to barium, but no pattern is seen at all in the ratios between manganese:strontium and gallium:strontium. This may be because strontium does not exhibit a clear abundance trend with temperature. These results satisfy me that systematic error due to modelling errors is not a problem in the determined abundances.

7.1.4 Evidence for stratification by comparison of UV and optical abundances

Elements which were common to this work and the work of K.C. Smith were examined for discrepancies which may point toward stratification in the stellar atmosphere. This is because UV and optical lines form at different depths in the stellar atmosphere and so if concentration gradients of certain elements exist they might be expected to show greater abundances in the optical or the UV, depending on whether the lines are formed in the overabundant regions or not. Systematic discrepancies between optical and UV abundances may be an indicator as to the presence of stratified layers in the stellar atmospheres of some stars.

The elements aluminium, magnesium, silicon, manganese, iron, chromium, gallium and nickel were compared with the work of Smith (1993), Smith (1995) and Smith and Dworetsky (1993) for systematic deviations because these elements were present in both analyses. The deviations with respect to these results ($\log A_{\mathrm{SandD}} - \log A_{\mathrm{Allen}}$) are shown in Table 7.5.

Most of the deviations in Table 7.5 are within 2σ of the error on the abundances of the order of 0.2 dex and fluctuate beween positive and negative values. Of those with deviations above 3σ, gallium shows the most instances, but the negative value obtained for HR7664 does not make this conclusive of the presence of stratification; more data would give a better indication and it is worth remembering that the gallium abundances were calculated using blended lines.

The systematic deviation of magnesium from the results of Smith and Dworetsky is thought to be due to systematic error in the work of Smith and Dworetsky, discussed in Smith (1992) and elsewhere in this chapter (Section 7.2.2). It is not

Table 7.5: Deviations between the thesis abundances and Smith (1992)

Star	Mg	Al	Si	Cr	Mn	Ni	Fe	Ga
θ Leo	-0.23	+0.31	+0.07	+0.14	+0.07	+1.08	-0.07	–
α Lyr	-0.38	+0.10	+0.17	+0.02	+0.38	+0.01	-0.03	–
HR7098	-0.28	-0.01	-0.04	+0.55	-0.06	+0.30	-0.01	–
21 Peg	-0.14	+0.10	+0.07	-0.04	–	-0.11	-0.18	–
ζ Dra	+0.56	-0.06	+0.03	-0.13	–	-0.34	+0.76	–
21 Aql	-0.33	+0.13	-0.19	+0.39	–	-0.07	-0.03	–
τ Her	-0.34	–	-0.17	+0.19	–	-0.08	-0.37	–
ϕ Her	-0.18	+0.25	+0.18	+0.05	-0.05	-0.22	-0.08	+0.40
υ Her	-0.04	+$\leq$0.38	+0.12	+0.06	-0.01	+1.15	+0.13	+0.05
87 Psc	-0.14	+0.41	+0.06	-0.60	+0.12	-0.52	+0.64	+0.90
HR7664	+0.25	+$\leq$0.48	-0.05	+0.02	+0.08	-0.24	+0.20	-0.40
HR7361	+0.06	+$\leq$0.88	+0.15	-0.08	-0.11	-0.38	+0.10	+0.80
HR6997	-0.63	+0.30	-0.20	–	+0.18	-0.63	-0.65	–

thought to be indicative of stratification.

7.1.5 Abundances obtained from different ionisation stages

Manganese showed a systematic difference between the abundances obtained from the first and second ionisation stages; this was more pronounced in the cooler stars, especially Vega and θ Leo and confirms the work of Adelman (1991).

These discrepancies may be due to the low population of an ionisation stage giving rise to nLTE effects and could be temperature based as Vega is close in $T_{\rm eff}$ to θ Leo.

Lemke (1989,1991) saw a discrepancy between the first and second ionisation stages for iron but, curiously, the difference increased under nLTE modelling, implying another mechanism may be responsible. This problem remains unresolved.

7.2 Anomalies

Some interesting anomalies were found or confirmed in this work and these are highlighted and discussed below.

7.2.1 The peculiarly low abundances for ζ Dra found by Smith (1992)

Smith obtained a very high value for ξ, the microturbulence parameter for ζ Dra, of $2.5\,\mathrm{kms}^{-1}$, which is not in agreement with what has been found for the hotter stars in this work, *i.e.*, hot stars have low (less than $1.0\,\mathrm{kms}^{-1}$) or 'imaginary' microturbulent velocities. Smith's adopted value for ξ was derived from UV lines as Smith had no optical data for ζ Dra which could be used as a comparison against the UV data.

This high value for ξ is very different from the optically derived value of ξ=0 kms^{-1} for ζ Dra, and also different from that obtained by Smith for the other sample stars. It will most likely be responsible for the systematically low abundances derived by Smith for ζ Dra. This implies that other relatively high-temperature sample stars with high microturbulences derived by Smith may also have underestimated abundances. These stars are 36 Lyn, with a ξ of $2.0\,\mathrm{kms}^{-1}$ and a T_{eff} of 13 700K, HR6997 with a ξ of $1.5\,\mathrm{kms}^{-1}$ and a T_{eff} of 14 500K, and HR2676, with a ξ of $1.0\,\mathrm{kms}^{-1}$ and T_{eff} of 14 050K.

7.2.2 The magnesium abundance overestimation found by Smith (1992) and Smith (1993)

Smith states in his thesis that the magnesium abundances (published Smith 1993, recalculated, but little different from those in his thesis) may be overestimated by 0.15-0.20 dex and this appears to be the case, according to the results in this project and those in the literature. Smith suggests that this overabundance may be due to differences between LTE and nLTE W_λ values for the UV lines used by Smith in this analysis; i.e. in nLTE lines are stronger, which means the abundances derived by Smith are too high.

The thesis results agree well with Guthrie (1984); both find low abundances in

the same stars for magnesium, implying the scatter seen is not experimental but indeed a property of the stars.

7.2.3 The barium and strontium enhancement in cooler A/B stars

Lemke (1990,1991) found that strontium and barium were enhanced in a sample of A-type normal stars in the $T_{\rm eff}$ range 8 800 - 10 900K and $v \sin i$ values less than $50\,{\rm kms}^{-1}$, including the stars θ Leo and α Lyr, which are present in the sample. It is stated that this overabundance pattern is reminiscent of Am stars.

Lemke never did find a typical A-star in his sample although Vega was closest when the metal abundances were normalised to iron. No typical non-solar abundance patterns were to be found.

Lemke suggests that a stellar wind producing a low but significant mass loss can give rise to abundance anomalies. Different wind rates will give different results. This model was devised by Michaud and Charland (1986) who suggest that the relatively different abundances may reflect the age of the star. Lemke suggests that the slowly-rotating A/B- type stars may be cool HgMn precursors.

No barium line was seen in the hotter stars in this project so it is not possible to tell if Lemke's results apply to hotter stars. Strontium is less abundant in hotter normal stars but even more enhanced in the HgMn stars. The sample size is not large enough to determine if this is a statistical anomaly or a typical property of hot narrow-lined B-stars.

The LTE results in this thesis for Vega and θ Leo bear out Lemke's work.

7.2.4 The systematic abundance enhancement in Heacox's work

Heacox obtained his abundances from the measured photographic equivalent widths of Gaussian profiles fitted to spectral lines from a sample of 22 HgMn stars. Line blends and Voigt profiles were fitted with hand-drawn approximations.

It was found that Heacox used effective temperatures for his stars which were lower than other determinations in the literature for the same stars; Heacox credits this to line blanketing effects unaccounted for by the model atmosphere. Heacox used

ξ=0 kms^{-1} for all HgMn stars, which is what I used, so this cannot be responsible for the abundance enhancement. The difference could also be due to a different line sample, but it can be seen that the Heacox line sample is not so very different to that used in this project, except for a few extra blue lines in the Heacox sample. The manganese enhancement is certainly not due to his usage of λ4206 (see 7.2.5 for further details) as the effect of this line would be diluted by Heacox' large sample of Mn lines.

It does appear that Heacox neglected to compensate for the effect of interstellar reddening in the hotter, more luminous and more distant stars in his sample. This may have given rise to an error in Heacox's derived temperatures and therefore in his model atmospheres and abundances.

Generally the elements strontium, titanium, manganese, chromium and iron analysed by Heacox are enhanced above other work in the literature, including my own.

7.2.5 The anomalously strong manganese line at λ4206

The strong manganese stars ϕ Her, υ Her, HR7361, HR6997 and 87 Psc exhibited an anomalously strong line at λ4206, whereas HR7664, with a low Mn abundance compared to the other HgMn stars, did not. Figure 7.19 shows how the equivalent width of a synthesised λ4206 line increases with temperature at the mean derived abundance for manganese in each star. This is compared with the *observed* equivalent widths for this line; the comparison shows an obvious discrepancy and implies that a temperature-sensitive blending species may be responsible. However, tests using the lists of Moore (1959), Kurucz and Peytremann (1975) and Kurucz (1988) reveal no obvious line blend.

To investigate the anomaly the mean abundances for manganese were first calculated without a contribution from the line at λ4206. These results are plotted in Figure 7.20 against the abundances derived only from the line at λ4206. In the HgMn stars the divergence of the abundance of λ4206 from the other lines can be seen clearly. Such behaviour cannot be explained by an error in the $\log gf$ as it does not show a constant shift in abundance.

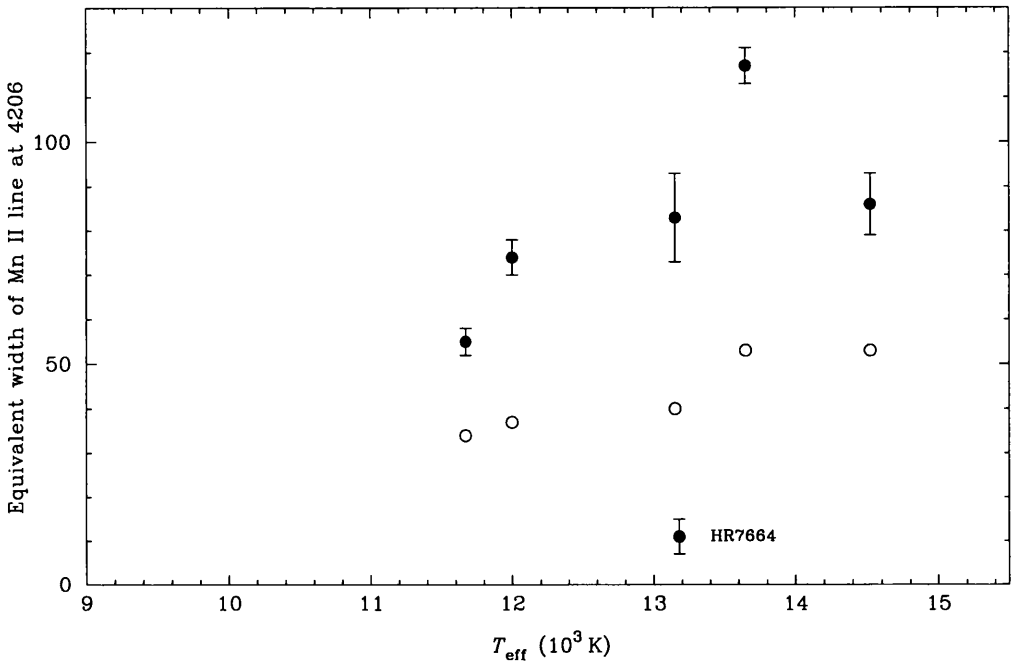

Figure 7.19: Measured line equivalent width for the 4206 line (filled circles) and predicted 4206 line equivalent width (open circles) plotted against effective temperature. [The synthetic equivalent width for λ4206 was determined from a mean abundance which was calculated from the abundance of four other optical lines.] Note that HR7664, with a low manganese abundance, does not exhibit an obvious strengthening of 4206

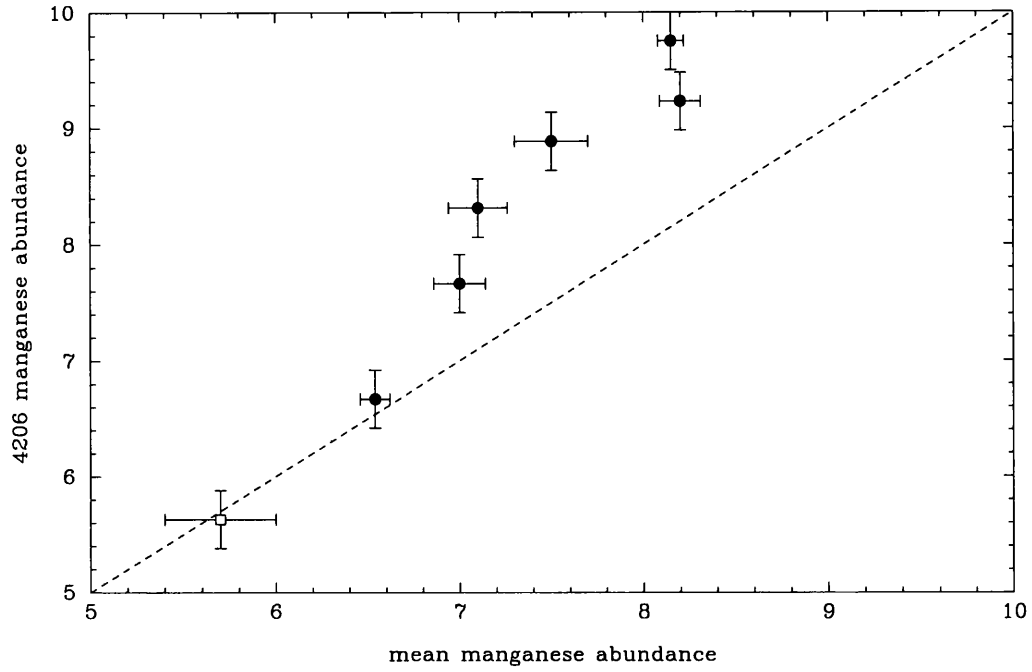

Figure 7.20: A comparison between the abundance for manganese obtained using the line at 4206.37 and the mean abundance using a selection of strong lines but omitting 4206.

It is likely that this behaviour is due to hyperfine structure, which is more important in strong lines which can be partially desaturated.

7.2.6 Gallium

Smith (1995) found that Ga II and III ions gave systematically very different abundances and postulated that a stratification model could account for those differences. He also suggested that the LTE ionisation equilibrium for gallium is not well-known above 12 500K. Smith's stratification model has a two-layer structure with a 'rich' gallium layer above a specified optical depth overlaying the normal abundance region. Smith admits this may be an oversimplified model as it is unlikely a two-layered situation would evolve naturally; however, this model was proposed to begin to explain peculiarities seen in gallium.

Smith found that most of the stars he looked at gave results under the new model which fitted to the Ga II and Ga III lines at a single abundance.

Smith then looked at the blue region Ga II lines derived in the literature and

Table 7.6: Gallium abundances

Star	Ga I Thesis	Ga II UV	Ga III UV	Ga UV †	Ga II Optical
ϕ Her	5.9	6.0	5.6	6.2	6.0
υ Her	6.1	6.2	6.0	6.4	6.6
87 Psc	6.5	6.0	5.2	6.1	5.5
HR7664	6.1	5.6	5.6	–	5.9
HR7361	6.8	6.6	6.3	6.7	6.6
HR6997	–	6.6	6.4	6.7	7.3

All errors approx. ±0.2 dex. All data from Smith (1995), except for the first column, which this work is from. † represents abundances obtained using stratification model

found them to be on average ~1 dex higher than the UV values; however, he found the then current explanation (optical lines are formed deep in the gallium rich layer) lacking because optical lines should be formed at the same depth as those in the UV at λ1414 and that the discrepancy between the regions should be no more than 0.1 dex.

Instead, he suggests that the Ga II optical lines may be prone to hyperfine splitting (Isberg and Litzen 1985). Ga I is not known to have hyperfine structure so currently there is not a suitable model to account for any unusual behaviour for this species.

The results obtained in this thesis can be compared favourably to those of Smith (1995) and the results appear to match fairly well within the bounds of experimental error, except for 87 Psc, where the Ga I results are enhanced (see further discussion in section 7.1.4). Comparisons of the unsplit neutral gallium lines with the singly ionised gallium lines in the optical region must wait on the work of Dworetsky *et al* (1997, submitted) for a full discussion.

7.3 Comparison of results to theoretical predictions

7.3.1 Deep nucleosynthesis

The nucleosynthesis theory proposed by Fowler *et al* (1965) suggests that Ap stars form through the manufacturing of rare earth elements from iron peak elements. These elements would then be expected to be seen in the atmospheres of HgMn stars. Wahlgren et al (1995) suggests that a study of the abundance ratios of gold and platinum would shed light on the possibilities of this mechanism being a valid explanation. The problem with this is that Sargent and Searle (1967) found evidence to suggest that the HgMn anomalies are found in the photosphere and are not mixed throughout the star. The results in this thesis show no evidence of an overabundance of rare earth elements. Fowler *et al*'s theory makes no attempt to account for the presence of manganese in the spectra of these stars. It was not possible to measure the gold to platinum ratio as gold was not seen in the spectra of these stars at the resolution and noise level of the data. In general it appears to be an unlikely explanation for the formation of stars with the mercury-manganese overabundance pattern.

7.3.2 Accretion by a white dwarf

Fowler *et al* (1965) presented a theory for Ap-star formation in which a white dwarf is a companion to a main sequence star; mass transfer takes place because both stars are linked by a magnetic field.

This theory has a disadvantage in that HgMn spectroscopic binary stars have so far not appeared to have evolved companions, nor have they been found to be magnetic. The HgMn programme stars studied in this project show abundance trends with temperature for the elements gallium and manganese, which should not be the case if this theory is the only explanation for the HgMn phenomenon as accretion is not a temperature dependent phenomenon. The presence of rare-earth elements are predicted and these are not seen in the atmospheres of HgMn stars. The theory does, however predict overabundances in strontium, and some of the HgMn stars in this sample show strontium overabundances.

The suggestion by Wahlgren et al (1995), that the Au/Pt ratios can be used to diagnose the s-process is indeterminate at current experimental precision.

7.3.3 Accretion from AGB companion

The class of non main-sequence stars known as BaII stars are thought to be a product of accretion from companion AGB stars in binary systems (Proffitt and Michaud 1989). These authors proposed that the main-sequence counterparts of these stars should exist and should have been observed, but they have not. This is curious, because the thinner envelopes of main-sequence stars should show s-process chemical peculiarities accreted from an AGB companion more clearly.

The authors predict that only 1.5% of all magnetic B stars could have accreted s-process elements during the thermally pulsing AGB phase of the companion star. It is therefore unlikely that the apparently non magnetic HgMn stars can be formed by this method, and of the magnetic Am stars, only 5% are predicted to be formed this way, which leaves 95% of Am cases unexplained. HgMn stars do not have a detectable magnetic field, so accretion of gas through a magnetic field is very unlikely to occur.

7.3.4 Supernovae

A supernova outburst close to an HgMn star precursor would shower the stellar atmosphere with heavy elements. Cameron (1971) suggests that a supernova could remove the outer atmosphere of the star and give it a radial velocity in excess of $10\,\mathrm{kms}^{-1}$. The pattern of heavy elements in the atmosphere of such a star would be an enhancement in all iron group elements by $\sim$ 1.0 dex compared to solar metallicities because this is the pattern of elements ejected by a supernova. It was predicted that only 0.06 of all CP stars can be created this way when the probability of CP formation is considered.

Abt (1979) found no evidence of large radial velocities in his study of HgMn stars in clusters. The iron group elements in the programme stars do not show a general enhancement, instead they show the signature manganese and gallium enhancement; the iron group elements are basically normal and are certainly not enhanced by a

$\sim$ 1 dex over the entire sample. The presence of the iron weak stars Vega and 87 Psc further suggests that this process alone cannot possibly account for the HgMn phenomenon.

7.3.5 Binarity and close binaries

Few normal low $v \sin i$ stars are known to be in binary systems; it is also unlikely that all normal A and B stars are binaries. It is unlikely that mass transfer *causes* the HgMn phenomenon either; studies of HgMn binary systems by Conti (1970) also show primary and secondary stars with different abundance patterns in primary and secondary stars. If mass transfer did take place in these systems the abundances should be identical. This theory also offers no explanation as to why A- and B-type stars should develop as HgMn stars to the exclusion of other stellar classes. Furthermore, the lack of stars with $m_2/m_1 \leq 0.1$ is inconsistent with secondaries in systems containing HgMn stars having passed through the red giant phase and having transferred matter onto the HgMn star (Wolff and Preston 1978).

Close non-synchronous binaries were examined by Wolff and Preston (1978). The authors found only a few HgMn stars with periods of less than 15 days in binary systems. The proximity of HgMn stars to a companion's radiation field could quite possibly disrupt the quiescent atmosphere needed for radiative diffusion to take place. Therefore HgMn stars in close binary systems may need another mechanism to explain their presence.

7.3.6 Surface nucleosynthesis

Burbidge and Burbidge (1955), and Fowler, Burbidge and Burbidge (1955) proposed that magnetic CP stars could be formed using surface nuclear reactions. HgMn stars are not detectably magnetic (Preston 1971). One of the characteristics of nuclear reactions is that stable elements with even-Z atomic numbers are more abundant that adjacent elements with odd-Z atomic numbers. Guthrie (1984) notes that some HgMn stars show a violation of this rule and some show an enhancement. This implies that nucleosynthesis may not be valid as the sole mechanism for the formation of HgMn stars.

Table 7.7: Even-odd Z ratios for HgMn stars.

Even-odd ratio	ϕ Her	υ Her	87 Psc	HR7664	HR7361	HR6997
Mg:Al	1.31	–	1.23	–	–	1.35
Si:Al	1.34	–	1.28	–	–	1.42
Si:P	–	1.19	1.24	1.03	1.01	1.00
S:P	–	1.12	1.17	0.88	0.83	0.94
Ca:Sc	0.56	2.30	1.54	2.11	1.54	–
Ti:Sc	1.31	2.03	1.54	1.85	1.21	–
Ti:V	1.59	1.51	1.57	1.40	1.31	1.13
Cr:V	1.94	1.54	1.51	1.22	1.23	1.13
Cr:Mn	0.95	0.85	0.86	0.79	0.76	0.71
Fe:Mn	1.08	1.03	0.93	1.30	0.96	0.97
Sr:Y	0.83	0.27	0.58	–	0.64	–
Zr:Y	0.83	–	–	–	–	–

No evidence of this signature of nucleosynthesis was seen in the present data. When abundance ratios of adjacent even-odd elements in this project were examined (Table 7.7) the abundance ratio was close to unity for the majority of stars and elements. If nucleosynthesis was a suitable single explanation for HgMn stars then chromium and iron should be more abundant than manganese, but the opposite is the case, especially at higher temperatures, implying iron and chromium are not affected by temperature dependent phenomena in the same way as manganese. These results confirm Guthrie's conclusions.

7.3.7 Planetesimals

Planetesimal impacts can contribute heavy elements to the atmospheres of HgMn stars but this theory cannot stand alone as an explanation for the formation of CP stars because it does not address either the presence of underabundant elements or the isotopic element patterns seen in mercury and platinum.

7.3.8 The predictions of diffusion theory

Diffusion theory predicts that the effects of radiation pressure and gravity in a quiescent atmosphere can give rise to diffusion currents inside a stellar envelope, leading to layers of enhanced abundance inside the atmosphere which appear in the stellar spectra. Published predictions calculated using the diffusion hypothesis are discussed below and compared to the results obtained here.

Magnesium

Borsenberger, Michaud and Praderie (1984) studied magnesium and predicted that this element should be sensitive to gravitational settling below the helium convection zone in the initial stages of stellar evolution. They calculated that stars with a relatively small $\log g$ require less radiation pressure in order to support magnesium, so stars with lower $\log g$ values should have higher magnesium abundances. However, Smith (1993) and Smith and Dworetsky (1993a) were unable to confirm a correlation between $\log g$ and element abundance patterns in magnesium and most other elements, which means the effect of gravity may be at most a second order consideration.

The results in this thesis compare well with the calculations. Between 12 500-15 000K the theory predicts that magnesium should be no more than 0.48 dex underabundant, which encompasses the range of abundances calculated for this project.

Aluminium

Michaud (1970) briefly mentioned aluminium and predicted that this element will sink in Ap-star atmospheres, which is borne out by the fairly consistent underabundances seen in the HgMn stars in this sample.

Silicon

Vauclair, Hardorp and Peterson (1979) looked at the behaviour of 126 lines of silicon over a range of effective temperature between 12 000 and 14 000K. The authors found that the abundances should be within 0.3 dex of the solar value for normal stars,

but for Ap stars the neutral silicon moves into the line forming region and manifests itself as an overabundance.

The results in this thesis show consistently solar values for silicon in both HgMn and normal stars with the exceptions of HR7361, which is overabundant by 0.4 dex, and α Lyr, which is more than 0.3 dex underabundant.

Manganese

Alecian and Michaud (1981) produced an abundance envelope which represented the maximum overabundance which can develop in the stellar atmosphere. This does not represent the abundance which may actually be visible in the spectrum of the star because the time dependence of the HgMn phenomenon and optical depth of any layers of manganese are not taken into account. Smith (1992) computed a series of envelopes for various depth dependent layers of manganese, but although this model is a very simplified version as it is not likely that such clear cut layers exist in real stellar atmospheres, as a test for stratification in stellar atmospheres Smith's results bear up well.

The results presented here all lie below the maximum abundance envelope derived by Alecian and Michaud. The only star in this sample which does not fit the general positive correlation in manganese is HR7664, which has a much lower abundance than the other sample stars. This still fits the work of Alecian and Michaud as the envelope derived by these authors is only the maximum possible abundance supportable in a stellar atmosphere, not the expected abundance.

Iron

Two papers have been published recently which discuss the iron abundances and radiative acceleration on iron. The first work, Alecian, Michaud and Tully (1993) was an investigation on the radiative acceleration on iron using opacity project data. They compared g_R against g for iron and found for $T_{\rm eff}$=6 000K, Δg is small, but in hotter stars, a larger iron abundance should be seen. However, only iterative evolutionary calculations using both helium and iron can be used to determine the exact size of the iron overabundances and this is still awaiting completion.

Later work by LeBlanc and Michaud (1995) stated simply that evolutionary data and exact $T_{\rm eff}$ and $\log g$ values are needed to obtain accurate quantitative g_R values for iron. Abundance changes in iron can also alter the Rosseland mean opacity and so need to be taken into account, possibly by iterative methods, in the calculations.

A plot given in the paper shows an increase in iron abundance as $T_{\rm eff}$ rises between 9 000 – 10 000K. Recent observational work by Burkhart and Coupry (1991) indicated that g_R must be higher than currently predicted to account for the observed iron overabundances which were 0.25 dex in excess of theoretical predictions. It is possible that simultaneous diffusion of carbon, nitrogen, oxygen and helium can make it possible for the amount of iron supportable in the stellar atmosphere to increase by 0.5 dex, which may explain the observational results.

The iron abundance observations for HgMn stars in this thesis show a widely varying scatter between stars, even those of similar effective temperature. This is not so evident in normal stars which, with the exception of Vega, show a solar abundance. The predictions here indicate that overabundances should be observed but do not account for the underabundance observed in the hotter HgMn star 87 Psc; indeed this result contrasts with the theoretical prediction of hotter stars having higher iron abundances.

Nickel

Michaud (1970) predicted that nickel would be underabundant in HgMn stars but no detailed calculations have been performed yet for this element. The results in this thesis show three of the HgMn stars have a significant nickel underabundance and agree with the theoretical predictions.

Gallium

The behaviour of gallium was first modelled by Alecian and Artru (1987). They found that at solar abundance g_R is greater than g over the optical depth range $-4 \leq \log \tau_0 \leq 3$ and this difference increases with effective temperature over the range 10 000 – 15 000K. At higher temperatures the flux maximum of the stellar spectrum shifts towards the wavelength region containing the Ga II and Ga III lines. The

authors estimate that in a 10 000K star the expected overabundance can be as high as 3 dex, whereas at 15 000K the maximum overabundance is ~4.5 dex. 'Hydrodynamic mechanisms' are proposed by the authors to account for any scatter in the results. It is also likely that the diffusion of gallium is time-dependent. The authors further proposed that gallium overabundance could be stratified over the optical depth range $-1 \leq \log \tau_0 \leq 0$ and performed a calculation using this model. The apparent gallium overabundances were ~0.5 dex lower than in the non- stratified solution, however it should be remembered that the stratified model is a *basic* model.

The results obtained in this thesis show a fairly consistent overabundance in gallium, with little obvious temperature dependent correlation, which fits with the qualitative predictions offered by Alecian and Artru (1987). Quantitatively, the abundances seen at 11 000K are approximately 3 dex overabundant, which fits the maximum supportable abundance at 10 000K of 3 dex. At 13 650K HR7361 shows an overabundance of 4 dex, and at 14 520 HR6997 shows an enhancement of 3.5 dex, which match theoretical predictions of the maximum possible gallium abundance in the stellar atmosphere; certainly abundances in excess of 4.5 dex are not seen in the thesis results.

7.4 Summary

It seems quite likely that HgMn stars are the norm at low rotational velocities where the atmosphere is stable enough to allow diffusion; single stars not in binary systems appear to have the capacity to become HgMn stars. It may then be that the low $v \sin i$ normal stars are rapid rotators with a pole-on or close to pole-on inclination, and that HgMn stars are true slow-rotating B-stars. 12% of the sample examined by Wolff and Preston (1978) were HgMn stars, which, if this is extended, implies 12% of B-stars are slow rotators ($\leq 100\,\mathrm{kms}^{-1}$). This suggestion can be tested by examining the profile of the weak Fe I line at λ4528, because a trapezoidal shape will imply that the inclination of the star (Gulliver *et al* 1994) is close to zero.

Diffusion theory also does not predict the presence of He-rich stars, which require a mechanism to re-elevate the helium in the stellar envelope after it has been lost from the helium convection zone.

Chapter 8

Final comments and conclusions

This work has shown that it is possible to obtain high-quality abundance determinations with a carefully-selected line sample and a combination of iterative and synthesis-based techniques. As a direct consequence of the improved methods used it has been possible to draw a number of conclusions and suggest some ideas for future work in this field which are described and discussed in the sections which follow.

8.1 Conclusions

8.1.1 Data reduction and analysis

The data in this project were obtained using an 800×800 CCD chip, which provided excellent response in the blue spectral region of 3900–4900Å. In order to fit all of the free-spectral- range (FSR) onto this chip it was necessary to adjust the grating angles which meant it was necessary obtaining data in 'batches' of one setting to reduce the time spent recalibrating the spectrograph for each setting. This also meant it was necessary to re-acquire objects, sometimes on consecutive nights, thereby reducing the sample it was possible to obtain during an observing run. It seems that a larger CCD chip with a wider wavelength coverage should be used in future which means only one exposure of an object will then be necessary, which will improve the number of stars obtainable on an observing run. Improved redundancy in the face of cosmic

ray events will also be an advantage, as the gaps in data from a combination of bad pixels and cosmic rays, though not always sigificant, can be a real enough difficulty, especially when a cosmic ray lands upon an important line. The large unthinned CCD currently available at the time of writing at Lick Observatory will yield a reduced signal-to-noise for a comparable exposure time on the small chip, however, two consecutive exposures of an object will probably overcome this and provide twice the number of spectra as a similar exposure on the small chip. A new thinned CCD, although afflicted by numerous bad columns and cosmetic defects, has already been used to observed HgMn stars (Dworetsky *priv comm*).

The presence of cosmic rays is a problem in long-exposure spectra, so the spectra were taken as a series of short exposures to compensate for this effect. In this project cosmic rays are removed by the multiplication through the data of a binary mask, rather than by the 'snip and smear' technique available in FIGARO. This is because FIGARO artificially destroys and replaces several pixels of data which can easily give rise to artificial results being presented as 'data'. It is far better instead to completely remove one or two pixels, which in most cases can be replaced by the corresponding sister exposure. This is especially important in narrow-lined stars, where a profile can be partially recovered from the latter, adopted, technique but is at least distorted, if not totally lost, by the other technique.

The software package VISTA should be used in preference to the early releases of ECHOMOP, as in comparison VISTA is user-friendly, fast at running batch processes of data and internally fairly stable. It is not possible to make any statements about the latest release of ECHOMOP or the current standard reduction package IRAF. The data reduced by VISTA were artifact-free and with a signal-to-noise in excess of 100:1. Investigation of spectra during investigation of the line-profile asymmetry proved that the background subtraction performed by VISTA was sufficient. One pitfall of using VISTA is the occasional 'quantisation' of data when saving a flat-fielded but un-normalised spectrum to disk. It is recommended the worker be aware of this and that the data are scaled upwards by several orders of magnitude to prevent this from occurring.

The technique for measuring and removing parasitic light presented and adopted in this work is an essential one wherever uncertainty as to the amount of parasitic or

scattered light is present. This technique involves first measuring the profile of the comparison-spectrum and convolving this through the spectrum of a standard star, then comparing the resulting spectrum against the data and measuring the difference between the equivalent widths of both spectra. As the presence of scattered and parasitic light can introduce an important systematic error into the final abundances of several percent (comparable, for example, with the effect of nLTE on the UV abundances of magnesium, Smith 1992) this technique, which is convenient and easy to apply, should be adopted for future abundance analyses.

When performing the flat-field technique on echelle spectra it is desirable that a wide-dekker (long slit) dispersed flat-field spectrum is used in preference to a narrow-dekker spectrum. This has the effect of increasing the photon counts in the 'tail' of the spatial profile and so increases the signal-to-noise of the collapsed flat-field spectrum. This in turn has the effect of increasing the signal-to-noise of the flat-fielded stellar spectrum.

Before final summation it was necessary to reduce the spectra to the laboratory scale by comparison between the RMT wavelengths of strong lines and the measured line-core wavelengths (not the line centroids). This technique is preferable to that of cross-correlation for a number of reasons. Firstly, the construction of a full synthetic spectrum before analysis began would be necessary, and secondly, because cross-correlation is a fundamentally linear technique, it would have been necessary to split the spectrum into a number of short segments where the linear variation of the radial velocity along the wavelength scale can be said to be neglible. The sheer volume of data precluded this approach. Finally, an additional correction for a constant wavelength shift, because of problems with the profile asymmetry, may have been required.

8.1.2 Spectrum analysis

Only one star, υ Her, was used to select the lines used in the abundance analysis; in future it could have possibly been more thorough to examine the spectra of the other sample stars in greater detail, if only to discover the presence of other unusually overabundant elements such as zirconium or gold in their spectra. However, the approach used here sufficed as it was essential to rationalise the line sample and,

where possible, examine the same blend-free lines in each star in order to show more clearly any stellar systematics in the line abundances.

Three selection criteria should be used to enable choice of lines types appropriate to this analysis. It is suggested that line types best suited for this type of analysis are:

a.) lines that are on the linear part of the curve-of-growth and are well-defined;

b.) lines that are not blended;

c.) lines with high-quality atomic data.

Justification for these criteria has been demonstrated both by theoretical argument and in that the final abundances presented in this project for normal stars are generally consistent with those in the literature.

In this project, line selection was made prior to the abundance calculations so as to effectively avoid 'positive discrimination' which would introduce systematic error into the abundances. Line selection must proceed carefully to avoid the pitfall of selecting lines because they give the 'right answer'. It is further recommended that the line list in Tables 3.1 and 3.2 be considered as the basis for abundance determinations in the future.

8.1.3 The stellar and line parameters

The effective temperatures and surface gravities used for the programme stars are taken from the work of Smith and Dworetsky (1993). This is because the parameters have been calculated from a combination of spectrophotometric and photometric data rather than from one single photometric source, and then the parameters which give the minimum reduced χ^2 for the variables on a $T_{\rm eff}/\log g$ grid are adopted.

Microturbulences were calculated according to the method of Magain (1984); this is a widely adopted method of determining microturbulence for abundance analysis, *in spite of some anomalous results*, as its method of dealing with random error in equivalent width measurements make it far superior to the classical technique for determining abundance. The microturbulences provided by this method produce abundances for the normal and HgMn stars consistent with the literature and in some

cases are an improvement upon these (*i.e.*, ζ Dra), but for some hot stars anomalous imaginary values for the microturbulence were found, which was a consequence of a negative correlation coefficient. It is worth remembering a very well-correlated data set with a very small gradient can have a correlation coefficient close to $\pm$ unity.

8.1.4 Abundance analysis

The two methods of analysis used in this thesis, spectrum synthesis and line abundance iteration, give satisfactory results when applied sensibly. When calculating the mean abundance for an element it is recommended this not be weighted by the line equivalent width. Weak lines and broadened lines have a large random fractional error in their measured equivalent widths, but strong lines often lie on the flat part of the curve-of-growth and so have a large uncertainty in their calculated abundance. It is therefore sensible to avoid favouring lines from any particular part of the curve-of-growth, especially with such a small sample size, and simply to take an unbiased mean of the abundances.

When combining mean abundances of more than one species for a single element the abundances should be weighted by the number of lines analysed for each species.

The method for determining the errors in the calculation (first described by Smith 1993) and adopted here should be used in the future as it allows the covariance between dependent variables used in calculating the abundance to be taken into account. The error due to uncertainties in independent variables was measured directly and is highly variable.

8.2 Future work

8.2.1 The abundances of cluster stars

It is important to obtain the abundances of cluster stars in order to obtain information which can be related to the ages of these stars and the evolutionary context of the HgMn phenomenon as well as the temperature-dependent trends seen in this and other work. There are many HgMn stars in open clusters (Abt 1979) but it was

not possible to undertake such a study in this project because the telescope integration time required for these objects, often with magnitudes fainter than m_V=8, makes such a study difficult, in terms of the high competition for telescope time, the time spent observing, and the many data frames requiring reduction. Instead, an international collaboration, with a pool of spectra and data reduction hours, may make such a project feasible. Such a project would require a telescope with a large light-gathering capability, an échelle spectrograph and high-sensitivity detectors.

8.2.2 nLTE models

Work by Lemke on normal stars has already illustrated the differences which can be found in abundance analysis using nLTE models. Some of the peculiar differences seen here and in previous work on normal stars could be explained by the presence of nLTE effects on subordinate ionisation stages in the stellar atmosphere and the ionisation balance being shifted in favour of one ion. Use of the correct nLTE models should produce abundances similar between two or more stages. The UV analysis of doubly ionised yttrium and zirconium by Redfors and Cowley (1993) illustrates again the importance of modelling stellar atmospheres to take nLTE effects into account. Curiously, the unpublished work by Gigas (1986) quoted by Lemke (1990) increased the discrepancy between iron ionisation stages in Vega.

8.2.3 The imaginary microturbulence

It would be worth investigating further the microturbulence parameters of stars with $T_{\rm eff}$ values above 11 000K to see if the imaginary microturbulence parameters obtained here could be repeated in other work with different data and spectrum synthesis packages and, if so, to account for this phenomenon. It would be useful for this investigation to include the sample HgMn and normal stars analysed here, as well as other B-type stars above 11 000K.

8.2.4 Abundance analysis with higher resolution spectra

The resolution of spectra with $v \sin i$ below 9kms^{-1} obtained for this project was compromised by the broad, distorted instrumental profile of the Schmidt camera.

This camera has since been replaced and it would be useful to observe the very narrow lined normal and HgMn stars with this new set-up in order to resolve line blends. Indeed, during this study another observing run was scheduled on the Hamilton Échelle Spectrograph using a Schmidt camera with an improved point-spread-function. This means these new data are free of the asymmetrical 9kms^{-1} instrumental profile and so the resolving power was indeed much closer to the quoted 48 000; a measured value, R=46 500, was obtained in July 1995 (Dworetsky, *priv. comm*). A new blue-sensitive CCD with a much larger area is now also available. Unfortunately it was too late to analyse these data in time for this project, but future work can be suggested which uses these new data; firstly, stars with $v \sin i$ values lower than 9kms^{-1} can be analysed and the spectral lines distinguished and secondly, the mercury and platinum lines, which it has not been feasible to analyse here, can be resolved and synthesised.

8.2.5 Binary star systems

Doubled lined binaries were not examined in this thesis because of the complications that can arise from examining and anlysing their spectra (and time constraints). However, these stars contain interesting data and it would be useful to analyse these systems in the future. (Dworetsky and Jomaron, work in progress).

8.2.6 Analysis of large amounts of data

The problem which exists currently is the presence of a great deal of abundance data from different sources. These data cannot be combined into a database of HgMn star abundances to give a single, definitive abundance for each element and each star. This is because of the differences between the techniques used by the different workers in this field. It would be useful to come to some agreement on the techniques used and to produce a 'standard' technique used by all researchers. The problem with this approach is that science advances and methods are being improved continuously and it is the nature of science that new and original ideas will be proposed, superseding the standardised technique before it has time to be used.

Automatic data reduction can reduce the amount of time spent on data processing, which can increase the volume of data considerably. However, some work, such as the identification and measuring of spectral lines, needs close supervision. It seems therefore that this problem is a difficult one to solve and at some point a standard technique should be adopted, possibly through shared authorship, in order to increase the throughput of results.

8.3 Acknowledgements

I would like to thank the following people for their assistance with this thesis:

- Mike Dworetsky for supervising this project, proof reading the thesis and giving encouragement;

- Keith Smith, Barry Smalley, Ian Howarth and Chris Jomaron for advice on LaTeX coding and data reduction;

- Andy Reid for advice on incorporating graphics into the thesis;

- Martin Dean for his friendship;

- Ron, Mary and Graham Allen for their support and use of their PC;

- Tony Misch for advice and unstinting support at Lick Observatory;

- PCD Maltron for supplying me with the ergonomic keyboard I needed to complete this project;

and finally

- this thesis would not have been possible without the funding from the Science and Engineering Research Council (SERC)/ Particle Physics and Astronomy Research Council (PPARC) (Studentship number 92 30088X).

Thank you all!

Appendix A

Full line-list

This table lists the lines and equivalent widths measured for υ Her. All wavelengths and equivalent widths were measured using DIPSO. Equivalent widths are the mean of two measurements measured through integration; no synthesised or fitted equivalent widths are listed. A series of labels have been devised to help describe the spectrum in more detail. The equivalent width of a line of a species which is blended is uncertain and labelled with a colon ':' next to the measurement. Line blends are dealt with in the 'Comments' heading and the following symbols are used; '$\surd$', which means 'used in line analysis', 'B', which means 'blended, not suitable', 'S', which means 'blended but synthesised' and 'H', which refers to the presence of hyperfine structure. The blend parameter 'BX' (*i.e.* B2, B3) indicates the presence of X adjacent lines, listed individually in the Table, which are blends of each other but are separable. A question mark '?' located in the margin means the ID is uncertain; if this is located in the line-blend column it means a blending species has not been identified. Additional blending species indicators are also given in the comments heading (*i.e.* Hβ). All wavelengths were adopted from Adelman (1991,1990,1989) unless labelled †† (Kurucz and Peytremann 1975) or † (Iglesias and Velasco 1964).

Table A.1: The measured line-list for υ Her

λ_{obs}	ID	λ_{lab}	Blends	W_λ/mÅ	Comments
3913.45	Ti II	3913.464	–	70	√
3917.36	Mn II	3917.32†	–	28	√
3918.43	Fe II	3918.51	–	14:	B2
3918.89	–	–	–	13:	B2
3920.67	Fe I	3920.65	C II 3920.677	27:	B
			Fe I 3920.839		
3926.09	–	–	–	15:	B2
3926.40	–	–	–	22:	B2
3928.06	Fe I	3927.92	–	9	
3933.60	Ca II	3933.664	Ti II 3932.01	202:	B
3935.88	Fe II	3935.942	–	20	√
3935.99	–	–	–	21	
3938.28	Fe II	3938.29	–	12	
3938.99	–	–	–	16	
3941.23	Mn II	3941.22†	Fe I 3941.283	19	B
3943.84	Mn II	3943.86†	Al I 3944.009	53:	S √
3945.21	Fe II	3945.21††	–	11	√
3950.38	Y II	3950.35††	–	26	√
3952.47	Mn II	3952.418†	Fe I 3952.606	10:	B
			Cr I 3952.399		
3960.95	Al I	3961.52	–	4	√
3968.41	Ca II	3968.470	–	78:	B (Hβ)
3975.01	Fe II	3975.016††	–	6	
3975.77	Fe II	3975.743	Mn II 3975.74†	13:	B
3979.48	Cr II	3979.51††	–	15	B √
3982.02	Ti II	3981.998††	–	7	
3982.61	Y II	3982.59	–	6	√
3984.01	Hg II	3983.99	–	116	
3986.66	Mn I	3986.826	Mg I 3986.753	16:	B
3994.16	Fe I	3994.117††	–	4	
3995.28	Mn II	3995.32†	Co I 3995.306	8	
3996.57	–	–	–	9	
4002.04	Fe II	4002.073††	–	7	

λ_{obs}	ID	λ_{lab}	Blends	W_λ/mÅ	Comments
4002.55	Fe II	4002.549	Fe I 4002.665	14:	B
4002.83	V II	4002.94	–	2:	B
4003.32	Cr II	4003.28[tt]	–	10	√
4004.92	Fe I	4005.241	–	4	
4005.24	V II	4005.706	–	4	
4011.78	Fe I	4011.71	–	3	
4012.42	Ti II	4012.372	Cr II 4012.50	47:	S √
			Fe II 4012.74[tt]		
4013.44	–	–	–	5	
4017.56	–	–	–	3	
4018.06	–	–	–	6	
4024.38	Fe II	4024.552	Fe I 4024.735	20:	B (He I)
4024.86	Cr I	4025.012	Ti II 4025.136	13:	S √ (He I)
4026.13	He I	4026.189	He I 4026.362	–	B
4028.40	Ti II	4028.332	–	35:	S √ (He I)
4028.84	S II	4028.791	Mn I 4028.59[t]	3:	B √
			Ti II 4028.33		
4030.32	–	–	–	3	
4030.72	Mn I	4030.755	Fe II 4030.35[tt]	19:	S √
4031.49	Fe II	4031.44	–	5	
4033.01	Ga I	4032.94	S II 4032.81	51:	B
			Fe II 4032.94		
			Mn I 4033.06		
4034.42	Mn I	4034.490	Fe II 4034.24	11:	S √
4035.74	V II	4035.63	–	6	√
4038.02	Cr II	4038.03[tt]	–	11	
4041.41	Mn I	4041.361	Fe II 4041.64	18:	B √
			Fe II 4041.27		
4044.06	–	–	–	6	
4044.60	Fe II	4044.61[tt]	–	7	√
4045.17	–	–	–	4	
4045.85	Fe I	4045.84[tt]	–	18	√
4048.85	Fe II	4048.831[tt]	V II 4048.67	24:	B
4049.08	Cr II	4049.14[tt]	?	24:	B
4050.59	–	–	–	6	

λ_{obs}	ID	λ_{lab}	Blends	W_λ/mÅ	Comments
4051.96	Cr II	4051.97[††]	–	11	
4053.80	Ti II	4053.81	Cr II 4053.43	38:	B
			V II 4053.59		
			Mn II 4054.05		
4055.49	Fe II	4055.24	Mn I 4055.55	7	√
4057.33	Fe II	4057.46	–	7	
4059.56	Mn I	4059.39	Fe II 4059.71	2	
4061.83	Fe II	4061.787[††]	–	5	
4063.59	Fe I	4063.597[††]	–	13	√
4065.03	–	–	–	4	
4065.82	–	–	–	3	
4066.68	–	–	–	2	
4067.12	Ni II	4067.051	Fe I 4066.98	9:	S √
4071.87	Fe I	4071.740	–	10	√
4072.57	Cr II	4072.56	–	2	
4072.66	Cr II	4072.56	–	7	
4075.63	Si II	4075.45	Fe II 4075.95	14:	B
4076.89	Si II	4076.78	Cr II 4076.87	14:	B
4077.93	Sr II	4077.714	Cr II 4077.51	45:	B
4079.32	–	–	–	8	
4081.48	Fe II	4081.42	Mn II 4081.45	33:	B
4083.73	Mn II[†]	4083.66	–	17	
4085.09	–	–	–	10	
4085.41	–	–	–	18	
4105.17	–	–	–	22	
4110.62	Cr II	4110.68[††]	–	23:	B2
4111.00	Cr II	4110.99[††]	–	9:	B2
4111.94	Fe II	4111.88[††]	–	5	
4113.22	Cr II	4113.21[††]	–	3	
4114.11	–	–	–	5	
4120.03	–	–	–	4	
4120.90	–	–	–	16	
4122.69	Fe II	4122.638	Fe I 4122.52	20:	S √
4124.86	Fe II	4124.78[††]	–	7	
4128.11	Si II	4128.071	–	123	√

λ_{obs}	ID	λ_{lab}	Blends	W_λ/mÅ	Comments
4130.89	Si II	4130.884	Ba II 4130.648	103:	S √
4132.45	Fe I	4132.06	–	3	
4137.02	Mn II	4136.91†	Fe I 4136.997	73:	B
4140.43	–	–	–	13	
4143.89	Fe I	4143.83††	–	7	
4145.76	Cr II	4145.77	–	14	√
4153.08	S II	4153.098	–	10	√
4161.59	Ti II	4161.52††	–	8	√
4162.69	S II	4162.698	–	9	√
4163.27	Ti II	4163.55††	–	51	√
4167.20	Mg II	4167.26	Fe II 4167.30	5:	S √
4171.11	–	–	–	16	
4171.67	–	–	–	15	
4172.02	Ga I	4171.99	Ti II 4171.91	68:	S √
			Cr II 4171.90		
4173.51	Fe II	4173.45	Ti II 4173.537	55:	B
4174.35	Ti II	4174.07††	Mn II 4173.32†	42:	B
4177.50	Fe II	4177.70	Mn II 4177.48	58	B
4178.85	Fe II	4178.86††	–	40	
4179.45	Cr II	4179.43††	–	16	
4180.11	–	–	–	8	
4184.37	Ti II	4184.29††	Fe II 4184.285	26	B
			Mn II 4184.46		
4187.79	Fe I	4187.802††	–	5	
4189.03	–	–	–	6	
4189.70	–	–	–	5	B2
4190.67	Si II	4190.738	–	15:	B2
4195.28	Fe II	4195.337	Cr II 4195.41	8:	B
4196.12	Fe I	4196.218	–	3	
4198.11	Si II	4198.124	–	3	
4198.20	Fe I	4198.268	Fe I 4198.310	5:	B
4199.08	Y II	4199.10	?	13:	B
4205.34	Mn II	4205.37	Fe I 4205.48	52:	B
4206.35	Mn II	4206.375	–	72	H √
4207.24	Cr II	4207.35	–	5	

λ_{obs}	ID	λ_{lab}	Blends	W_λ/mÅ	Comments
4215.48	Sr II	4215.524	Cr II 4215.74	34:	S √
			Mn II 4215.54		
4216.43	–	–	–	11	
4217.88	–	–	–	5	
4218.37	–	–	–	6	
4224.87	Cr II	4224.85	–	13	
4226.70	Ca II	4226.73	–	4	√
4227.39	Fe I	4227.42	–	8	
4233.20	Cr II	4233.25	Fe II 4233.17	91:	B
4235.77	Fe I	4235.942	Y II 4235.73	5:	S √
4237.85	–	–	–	11	
4238.75	Mn II	4238.79	Fe II 4238.816	36:	B2
4239.17	Mn II	4239.19†	–	32:	B2
4242.35	Cr II	4242.38	Mn II 4242.33	70:	B2 S √
4242.96	Mn II	4242.92	–	13	B2
4244.25	Mn II	4244.26	–	30	
4246.82	Sc II	4246.829	–	8	√
4247.94	Mn II	4247.95††	–	29	
4250.46	Fe I	4250.12		2	?
4251.18	Fe I	4250.90	–	42	
4251.78	Mn II	4251.74†	Ti II 4252.036	49	B
			Fe II 4252.335		
4253.04	Mn II	4252.96†	Cr I 4254.346	19:	B
4254.58	Cr II	4254.56	–	8	√
4255.70	–	–	?	28	B
4258.17	Fe II	4258.155	Fe II 4258.35	13	S √
4259.23	Mn II	4259.203	S II4259.17	74:	B
4260.46	Mn II	4260.47	Fe I 4260.479	15:	B
4261.93	Cr II	4261.92	Cr II 4261.85	52:	B
4263.11	–	–	–	5	
4263.92	Fe II	4263.895	–	4	
4265.91	–	–	–	4	
4267.23	C II	4267.02	C II 4267.27	36:	B
4267.86	–	–	–	7	
4269.52	Cr II	4269.28	–	10	

λ_{obs}	ID	λ_{lab}	Blends	W_λ/mÅ	Comments
4273.30	Fe II	4273.22	–	15	√
4274.77	Cr I	4274.80	–	2	√
4275.55	Cr II	4275.58	Mn II 4275.88	28:	B
4278.17	Fe II	4278.128	–	9:	B2 S √
4278.62	–	–	–	18:	B2
4279.38	–	–	–	6	
4282.06	–	–	–	27:	B2
4282.57	Fe I	4282.406	–	51:	B2
4283.86	Mn II†	4283.86	–	39:	B2
4284.37	Mn II	4284.425	Cr II 4284.21	47:	B2
4286.30	Fe II	4286.311	–	5	
4287.87	Ti II	4287.893	Mn II† 4288.065	33:	S √
4289.70	Cr I	4289.721	–	10	√
4290.21	Ti II	4290.222	–	54	√
4291.43	–	–	–	5	
4292.27	Mn II	4292.246	Mn II4292.383	63:	B
4293.30	Mn II	4293.226	–	5	?
4294.16	Fe I	4294.128	Ti II 4294.101	57:	B
4296.63	Fe II	4296.567	–	27	√
4300.04	Ti II	4300.052	Mn II 4300.23	86:	√
4301.90	Ti II	4301.928	–	39	√
4303.16	Fe II	4303.166	–	55	√ distorted
4307.90	Fe II	4307.906	Ti II 4307.900	53:	B2
4308.19	–	–	?	35:	B2
4309.67	Y II	4309.62	–	16	√
4310.76	–	–	–	9	
4312.85	Ti II	4312.861	–	48	√
4314.32	Fe II	4314.289	–	22	
4315.06	Fe II††	4315.09	Ti II 4314.98	44:	S √
4321.01	Fe II	4321.341	Ti II 4320.96	24:	B
4325.18	Fe II††	4325.43	Fe II 4325.54 ††	24:	B
4325.76	Fe I	4325.765	?	11:	B
4326.68	Mn II†	4326.63	–	88	√
4330.25	Ti II	4330.264	–	9:	B2
4330.72	Ti II	4330.708	–	9:	B2

λ_{obs}	ID	λ_{lab}	Blends	W_λ/mÅ	Comments
4337.89	Ti II	4337.916	–	24	B (H balmer line)
4343.92	Mn II	4343.987	?	75	B (also in H line wing)
4345.59	–	–	–	12	
4346.43	–	–	–	6	
4348.55	–	–	–	40	
4350.86	Ti II	4350.834	–	8	
4351.88	Mg I	4351.8941	Mg II 4351.956	50:	S √
			Fe II 4351.77		
4352.65	–	–	–	2	
4356.64	–	–	–	26	
4357.57	Fe II	4357.574	–	11	
4358.25	Hg I	4358.343	–	4	
4358.73	Y II	4358.73	–	4	√
4361.30	Fe II	4361.249	–	6	
4362.05	Ni II	4362.10	–	3	√
4363.25	Mn II†	4363.26	–	25	√
4365.26	Mn II†	4365.22	–	27	√
4367.62	Ti II	4367.657	–	25	
4368.17	Fe II	4368.262	–	11	
4369.35	Fe II	4369.404	–	7	
4371.90	–	–	–	3	
4374.93	Y II	4374.94	Ti II 4374.82	50:	S √
4377.72	–	–	–	15	
4379.70	–	–	–	23	
4383.57	Fe II	4383.547	–	12	
4384.28	Fe II	4384.33	–	13:	B2
4384.66	Mg II	4384.643	Ni II 4384.6	18:	B2
4385.43	Fe II	4385.381	Mn II 4385.76	40:	S √
4386.91	Ti II	4386.858	–	22	
4388.17	He I	4387.928	–	–	
4390.60	Mg II	4390.585	–	29	√
4391.85	–	–	–	7	
4393.42	–	–	–	13	
4394.07	Ti II	4394.057	–	18	√
4395.03	Ti II	4395.031	–	67	√

λ_{obs}	ID	λ_{lab}	Blends	W_λ/mÅ	Comments
4395.86	Ti II	4395.848	–	14	√
4398.04	Y II	4398.02	–	14	√
4399.78	Ti II	4399.767	–	32	√
4402.84	Fe II	4402.875	–	7	
4403.46	Mn II†	4403.51	–	14	
4404.81	Fe I	4404.752	–	10	
4405.72	–	–	–	2	
4406.78	–	–	–	2	
4407.77	–	–	–	7	
4409.55	–	–	–	10	
4411.02	Ti II	4411.080	–	22	
4411.88	–	–	–	4	
4412.90	–	–	–	2	
4413.52	–	–	–	5	
4414.85	–	–	–	6	
4416.82	Fe II	4416.817	–	35	√
4417.81	Ti II	4417.718	–	40:	B2 S √
4418.34	Ti II	4418.34	–	11:	B2 S √
4419.73	Fe III††	4419.65	–	7	
4421.96	Ti II	4421.949	–	10	
4422.62	Y II	4422.59	Fe I 4422.57	8:	B
4428.01	Mg II	4427.995	TiII†† 4427.88	10:	S √
4430.98	–	–	–	3	
4431.58	Fe II	4431.64	–	3	
4434.04	Mg II	4433.991	Mn II† 4434.07	35:	S √
4435.72	–	–	–	8	
4437.66	–	–	–	4	
4441.84	Ti II	4441.73	Fe I 4442.343	17:	B
			Mn II† 4441.99		
4443.76	Ti II	4443.802	?	63	B
4444.44	Ti II	4444.559	Fe II 4444.563	14:	B2
4444.63	–	–	–	14:	B2
4445.98	Fe II	4446.24	–	6	
4450.55	Ti II	4450.487	–	35	
4451.61	Fe II	4451.545	–	18	

λ_{obs}	ID	λ_{lab}	Blends	W_λ/mÅ	Comments
4453.22	–	–	–	4	
4455.36	Fe II	4455.258	–	14	
4455.82	–	–	–	2	
4456.65	Ti II	4456.65	–	8	?
4457.56	–	–	–	3	
4458.25	–	–	–	4	
4461.77	Fe I	4461.654	Fe II†† 4461.71	13:	B2 S √
4462.00	–	–	–	6:	B2
4463.60	–	–	–	3	
4464.53	Ti II	4464.458	–	19	√
4465.84	CrII	4465.77	–	3	?
4466.63	–	–	–	3	
4468.48	Ti II††	4468.54	–	63	√
4469.12	TiII	4469.12	–	4	?
4470.86	Ti II	4470.864	–	8:	B (He I)
4471.51	He I	4471.688	–	–	
4472.94	Ti II	4472.92	–	13:	B (He I)
4475.25	P II	4475.27	–	5	√
4476.01	Fe II	4476.08	–	2	
4478.65	Mn II†	4478.64	–	44	√
4481.15	Mg II	4481.129	Mg II 4481.1327	248:	B (doublet)
4483.42	P II	4483.69	–	6	√
4488.39	Ti II	4488.319	–	28	
4489.28	Fe II	4489.185	–	27	
4491.47	Fe II	4491.401	Mn I 4491.65	33:	S √
4493.55	Fe II	4493.579	–	7	
4497.00	Fe II	4496.96	–	2	
4499.24	P II	4499.18	–	4	√
4500.47	Mn II†	4500.543	–	13	
4501.24	Ti II	4501.27	–	69	√
4503.15	–	–	–	12	
4508.21	Fe II	4508.283	–	46	√
4510.37	–	–	–	7	
4511.79	–	–	–	3	
4515.32	Fe II	4515.337	–	45	√

λ_{obs}	ID	λ_{lab}	Blends	W_λ/mÅ	Comments
4518.98	–	–	–	4	
4519.24	Mn II†	4518.96	?	38:	B (of several lines)
4520.23	Fe II	4520.225	–	38	√
4522.71	Fe II	4522.634	–	53	√
4525.35	Mn II†	4525.33	?	23:	B
4528.37	–	–	–	2	
4529.47	Ti II	4529.46	–	16	?
4533.99	Fe II	4534.166	Ti II 4533.97	82:	S √
4539.61	Cr II	4539.62	–	7	
4541.49	Fe II	4541.523	–	30	
4544.00	–	–	–	5	
4545.01	Ti II	4545.144	–	5	
4546.60	–	–	–	3	
4549.31	Fe II	4549.214	Fe II 4549.467	161:	B
			Ti II 4549.82		
			Ti II 4549.622		
4552.42	–	–	–	10	
4554.03	Ba II	4554.033	–	11	√
4554.98	Cr II	4555.02	–	45	
4555.90	Fe II	4555.890	–	45	√
4558.68	Cr II	4558.659	–	67	√
4563.74	Ti II	4563.761	–	57	√
4565.74	–	–	–	13	
4571.26	–	–	–	4	
4571.98	TiII	4571.97	–	72	√
4576.32	Fe II	4576.331	–	24	√
4578.99	Fe II	4579.32	–	2	?
4580.06	Fe II	4580.055	–	6	
4582.84	Fe II	4582.835	–	19	√
4583.82	Fe II††	4583.63	–	69	
4588.22	Cr II	4588.217	–	62	√
4589.90	Cr II	4589.89	Ti II 4589.961	30:	B
4592.10	Cr II	4592.09	–	29	
4596.01	Fe II	4596.06	–	16	
4598.48	Fe II	4598.528	–	6	

λ_{obs}	ID	λ_{lab}	Blends	W_λ/mÅ	Comments
4602.09	P II	4602.08	–	7	√
4603.08	–	–	–	7	
4603.35	–	–	–	3	
4605.38	–	–	–	4	
4610.59	Fe II	4610.59	–	3	
4616.57	Cr II	4616.64	–	24	
4617.30	–	–	–	9	
4618.77	Cr II††	4618.83	–	43	
4620.49	Fe II	4620.513	–	16	√
4621.44	Si II††	4621.42	Si II 4621.72	17:	B (doublet)
4625.91	Fe II	4625.911	–	4	√
4628.85	Fe II	4628.821	–	3	
4629.36	Fe II	4629.336	–	42	√

Appendix B

The abundance tables

The abundances are quoted relative to the stellar hydrogen abundance and are listed in order of increasing effective temperature, whilst the elements are ranked in order of atomic number Z. In the abundance tables which follow the following symbols are used, (c.f. Tables 3.1 and 3.2), 'B' denotes a blend where the blending species dominates, 'C' labels a line profile destroyed by a cosmic ray, 'Z' a 'zapped' line profile not present in the spectrum (edge effects, bad columns etc.) and '–' means that the line is not present.

Table B.1: Abundances for normal stars

Line		θ Leo	α Lyr	HR7098	21 Peg	ζ Dra	21 Aql	τ Her
Ti II	3913.46	B	Z	Z	4.87	–	4.69	–
Mn II	3917.23	B	–	–	–	–	–	–
Fe II	3935.94	B	7.05	–	B	7.13	7.67	–
Al I	3944.01	6.53	5.74	6.47	6.25	6.27	6.35	–
Fe II	3945.21	B	6.86	7.49	7.29	B	7.41	–
Y II	3950.35	2.83	Z	B	–	–	–	–
V II	3951.97	4.27	4.44	4.08	–	–	–	–
Zr II	3958.22	–	–	–	–	–	–	–
Al I	3961.52	6.65	5.85	6.25	–	–	–	B
Cr II	3979.51	6.02	–	5.67	5. 42	5.45	5.37	–
Y II	3982.59	2.74	–	–	–	–	–	–
Zr II	3991.13	3.27	–	2.65	–	–	–	–
Zr II	3998.97	B	–	–	B	–	–	–
Cr II	4003.28	B	–	–	5.59	–	–	–
V II	4005.71	B	B	3.89	3.88	–	–	–
Ti II	4012.37	B	4.62	5.65	5.16	B	4.90	–
Ni II	4015.50	5.68	5.99	6.50	6.28	B	6.09	6.00
Ti II	4025.14	B	B	B	4.34	–	–	–
Ti II	4028.33	5.67	B	B	B	–	–	–
S II	4028.79	–	B	B	–	B	B	B
Mn I	4030.76	B	5.32	–	B	–	–	–
Ga I	4032.99	–	–	–	–	–	–	–
Mn I	4034.48	B	5.35	–	–	–	–	–
V II	4035.63	4.43	–	B	3.94	–	–	–
Mn I	4041.36	5.39	5.43	–	–	–	–	–
Fe II	4044.61	7.53	–	7.39	7.28	7.47	6.97	–
Fe I	4045.82	B	B	7.80	7.31	–	7.32	B
Zr II	4048.67	B	–	B	–	B	–	–
Ti II	4053.81	5.29	B	B	B	–	–	–
Mn I	4055.54	–	–	–	–	–	–	–
Fe I	4063.60	7.68	7.01	7.63	7.25	7.32	–	–
Ni II	4067.05	5.97	5.80	5.41	Z	5.16	5.99	5.98
Fe I	4071.74	7.60	6.99	7.56	Z	–	–	–

Line		θ Leo	α Lyr	HR7098	21 Peg	ζ Dra	21 Aql	τ Her
Sr II	4077.71	3.72	2.17	3.66	C	2.57	2.74	–
Fe II	4122.64	7.65	7.01	7.66	7 .41	B	7.40	7.40
Si II	4128.07	7.55	7.02	7.56	7.51	7.62	7.37	7.51
Ba II	4130.65	B	B	B	B	B	B	B
Si II	4130.889	7.79	7.22	7.55	7.44	7.64	7.46	7.37
Cr II	4145.76	B	B	B	B	B	B	B
S II	4153.10	$\leq$7.59	$\leq$7.57	6.75	7.27	7.58	7.45	7.45
Zr II	4156.24	B	–	–	–	–	–	–
Ti II	4161.52	B	4.81	5.12	B	–	–	–
S II	4162.70	$\leq$7.40	$\leq$7.37	–	–	7.30	7.33	7.37
Ti II	4163.64	B	C	5.47	5.05	–	–	–
Mg I	4167.26	7.41	6.97	7.65	7.29	–	–	–
Ga I	4172.04	–	–	–	–	–	–	–
Mn II	4206.37	H	H	H	–	–	–	–
Zr II	4208.985	B	–	–	–	–	–	–
Zr II	4211.88	3.16	–	–	–	–	–	–
Sr II	4215.52	3.55	2.14	B	2.91	2.75	2.92	–
Ca I	4226.73	6.18	5.90	6.65	5.99	–	$\leq$6.50	$\leq$6.50
Cr II	4242.38	6.07	–	5.89	5.80	B	B	5.65
Ni II	4244.82	–	–	–	–	B	–	–
Sc II	4246.83	2.87	2.84	2.72	2 .32	2.91	2.99	$\leq$3.46
Cr I	4254.35	5.87	5.35	–	B	–	–	–
Fe II	4273.22	7.67	6.98	7.74	7.46	7.30	7.44	7.79
Cr I	4274.80	5.80	5.39	5.98	5.73	–	–	–
Fe II	4278.13	7.53	6.93	7.46	7.20	B	–	–
Ti II	4287.89	5.25	4.91	5.11	4.79	–	–	–
Cr I	4289.72	B	B	5.96	5.89	–	–	–
Ti II	4290.22	B	5.03	5.69	5.08	4.75	4.95	–
Fe II	4296.57	B	7.01	7.78	7.39	7.45	7.41	7.41
Ti II	4300.05	5.47	5.13	B	4.83	B	4.65	4.90
Ti II	4301.93	Z	Z	Z	4.74	B	B	–
Fe II	4303.16	7.72	6.88	7.79	7.47	Z	Z	7.15
Y II	4309.62	B	1.91	B	–	–	–	–
Ti II	4312.86	5.33	4.80	5.23	4.78	4.90	4.96	–
Zr II	4317.32	B	–	–	–	–	–	–

Line		θ Leo	α Lyr	HR7098	21 Peg	ζ Dra	21 Aql	τ Her
Mn II	4326.68	B	–	–	–	–	–	–
Mg I	4351.90	7.40	B	7.60	7.31	B	B	B
Ni II	4362.10	5.52	–	6.66	6.38	B	6.16	–
Mn II	4363.26	B	–	5.55	–	–	–	–
Mn II	4365.22	–	–	–	–	–	–	–
Fe II	4369.40	7.84	Z	7.55	7.43	7.28	7.73	–
Y II	4374.94	B	2.20	2.63	2.30	–	–	–
Zr II	4379.78	B	–	–	–	–	–	–
Fe II	4385.38	7.69	6.86	7.83	7.42	B	B	B
Mg II	4390.58	7.51	7.05	7.70	7.71	7.69	7.64	7.71
Ti II	4394.06	4.97	4.42	4.95	4 .54	–	–	–
Ti II	4395.03	B	4.86	5.62	4.95	4.66	4.47	B
Ti II	4395.85	B	4.48	5.34	4.83	–	–	–
Y II	4398.02	–	2.25	2.54	–	–	–	–
Ti II	4399.78	B	B	5.19	4.75	–	–	B
Ni I	4401.55	–	5.88	6.25	6.48	B	–	–
Fe I	4404.75	7.80	7.05	7.68	7.36	7.60	–	–
Fe II	4416.82	7.69	6.98	7.60	7.41	7.51	7.41	7.42
Ti II	4417.72	B	4.77	5.19	4.82	–	–	–
Ti II	4418.34	B	4.92	5.23	4.96	–	–	–
Mg II	4427.99	7.57	6.85	7.50	7.47	7.56	7.51	7.60
Mg II	4433.99	7.58	6.95	7.65	7.52	7.51	7.59	7.67
Ti II	4464.53	5.33	4.98	5.32	4.95	B	B	B
Ti II	4468.54	B	4.72	5.47	4.77	–	4.45	–
P II	4475.26	–	–	–	–	–	–	–
Mn II	4478.64	5.75	–	5.65	–	–	–	–
P II	4483.68	–	–	–	–	–	–	–
Fe II	4491.40	7.59	6.99	7.72	7.46	7.74	7.26	7.25
P II	4499.24	–	–	–	–	–	–	–
Ti II	4501.24	B	4.71	5.37	4.91	4.42	4.59	–
Fe II	4508.28	7.74	6.91	7.67	7.39	7.25	7.33	7.19
Fe II	4515.34	7.67	6.96	7.69	7.55	7.57	7.44	7.23
Fe II	4520.22	7.67	7.06	7.24	7.40	7.41	7.31	–
Fe II	4522.63	7.78	6.98	7.45	7.31	7.30	7.29	7.12
Fe I	4528.62	B	7.06	7.81	7.54	–	–	–

Line		θ Leo	α Lyr	HR7098	21 Peg	ζ Dra	21 Aql	τ Her
Fe II	4533.99	B	B	B	B	B	B	B
Ba II	4554.03	3.34	–	3.00	2.76	–	–	–
Fe II	4555.89	7.82	B	Z	7.36	7.38	7.16	7.45
Cr II	4558.66	6.13	5.61	5.81	5.82	5.40	5.29	5.36
Ti II	4563.76	5.34	4.81	5.33	4.78	4.48	4.56	–
Ti II	4571.97	5.64	5.08	5.64	4.99	4.64	4.65	–
Fe II	4576.33	7.66	7.13	7.68	7 .44	7.24	7.41	7.54
Fe II	4582.835	7.49	6.82	7.61	7.30	B	B	–
Cr II	4588.217	6.15	5.56	5.77	5.68	B	5.35	–
Fe II	4620.51	7.48	Z	Z	7.42	B	7.03	B
Fe II	4625.91	7.41	–	7.46	7.02	–	–	–
P II	4626.70	–	–	–	–	–	–	–
Fe II	4629.336	7.81	B	C	B	B	B	7.10
Al II	4663.05	6.65	5.90	6.47	6.34	6.42	6.10	6.21
Mg I	4702.94	7.34	7.04	7.65	7.48	–	–	–

Table B.2: Abundances for HgMn stars

Line		ϕ Her	υ Her	87 Psc	HR7664	HR7361	HR6997
Ti II	3913.46	B	6.04	6.70	Z	–	5.87
Mn II	3917.23	6.85	7.06	7.21	Z	Z	8.21
Fe II	3935.94	B	7.38	B	8.20	7.76	8.00
Al I	3944.01	B	–	–	–	–	B
Fe II	3945.21	7.67	7.56	Z	7.97	7.65	B
Y II	3950.35	C	B	4.85	–	–	Z
V II	3951.97	3.49	–	Z	–	–	B
Zr II	3958.22	4.53	–	Z	–	–	–
Al I	3961.52	–	–	–	–	–	–
Ca II	3968.73	B	B	B	B	B	B
Cr II	3979.51	6.54	B	–	–	6.11	Z
Y II	3982.59	Z	3.68	4.51	–	4.66	–
Zr II	3991.13	4.79	–	–	–	–	–
Zr II	3998.97	4.94	–	–	–	–	–
Cr II	4003.28	6.49	5.82	6.34	–	6.09	–
V II	4005.71	3.37	3.89	Z	–	5.06	B
Ti II	4012.37	5.33	6.05	6.89	6.09	5.94	–
Ni II	4015.50	5.90	–	5.65	5.78	–	B
Ti II	4025.14	5.92	5.43	7.24	5.43	–	B
Ti II	4028.33	4.95	5.66	B	5.47	–	B
S II	4028.79	–	–	B	–	–	B
Mn I	4030.76	7.04	7.02	7.70	Z	7.84	8 .24
Ga I	4032.99	6.00	6.07	6.50	6.20	6.80	6.90
Mn I	4034.48	6.99	7.05	7.83	C	8.13	8.21
V II	4035.63	B	3.97	4.41	4.01	4.82	4.84
Mn I	4041.36	7.11	B	7.76	C	7.94	8.35
Fe II	4044.61	7.52	7.29	C	8.15	7.89	Z
Fe II	4045.84	B	7.31	B	8.32	–	–
Zr II	4048.67	B	–	–	–	–	–
Ti II	4053.81	B	5.95	6.58	5.45	–	5.53
Mn I	4055.54	6.91	–	–	–	–	–
Fe I	4063.60	7.15	7.37	7.64	–	–	B
Ni II	4067.05	5.97	4.22	5.72	5.74	6.18	6.14

Line		ϕ Her	υ Her	87 Psc	HR7664	HR7361	HR6997
Fe I	4071.74	7.50	7.39	Z	8.20	–	B
Sr II	4077.71	3.89	3.91	2.62	–	3.05	3.24
Fe II	4122.64	7.58	B	6.96	B	7.40	B
Si II	4128.07	7.71	7.47	7.49	7.48	8.07	B[1]
Ba II	4130.65	B	B	B	–	B	B
Cr II	4145.76	6.78	B	B	B	B	B
Si II	4130.889	7.46	7.54	7.20	7.43	7.80	7.40
S II	4153.10	7.28	7.22	6.94	6.49	6.68	6.98
Zr II	4156.24	4.72	–	–	–	–	–
Ti II	4161.52	B	5.80	6.22	–	–	B
S II	4162.70	7.17	6.95	6.88	6.30	6.08	6.99
Ti II	4163.64	5.74	6.07	6.96	5.96	5.62	5.86
Mg I	4167.26	B	–	–	–	–	–
Mg I	4172.04	6.50	6.04	6.80	6.70	6.70	7.00
Mn II	4206.37	H	H	H	H	H	H
Zr II	4208.985	4.08	–	–	–	–	Z
Zr II	4211.88	4.79	–	–	–	–	–
Sr II	4215.52	4.05	3.87	2.74	–	B	B
Ca I	4226.73	6.40	$\leq$6.48	–	–	–	–
Cr II	4242.38	B	B	B	B	B	B
Sc II	4246.83	4.61	2.91	4.35	3 .17	3.54	–
Ni II	4244.82	B	B	–	–	–	–
Cr I	4254.35	B	–	–	–	–	–
Cr I	4274.80	6.80	–	–	–	–	–
Fe II	4273.32	B	7.30	7.30	Z	7.80	B
Fe II	4278.13	7.51	B	B	8.02	–	B
Cr I	4289.72	B	–	–	–	–	B
Ti II	4287.89	B	B	7.00	5.80	B	B
Ti II	4290.22	B	6.22	7.12	6.06	5.90	B
Fe II	4296.57	7.68	7.37	7.07	8.27	7.89	–
Ti II	4300.052	Z	B	B	Z	Z	C
Ti II	4301.93	5.10	5.81	6.51	5.77	5.47	–
Fe II	4303.16	7.77	B	7.27	8.51	8.15	–
Y II	4309.62	3.15	4.50	4.90	–	4.74	–
Ti II	4312.86	5.69	5.96	6.60	B	5.53	5.97

Line		ϕ Her	υ Her	87 Psc	HR7664	HR7361	HR6997
Zr II	4317.32	4.59	–	–	–	–	–
Mn II	4326.68	B	B	B	B	B	B
Mg I	4351.90	B	B	–	–	–	–
Ni II	4362.10	6.19	4.57	5.81	5.69	–	B
Mn II	4363.26	B	7.12	7.49	6.54	8.18	8.00
Mn II	4365.22	6.88	7.11	7.33	6.52	8.00	7.93
Fe II	4369.40	7.86	7.28	7.22	8.33	7.84	B
Y II	4374.94	B	B	4.66	4.09	B	B
Fe II	4385.38	7.43	B	B	8.34	7.98	B
Mg II	4390.58	7.30	7.10	6.89	6.49	7.32	6.99
Ti II	4394.06	4.93	5.71	6.35	5.59	–	B
Ti II	4395.03	5.84	6.05	6.76	5.99	5.34	B2
Ti II	4395.85	5.60	5.86	6.64	6.53	B	B2
Y II	4398.02	3.40	B	B	–	–	–
Ti II	4399.78	5.68	5.70	6.68	C	5.02	5.26
Ni I	4401.55	–	–	–	–	–	–
Fe I	4404.75	B	7.42	–	8.49	–	B
Fe II	4416.82	7.46	7.26	6.96	8.17	7.43	B
Ti II	4417.72	5.89	5.95	B2	5.88	5.91	5.78
Ti II	4418.34	5.93	6.02	B2	5.98	6.33	5.75
Mg II	4427.99	7.32	6.93	7.03	6.83	7.18	7.02
Mg II	4433.99	7.53	6.99	7.03	6.80	7.04	7.12
Ti II	4464.53	B	6.03	6.86	6.02	6.05	B
Ti II	4468.54	5.79	5.98	6.44	5.66	5.42	–
P II	4475.26	–	6.27	5.91	7.12	7.71	7.45
Mn II	4478.64	6.85	7.23	7.27	6.45	7.95	8.35
P II	4483.68	–	–	–	7.24	7.87	–
Fe II	4491.40	7.43	7.32	6.78	8.20	7.26	–
P II	4499.24	–	–	–	7.22	7.85	7.37
Ti II	4501.24	5.10	5.90	6.65	5.91	5.19	Z
Fe II	4508.28	7.44	7.21	6.76	8.21	7.20	7.84
Fe II	4515.34	B	7.41	6.97	B	7.23	7.91
Fe II	4520.22	7.45	7.24	6.90	Z	7.73	7.77
Fe II	4522.63	7.45	7.23	6.81	8.10	7.13	7.64
Fe I	4528.62	–	–	–	–	–	–

Line		ϕ Her	υ Her	87 Psc	HR7664	HR7361	HR6997
Fe II	4533.99	B	B	B	B	B	B
Ba II	4554.03	4.07	3.35	3.66	$\leq$3.08	$\leq$3.21	$\leq$3.40
Fe II	4555.89	7.65	7.24	6.76	8.17:	7.36	B
Cr II	4558.66	B	6.15	6.62	5.08	6.11	5.89
Ti II	4563.76	B	5.94	6.83	5.77	5.88	5.90
Ti II	4571.97	5.31	6.20	6.88	5.97	5.32	5.21
Fe II	4576.33	7.62	7.41	7.11	8.20	7.55	7.87
Fe II	4582.835	7.39	7.28	B	8.17	7.81	B
Cr II	4588.217	6.81	6.16	6.60	B	B	5.49
Fe II	4620.51	7.47	7.35	7.11	–	–	–
Fe II	4625.91	7.40	7.00	–	7.88	7.50	B
P II	4626.70	–	–	–	–	–	–
Fe II	4629.336	B	7.17	6.73	8.42	7.64	7.93
Al II	4663.05[2]	B	$\leq$4.88	$\leq$5.71	$\leq$4.98	$\leq$4.98	–
Mg I	4702.94	B	B	–	–	–	–

[1]: Curious blend with narrow-lined contaminant [2]: Curious unknown blend (see text)

References

Abt, H.A., 1979. *Astrophys. J.*, **230**, 485

Adelman, S.J., 1973. *Astrophys. J.*, **182** 531

Adelman, S.J., 1986. *Astr. Astrophys. Suppl.*, **64** 173

Adelman, S.J., 1988. *Mon. Not. R. astr. Soc.*, **235** 763

Adelman, S.J., 1989. *Mon. Not. R. astr. Soc.*, **239** 487

Adelman, S.J., 1991. *Mon. Not. R. astr. Soc.*, **252** 116

Adelman, S.J., 1994. *Mon. Not. R. astr. Soc.*, **266** 97

Adelman, S.J., and Fuhr, J.R., 1985. *Astr. Astrophys.*, **152** 434

Adelman, S.J., and Gulliver, A.F., 1990. *Astrophys. J.*, **348** 712

Adelman, S.J., and Lanz, T., 1988. *Proceedings of the IAU Working Group on Ap Stars Workshop* Lausanne, Universite Inst. d'Astronomie 1988.

Aikman, G.C.L., 1976. *Publs. Dom. astrophys. Obs.*, **14** 379

Alecian, G., and Artru, M.C., 1987. *Astron. Astrophys.*, **186** 228

Alecian, G., and Michaud, G., 1981. *Astrophys. J.*, **245** 226

Alecian, G., Michaud, G., and Tully, J., 1993. *Astrophys. J.*, **411** 882

Aller, M.F. 1970. *Astr. Astrophys.*, **6** 67

Anders, E., and Grevesse, N., 1989. *Geochim. Cosmochim. Acta.*, **53** 197

Anderson, L.S., 1989. *Astrophys. J.*, **339** 558

Auer, L.H., Mihalas, D., Aller, L.H., Ross, J.E., 1966. *Astrophys. J.*, **145** 153

Bidelman, W.P., 1962a. *Sky Telesc.*, **23** 140

Bidelman, W.P., 1962b. *Astrophys. J.*, **67** 111 *Astron. J.*,

Bidelman, W.P., and Corliss, C.H., 1962. *Astrophys. J.*, **135** 968

Biemont, E, Grevesse, N., Hannaford, P., Lowe, R.M., (1981) *Astrophys. J.*, **248** 867

Böhm-Vitense, E., 1989. *Introduction to Stellar Astrophysics Volume II: Stellar Atmospheres.*, Cambridge University Press

Borra, E.F., Landstreet, J.D., 1979., *Astrophys. J.*, **228** 809

Borra, E.F., Landstreet, J.D., and Thompson, I., 1983. *Astrophys. J. Suppl.*, **53** 151

Borsenberger, J., Michaud, G., and Praderie, F., 1984. *Astr. Astrophys.*, **139** 147

Burbidge, G.R. and Burbidge, E.M., 1955. *Astrophys. J. Suppl.*, **1** 431

Burkhart, C., and Coupry, M.F., 1991. *Astron. Astrophys.*, **249** 205

Cameron, A.G.W., 1971. *Publ. Astr. Soc. Pac.*, **83** 585

Conti, P.S., 1970. *Astrophs. J.*, **160** 1077

Cowley, C.R., Cowley, A., Jaschek, M., Jaschek, C., 1969. *Astron. J.*, **74** 375

Cowley, C.R., 1980. *Bull. Astr. Soc. India.*, **8** 101

Cowley, C.R., Sears, R.L., Aikman,G.C.L., Sadakane, K., 1982. *Astrophys. J.*, **245** 191

Deutsch, A.J., 1947. *Astrophys. J.*, **105** 283

D'odorico, S., Ghigo, M., Ponz, D., 1986. *ESO Scientific Report.*, **6** Published by ESO

Dreiling, L.A., Bell, R.A., 1980. *Astrophys. J.*, **241** 736

Dworetsky, M.M., 1971. 'PhD Thesis', University of California, Los Angeles, U.S.A.

Dworetsky, M.M., 1986. *Upper Main Sequence Stars with Anomalous Abundances, IAU Coll. No. 90.*, 397 eds. Cowley, C.R., Dworetsky, M.M., Mégessier, C.D., Reidel, Dordrecht

Dworetsky, M.M., 1993. in: *Peculiar Versus Normal Phenomena in A-type and Related Stars, Proc. IAU Coll. No. 138.*, PASPC 44,1 eds Dworetsky, M.M.,

Castelli, F., Faraggiana, R., Reidel, Dordrecht.

Fowler, W.A., Burbidge, G.R., Burbidge, E.M., 1955. *Astrophys. J.,* **2** 167

Fowler, W.A., Burbidge, E.M., Burbidge, G.R., Hoyle, F., 1965. *Astrophys. J.,* **142** 432

Fuhr, J.R., Martin, J.R., and Wiese, W.L., 1988. *J. Phys. Chem. Ref. Data.,* **17** No. 4

Gerbaldi, M., and Faraggiana, R., 1993. In: *Peculiar vs. Normal Phenomena in A-Type and Related Stars, Proc. IAU Coll. No. 138.,* PASPC 44, eds Dworetsky, M.M., Castelli, F., Faraggiana, R., Reidel, Dordrecht.

Gray, D.F., 1992. *The Observations and Analysis of Stellar Photospheres.,* 2nd edition John Wiley and Sons, New York

Grevesse, N., Biemont, E., Lowe, R.M., Hannaford, P., 1981. *IAU Colloquium No. 23.,* University of Liege, Belgium

Griffin, R,F., 1969. *Mon. Not. R. astr. Soc.,* **143** 319-339

Gulliver, A.F., Hill, G., Adelman, S.J., 1994. *Astrophys. J.,* **429** L81

Guthrie, B.N.G., 1984. *Mon. Not. R. astr. Soc.,* **200** 85

Guthrie, B.N.G., 1985. *Mon. Not. R. astr. Soc.,* **216** 1

Hannaford, P., Lowe, R.M., Grevesse, N., Biemont, E., Whaling, W., 1982. *Astrophys. J.,* **262** 736

Hartoog, M.R., and Cowley, A.P., (1979) *Astrophys. J.,* **228** 229

Hauck, B., Mermilliod, M., 1980. *Astr. Astrophys. Suppl.,* **40** 1

Hauck, B., and Mermilliod, M., 1990. *Astr. Astrophys. Suppl. Ser.,* **86** 107

Hauck, B., and North, P., 1982. *Astr. Astrophys.,* **114** 23

Havnes, O., Conti, P.S., 1971. *Astr. Astrophys.,* **14** 1

Heacox, W.D., 1979. *Astrophys. J. Suppl.,* **41** 675

Hearnshaw, J.B., 1990. *The Analysis of Starlight.,* Cambridge University Press

Heber, U., 1983. *Astr. Astrophys.,* **118** 39

Hoffleit, D., and Jascheck, C., 1982.*The Bright Star Catalogue* Yale University Observatory, 4th revised edition

Holzmann, J., 1991. *The On-line Vista Manual*

Howarth, I.D., Murray, J., 1991. *SERC Starlink User Note No. 50.*

Hunger, K., 1955. *Zeitschr. Astrophys.,* **36** 42

Hunger, K., 1975, In: *Problems in Stellar Atmospheres and Envelopes.,* 57 New York, Springer-Verlag New York

Iglesias and Velasco 1964. *Publ. Inst. Opt. Madrid.,* **23** 1

Isberg, B., Litzén, U., 1985. *Phys. Scripta.,* **31** 533

Jaschek, M., 1958., *Zeitschr. Astrophys.,* **45** 35

Jaschek, M., Jaschek, C., 1967. *Astron. J.,* **72** 806

Jaschek, M., Jascheck, C., 1995 *The behaviour of chemical elements in stars*, Knudsen

Kurucz, R.L., 1979. *Astrophys. J. Suppl.,* **40** 1

Kurucz, R.L., 1988. *Physical Formation of Fe* II *Lines Outside LTE: IAU Colloquium* 94 p41

Kurucz, R.L., 1990. *Transactions of the International Astronomical Union.,* **10B** 168

Kurucz, R.L., Furenlid, I., Brault, J., and Testerman, L., 1984. *Solar Flux Atlas from 296–1500nm Univ. Publ. Harvard.,* Cambridge, MA. Available from the National Solar Observatory, Sunspot, New Mexico

Kurucz, R.L., and Peytremann. E., 1975. *Smithsonian Astrophys. Obs. Spec. Rep.,* **32**

LeBlanc, F., Michaud, G., 1995. *Astrophys. J.,* **303** 166

Leckrone, D.S., Johansson, S.E., Wahlgren, G.M., Brage, T., 1994. *BAAS.,* **184** 0704

Lemke., M., 1989. *Astr. Astrophys.,* **225** 125

Lemke., M., 1990. *Astr. Astrophys.,* **240** 331

Magain, G., 1984. *Astr. Astrophys.,* **134** 189

Martin, G.A., Fuhr, J.R., and Wiese, W.L., 1988. *J. Phys. Chem. Ref. Data.,* **17** No. 3

Mathys, G., Lanz, T., 1990. *Astr. Astrophys.,* **230** 21

Michaud, G., 1970. *Astrophys. J.,* **160** 641

Michaud, G., Martel, A., Montmerle, T., Cox, A.N., Magee, N.H., Hodson, S.W., 1979. *Astrophys. J.,* **234** 206

Michaud, G., 1982. *Astrophys. J.,* **258** 349

Michaud, G., 1986. *Upper Main Sequence Stars with Anomalous Abundances, IAU Coll. No. 90.,* p454. Eds. Cowley, C.R., Dworetsky, M.M., Mégessier, C.D., Reidel, Dordrecht

Michaud, G. and Charland, Y., 1986. *Astrophys. J.,* **311** 326

Mihalas, D., 1965. *Astrophys. J. Suppl.,* **13** 1

Mihalas, D., 1978. *Stellar Atmospheres.,* Second Edition, Freeman and Company, San Francisco

Milne, E.A., 1922. *Phil. Trans. Roy. Soc.,* **223A** 201

Misch, A., 1991. *The University of California Lick Observatory Technical Reports.,* **58**

Moore, C.E., 1959. *Nat. Bur. Stand. Tech. Note No 32.,* 1

Morgan, W.W., 1931. *Astrophys. J.,* **73** 104

Morton, D.C., 1991., *Astrophys. J.,* **77** 119

Pagel, B.E.J., 1974. *Publ. Astr. Soc. Pac.,* **30** 471

Pirronello, V., Strazzullla, G., 1981. *Astr. Astrophys.,* **93** 411

Pitts, R.E., Newsom, G.H., 1986. *J. Quantit. Spectrosc. Radiat. Transfer.,* **35** 383

Pogge, R.W., Goodrich, R.W., and Veilleux, S., 1988. *University of California Lick Observatory Technical Reports.,* **50** University of Califoria

Press, W.H., Witta, P.J., and Smarr, L.L., 1975. *Astrophys. J.,* **202** L135

Press, W.H., Teukolsky, S.A., Vetterling, W.T., Flannery. B.P., 1986. *Numerical Recipes in FORTRAN.,* p. 163. Cambridge University Press, Cambridge.

Preston., G.W., 1971. *Publ. Astr. Soc. Pac.,* **83** 571

Proffitt, C.R., Michaud, G., 1989. *Astrophys. J.,* **345** 998

Ramella, M., Gerbaldi., M., Faraggiana., R., Böhm., C., 1989. *Astr. Astrophys.,* **209** 233

Redfors, A., and Cowley, C.R., 1993. *Astr. Astrophys.,* **271** 273

Roberts, J.R., and Eckerle, K.L., 1985. *Phys. Rev.,* **159** 104

Roby, S.W., and Lambert, D.L., 1990. *Astrophys. J. Suppl.,* **73** 67

Roman, N.G., Morgan, W.W., Eggen, O.J., 1948. *Astrophys. J.,* **107** 109

Russell, H.N., 1929. *Astrophys. J.,* **70** 11

Rutten, R.J., van der Zalm, E.B.J., 1984. *Astr. Astrophys. Suppl.,* **55** 143

Sadakane, K., 1981., *Publ. Astr. Soc. Pac.,* **93** 587

Sadakane, K., and Nishimura, J., 1981., *Publ. Astr. Soc. Japan.,* **33** 189

Sadakane, K., Takada, M., Jugaku, J., 1983., *Astrophys. J.,* **274** 261

Sahal-Bréchot, S., 1969. *Astr. Astrophys.,* **2** 322

Sargent, W.L.W., 1965. *Astrophys. J.,* **142** 787

Sargent, W.L.W., and Searle, L., 1967. *Astrophys. J.,* **157** 757

Searle, L., and Sargent, W.L.W., 1964. *Astrophys. J.,* **139** 793

Shortridge, K., Meyerdierks, H., Currie, M., Clayton, M., Lockley, J., (1997) *Starlink User Note* 86.14

Smalley, B., Dworetsky, M.M., 1993. *Astr. Astrophys.,* **271** 515

Smith, K.C., 1992. *PhD Thesis.,* University of London

Smith, K.C., 1993. *Astr. Astrophys.,* **276** 393

Smith, K.C., 1994. *Astron. Astrophys.,* **291** 521

Smith, K.C., 1995. *Astr. Astrophys.,* **297** 237

Smith, K.C., 1996. *Astr. Astrophys.,* **305** 902

Smith, K.C., and Dworetsky, M.M., 1988. In:*Elemental Abundance Analyses.,* ed. S.J., Adelman, T. Lanz, p32 *Lausanne: Institut. d'Astronomie de l'Université de Lausanne, Switzerland*

Smith, K.C., and Dworetsky, M.M., 1990. *ESA-SP-310 Evolution in Astrophysics IUE Astronomy in the Era of New Space Missions.,* p.279

Smith, K.C., and Dworetsky, M.M., 1993. *Astr. Astrophys.,* **274** 335

Smith, M.A., 1974. *Astrophys. J.,* **189** 101

Smith, P.L., 1976. *Mon. Not. R. astr. Soc.,* **177** 275

Stover, R., 1988. In *Proceedings of the Ninth Summer Workshop, Santa Cruz, California.,* p443 Springer-Verlag

Straizys, V., 1985. In: *IAU Symposium 111, Calibration of Fundamental Stellar Quantities.,* 285 eds. Haynes, D.S., Fasinetti, L.E., Davis Philip, A.G.

Strömgren, B., 1966. *Ann. Rev. Astr. Astrophys.,* **4** 433

Takada-Hidai, M., Sadakane, K., Jugaku, J., 1986. *Astrophys. J.,* **304** 425

Tassoul, J.L., and Tassoul, M., 1982. *Astrophys. J. Suppl.,* **49** 317-350

van der Held, E.F.M., 1931. *Z. Phys.,* **70** 508

Vauclair, G., 1976., *Astr. Astrophys.,* **50** 435

Vauclair, S., Hardorp, J., and Peterson, D.M., 1979. *Astrophys. J.,* **227** 526

Vauclair, G., Vauclair, S., and Pamjatnikh, A., 1974. *Astr. Astrophys.,* **31** 63

Vogt, S.S., 1987. *Publ. Astr. Soc. Pac.,* **99** 1214

Voigt, W., 1912. *Münch. Ber.,* **603**

Wahlgren, G.M., Adelman, S.J., Robinson, R.D., 1994a, *Astrophys. J.,* **434** 349

Wahlgren, G.M., Brage, T., Gilliland, R.L., Johansson, S.E., 1994b, *BAAS.,* **184** 0705

Wahlgren, G.M., Leckrone, D.S., Johansson, S.G., Rosberg, M., Brage, T., 1995. *Astrophys. J.,* **444** 438

Warner, B., 1967. *Mem. R. astr. Soc.,* **70** 165

Wiese, W,L., Smith, M.W., and Miles, B,M., 1969. *NSRDS-NBS 22.,* **Volume II** US Government Printing Office, Washington

Wiese, W.L., and Martin, G.A., 1980. *NSRDS-NBS 68.,***Part II** US Government Printing Office, Washington

White., R,E., Vaughan, A,H., Preston, G.W., Swings, J,P., 1976. *Astrophys. J.,* **204** 131

Wolff, S.C., and Wolff, R.J., 1974. *Astrophys. J.,* **194** 65

Wolff, S.C., and Wolff, R.J., 1976. *IAU Coll.* 32, p503. Eds. Weiss, W.W., Jenner, H., Ward, H.J., Universitätssternwarte Wien mit Figl- Observatorium für Astrophysik, Wien, Österreich

Wolff, S.C., 1983. *Physics of A stars; problems and perspectives: Monograph series on nonthermal phenomena in stellar atmospheres. NASA SP-463, NASA, Washington DC*

Wolff, S.C., and Preston, G.W., 1978. *Astrophys. J. Suppl.,* **37** 371-392

Zimmerman, R.E., Aller, L.H., Ross, J.E., 1970. *Astrophys. J.,* **161** 179